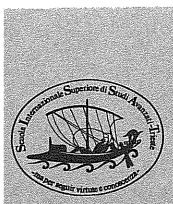

ISAS - INTERNATIONAL SCHOOL FOR ADVANCED STUDIES

APPLICATION OF MULTIGRID TO GENERAL RELATIVITY

Thesis submitted for the degree

of

Doctor Philosophiae

CANDIDATE

Antonio Lanza

SUPERVISOR

Marek Abramowicz

December 1986

TRIESTE

SISSA - SCUOLA
NTERNAZIONALE
SUPERIORE
STUDI AVANZATI
TRIESTE
Strada Costiera 11

APPLICATION OF MULTIGRID TO GENERAL RELATIVITY

Thesis submitted for the degree

of

Doctor Philosophiae

CANDIDATE

Antonio Lanza

SUPERVISOR

Marek Abramowicz

December 1986

To my wife

ACKNOWLEDGEMENTS

It is a pleasure to thank my supervisor Marek Abramowicz who introduced me to this very interesting subject. Also, thanks are due to him for continuous discussions, advise and encouragements.

Achi Brandt is acknowledged for having guided me towards the understanding of the Multigrid method and for the numerous suggestions during the development of the numerical code.

Useful discussions with Kei-ichi Maeda and John C. Miller have resulted in a number of crucial suggestions and clarifications. Special thanks are due to J.M. for reading the manuscript and for making useful comments.

I am grateful to Patrick Mann who brought to my attention the existence of the Multigrid and for his help on numerical work at the beginning of the project.

Particular thanks go to Dennis Sciama for his constant support and continuous encouragement.

Apart from my colleagues, I benefited from discussions with many other people, in particular I am indebted to M. Anile, F. De Felice, Y. Eriguchi, S. Motta, T. Piran and B. Schutz.

I wish also to thank my wife, Francesca, for her patience, encouragement and moral support over these years.

SISSA is acknowledged for the financial support during these years, which beyond the fellowship allowed for a number of useful trips in Italy and abroad.

The staff at the joined SISSA-ICTP computer center is acknowledged for their continuous assistance.

Finally, I am grateful for the facilities provided by the Weizmann Institute of Science, Rehovot, (Israel), where part of the work presented in this thesis has been done.

CONTENTS

Numerical solutions (Nakamura, 1981 and reference therein, Piran and Stark, 1984) of Einstein's equations following the collapse of axially symmetric rotating bodies show, for some value of the initial ratio a/m, the formation of structure with a toroidal shape around centrally condensed core. If by some mechanisms, the a/m ratio of the core is reduced (see Miller and De Felice, 1985 and De Felice et al., 1985 for a discussion of such mechanisms) to a value less than unity then a rotating black hole may be formed, which will be surrounded by a massive toroidal structure.

Other situations in which toroidal structures may be relevant are in the modelling of quasars, active galactic nuclei and other similar objects which most probably contain black holes and thick accretion disks.

So far the general relativistic description of these situations had been restricted to the case in which the self-gravity of the disk was negligible (Abramowicz et al., 1978 and Kozłowski et al. 1978) or to the case when both the self-gravity of the disk and the rotation of the black hole could be considered as perturbations (Will, 1974, 1975) to the Schwarzschild black hole. However there may be situations in which the mass of the disk or tori is comparable with that of a rotating hole (Wiita, 1985). In this case the full Einstein equations should be solved for the perturbations induced by the self-gravity of the matter to the Kerr black hole.

Moreover it is not clear yet whether the self gravity of the disk induces *runaway* instability. Abramowicz et al. (1980), using a very simple model of the black hole accretion disk system suggested that this kind of instability could act in a few dynamical time scales so that the disk itself could eventually be eaten by the black hole. This instability occurs because the growing black hole changes its gravitational field and therefore the location of the cusp through which matter is accreted changes. On the other hand, Wilson (1984), using models of

non-self-gravitating disks in the Kerr metric, concluded that there is no such kind of instability. A final answer to this problem can be given only after sequences of equilibrium configurations of self-gravitating disks or tori around black holes for different masses ratio have been constructed. This means solving numerically Einstein equations consistently with the given distribution of matter.

Since the problem is quite complicated in structure and a standard numerical method will not easily cope with it, we have decided to use the Multigrid method (Brandt, 1977) which although is complicated to program will deal naturally with the difficulties of the model. As one of the first applications of the method in general relativity (see Choptuik and Unruh, 1986, for a different one), we decided to solve few representative test problems before solving the entire one.

The plan of the thesis is as follows. In Chapter I we review the general theory of figure of equilibrium in Newtonian and relativistic theories. Chapter II contains a discussion of stationary and axisymmetric space-times and a derivation of Einstein's equations with the relative boundary conditions. Also, included is a discussion and derivation of the equations governing the fluid configuration. Chapter III reviews some numerical techniques used to solve Einstein's equations for stationary and axisymmetric configurations, with particular emphasis to the Multigrid which is the method applied by us. Chapter IV contains an application of Multigrid in general relativity in the case of vacuum stationary and axisymmetric space-times. In Chapter V we write down the equations for an infinitesimally thin disk around a black hole in Newtonian and relativistic theories. Also, an outline on how to apply the Multigrid in this case, is given. Finally, Chapter VI contains the outline of the application to the case of a self-gravitating toroidal structure around a rapidly rotating black hole.

CHAPTER I

FIGURES OF EQUILIBRIUM

It is well known that when rotation and magnetic field are neglected, an isolated self-gravitating star assumes a spherical shape, i.e. the surface upon which the total pressure p vanishes is a sphere.

If the body rotates around a fixed axis, then we have no apriori knowledge of its shape and stratification. Information on these is provided only by solving the hydrodynamical equations. In general, simplifying assumptions are made in order to approximate stars in a state of differential rotation by means of time-independent models. With this approximation sequences of models can be constructed for different amount of a rotation parameter.

The study of these stationary configurations contributes to understanding the mechanical properties of rotating bodies. Moreover the study of stability along these sequences has provided useful information about the fate in secular and dynamical time-scales of idealized evolving objects for increasing amount of rotation along the sequences.

This chapter is devoted to reviewing the important group of results that apply to rotating stars both in Newtonian and General Relativity theory.

1.1 The mathematical problem.

In this and next few sections we assume that the space-time is Euclidean and all the material velocities are small compared with the speed of light so that the Newtonian theory of gravity can be used. Moreover, we assume that the stars are composed of continuous and inviscid fluid so that the fundamental principles of classical mechanics hold. The hydrodynamical equations derived on the basis of this continuous model can be found in any book of classical mechanics. In particular, Tassoul (1978) derives them for a rotating star.

In the hydrodynamical description the state of the system is characterized by the density ρ, pressure p and velocity of the fluid $\underline{v}$ at a given point. The basic equations are the continuity equation

$$(1.1.1) \qquad \frac{\partial \rho}{\partial t} + \nabla \cdot (\rho \underline{v}) = 0$$

and the Euler equations

$$(1.1.2) \qquad \frac{d\underline{v}}{dt} \equiv \frac{\partial \underline{v}}{\partial t} + (\underline{v} \cdot \nabla)\underline{v} = -\frac{1}{\rho}\nabla p + \underline{F}$$

where $\underline{F}$ is the force per unit mass additional to the pressure force. In the case of self-gravitating system in Newtonian theory

$$(1.1.3) \qquad \underline{F} = -\nabla \Phi(\underline{r}, t)$$

where Φ is the gravitational potential. The relationship between $\underline{F}$, ρ and $\underline{v}$ is given by the Poisson equation

$$(1.1.4) \qquad \nabla^2 \Phi \equiv \frac{\partial^2 \Phi}{\partial x^2} + \frac{\partial^2 \Phi}{\partial y^2} + \frac{\partial^2 \Phi}{\partial z^2} = 4\pi G \rho$$

where G is the gravitational constant. It is well known (see any book on theoretical physics or potential theory, e.g. Morse and Feshbach, 1953) that the solution of equation (1.1.4) of physical interest is

$$(1.1.5) \qquad \Phi(\underline{r}, t) = -G \int \frac{\rho(\underline{x}, t)\, d\underline{x}}{|\underline{x} - \underline{r}|}$$

where the integration is extended over the entire volume of the system (that is, over all regions where ρ differs from zero).

The system of equations (1.1.1), (1.1.2) and (1.1.4) is incomplete and in general a relation between the pressure and the density (equation of state) must be provided. This constitutive equation (i.e. function of density, temperature T and chemical composition χ) is characteristic of the stellar material. In general

$$(1.1.6) \qquad p = p(\rho, T, \chi)$$

This equation introduces two additional variables, therefore the system has to be supplemented by the energy equation

$$(1.1.7) \qquad T\left[\frac{\partial s}{\partial t} + (\underline{v}\cdot\nabla)s\right] = -\frac{1}{\rho}\nabla\cdot\underline{Q} + \varepsilon$$

and by the equation expressing the change in time of the chemical composition due to nuclear reactions

$$(1.1.8) \qquad \frac{d\chi}{dt} = G(\chi,\rho,T)$$

In equation (1.1.7) s is the specific (per unit mass) entropy, $\underline{Q}$ is the radiative flux and ε is the rate at which energy is generated per unit mass. Constitutive equations for $\underline{Q}$ and ε must also be provided. Supposing that thermal energy is transferred from regions where the temperature is large to those where it is small, the diffusion equation gives

$$(1.1.9) \qquad \underline{Q} = -k\nabla T$$

where $k=k(\rho,T)$ is the transport coefficient. The energy generation ε per unit time and unit mass is in general a known function of ρ, T and the chemical composition χ of the star

$$(1.1.10) \qquad \varepsilon = \varepsilon(\rho,T,\chi)$$

Finally, in order to make a solution of the above system unique, initial data and boundary conditions must be specified. If the boundary $\partial\mathcal{V}$ (surface of the star) is expressed by the equation $\mathcal{S}(\underline{r},t)=0$ the simple boundary conditions are

$$(1.1.11) \qquad \frac{ds}{dt} = 0\ , \qquad p = 0\ , \qquad T = 0 \qquad \text{on } \partial\mathcal{V}.$$

These particular boundary conditions are valid only when the star is supposed to be non-radiating. Integration of equations (1.1.1), (1.1.2) and (1.1.7) over the entire volume gives as a result that mass, angular momentum and total energy must be conserved respectively.

Moreover combination of equations (1.1.2) and (1.1.5) gives as a result the second order virial theorem which should be

satisfied by any ideal and self-gravitating fluid model

$$(1.1.12) \qquad \frac{1}{2}\frac{d^2 I}{dt^2} = 2K + W + 3\int_{\mathcal{V}} p \, d\underline{x}$$

where I, K and W denote, respectively the moment of inertia, the kinetic energy and the gravitational energy

$$(1..1.13) \qquad I = \int_{\mathcal{V}} \rho x^2 d\underline{x} \qquad\qquad K = \frac{1}{2}\int_{\mathcal{V}} \rho v^2 d\underline{x}$$

and

$$(1.1.14) \qquad W = \frac{1}{2}\int_{\mathcal{V}} \rho\Phi \, d\underline{x}$$

The set of equations described so far can be reduced to stationary ones when the characteristic time scales for the fundamental physical processes involved are large.

1.2 Time scales and steady-state approximation.

There are three main time scales which are important during the life of a star: the dynamical time scale or *free fall* time scale t_{ff} (during which a unit of mass will fall freely under the action of the star's gravitational potential), the contraction time scale or *Kelvin* time scale t_k (during which the energy released by radiation is comparable with the gravitational energy) and the nuclear time scale t_n (during which a substantial fraction of the nuclear fuel is consumed). For the Sun these time scales are roughly one hour, 10^7 years and 10^{10} years respectively. For other stars the numbers can change, but the ratios t_{ff}/t_k and t_k/t_n are often still small. Different phases of stellar evolution can be treated by different approximations of the full hydrodynamical equations depending on which time scale dominates during that phase.

The first phase of a star's life, when the temperature is still low, is characterized by a rapid contraction or collapse. Here the dominant time scale is t_{ff} and the other ones can be considered infinite. In this case the full time-dependent

equations are needed and the mathematical problem is not trivial.

During protostars collapse when the temperature increases but is still below the value at which thermonuclear reaction are ignited the time scale of the contraction changes from t_{ff} to t_k and the star begins to radiate energy at the expenses of the gravitational energy. Here t_n can be still considered infinite. In this situation the characteristic velocity is comparable to the ratio of the radius of the star R to the Kelvin time which, in solar unit, is $v \sim R/t_k \sim 10^{-4}$. Such small velocities allow to neglect the local derivatives in equations (1.1.1) and (1.1.2) but not in equation (1.1.7). Therefore the star can be considered hydrodynamically, in steady state but not thermodynamically.

When the temperature reaches the thermonuclear reaction critical value the radiative losses are balanced by the energy released and the contraction stops. Here the dominant time scale is the nuclear one and the star can be considered hydrodynamically and thermodynamically in a steady state if we restrict our attention to short time intervals such that variations on chemical composition can be neglected.

After a succession of equilibrium core burning phases separated by periods of core contraction all of the available fuel is finally exhausted. At this stage the star cannot support itself against gravitational collapse by generating thermal pressure, then it will collapse till the pressure of degenerate electrons can support it forming thus a white dwarf or till when the support is provided by degenerate neutrons forming a neutron star or it will collapse for ever (no other means can support now the inward pull of gravity) forming a black hole. It is well know that the three situations will occurs for different values of the mass of the star. In table I (from Shapiro and Teukolsky, 1983) besides the range of typical masses for these objects (considered not rapidly rotating) one can read the radius, mean density and surface potential. It is clear from the table that these objects are very compact and have much stronger surface gravitational fields than a normal star. General relativistic corrections become progressively greater as one moves from ordinary stars to white dwarfs and then to neutron stars and black holes.

Table I

Object	Mass (M)	Radius (R)	Density ($g.cm^{-3}$)	Surface Potential (GM/Rc^2)
Sun	$M_\odot$	$R_\odot$	1	10^{-6}
White Dwarf	$\leq M_\odot$	$\sim 10^{-2} R_\odot$	$\leq 10^{7}$	$\sim 10^{-4}$
Neutron Star	$\sim 1 \div 3 M_\odot$	$\sim 10^{-5} R_\odot$	$\leq 10^{1}$	$\sim 10^{-1}$
Black Hole	$> 3 M_\odot$	$2GM/c^2$	$\sim M/R^3$	~ 1

The characteristic time scale for this phase of a star's life is given by the time during which the star releases the residual ion thermal energy cooling down. An estimate of this time scale (Shapiro and Teukolsky, 1983) is

$$t_c \sim 10^{9} \text{ yr}$$

for a white dwarf whose luminosity is $L \sim 10^{-3} L_\odot$. Here again the steady state approximation is valid.

The above analysis shows that in general the stars spend most of their life in hydrostatic equilibrium, therefore it is not a bad approximation for studying stellar structure to consider only the time-independent part of the system of equations discussed.

This even applies in the framework of General Relativity to study the structure of neutron stars and other configurations for which the above time scales can be neglected.

1.3 Some general results

Different situations can be described by different equations of state and different rotation law. The first model of star in hydrostatic equilibrium have been constructed supposing that the star does not radiate and it is in *permanent rotation* around a fixed axis (see Tassoul, 1978). The equations describing stationary configurations of rotating and self-gravitating gases are

$$(1.3.1) \qquad -(\underline{v}\cdot\nabla)\underline{v} = -\frac{1}{\rho}\nabla p + \nabla\Phi_g$$

$$(1.3.2) \qquad \nabla^2 \Phi_g = \begin{cases} 4\pi G\rho & \text{inside} \\ 0 & \text{outside} \end{cases}$$

The left hand side of equation (1.3.1) can also be written as

$$(1.3.3) \qquad -\frac{1}{2}\nabla v^2 - (\nabla \times \underline{v}) \times \underline{v}$$

therefore the integrability condition for equation (1.3.2) is

$$(1.3.4) \qquad \nabla \times \left[\frac{1}{\rho}\nabla p + (\nabla \times \underline{v}) \times \underline{v}\right] = 0$$

Using cylindrical coordinates (r, z, φ) the fluid velocity is given by

$$(1.3.5) \qquad \underline{v} = r\,\Omega(r,z)\underline{e}_\varphi$$

and equation (1.3.1) and (1.3.4) reduce to

$$(1.3.6) \qquad \frac{1}{\rho}\nabla p = -\nabla \Phi_g + r\,\Omega^2(r,z)\underline{e}_r$$

$$(1.3.7) \qquad zr\,\Omega\frac{\partial \Omega}{\partial z}\underline{e}_\varphi = \nabla\left[\frac{1}{\rho}\right] \times \nabla p$$

Here, $\underline{e}_\varphi$ and $\underline{e}_r$ are the unit vectors in φ- and r-direction, respectively, and Ω is the angular velocity. Equation (1.3.7) implies that for barotropes, where the pressure is a function of the density only, *the angular velocity distribution has to be constant over cylindrical surfaces*

$$(1.3.8) \qquad \frac{\partial \Omega}{\partial z} = 0$$

Moreover, if we consider a rotating star for which condition (1.3.8) holds, then equation (1.3.7) shows that *the isopycnic (equal density)- and the isobaric (equal pressure)-surfaces must coincide.* Furthermore, if equation (1.3.8) holds, the centrifugal force term in equation (1.3.6) can be obtained from a centrifugal potential Φ_c

$$(1.3.9) \qquad \Phi_c = \int_0^r \Omega^2(r) r \, dr$$

Another simplification is provided by the Lichtenstein's theorem: *rotating fluid masses for which the angular velocity does not depend on z have a plane of symmetry perpendicular to the axis of symmetry*. This theorem, first proved for rigid rotation and uniform density has been extended even to differential rotation with non uniform density (see Stoeckly, 1965). When the potential is expanded using orthonormal polynomials this symmetry requires only even terms in the series.

All these results are derived from the condition of mechanical equilibrium and are valid for any rotating systems. However, they do not provide any idea on the distribution of angular momentum or the rotation law. Constraints on it come from considerations of dynamical and thermal stability.

The usual approach to stability is the normal-mode one. This consists of considering small perturbations of the system and therefore studying the linearized time dependent equations of hydrodynamics. Since the problem is linear the space variable r can be separated from the time so one search for normal-mode solutions for the displacement of the form

$$(1.3.10) \qquad \xi(\underline{r},t) = \xi(\underline{r},\omega) e^{i\omega t}$$

The equations then will provide a dispersion relation from which one can study the sign of ω^2. It turns out that if $\omega^2<0$ the system will be unstable since perturbation will increase in time, and if $\omega^2>0$ the system will be stable. The onset of instability occurs when $\omega^2=0$, the modes corresponding to these values of ω are called neutral modes.

When the system is unstable we say that it is dynamically or thermally unstable if the characteristic time scale of the instability is of the order of the free fall time $(G\rho)^{-1/2}$ or of the order of the Kelvin time GM^2/LR respectively.

The main condition governing the rotation law criterion is the Høiland which states that *a general non-isentropic*

configuration is dynamically unstable if on each surface of constant entropy s the specific angular momentum $\ell = |r^2\Omega|$ *must be increasing function of* r

$$\frac{d\ell}{dr} > 0. \qquad (1.3.11)$$

In view of these results a model of a rotating configuration can be specified giving the total mass M, the total angular momentum J and a distribution of specific angular momentum satisfying the above criterion. Then fixing the mass one can construct a sequence of models with different amounts of rotation. Instead of J, one can use another parameter to characterize the main features along the sequences. In the case of a spheroid it is natural to use as a parameter the eccentricity *e* since it gives an idea of how oblate the object is. The most convenient measure is the ratio of rotational kinetic energy to the gravitational energy

$$\tau = \frac{K}{|W|} \qquad (1.3.12)$$

By virtue of the virial theorem, a rotating configuration in equilibrium composed by perfect fluid must satisfy

$$2K + W + 3(\Gamma - 1)U = 0 \qquad (1.3.13)$$

where Γ is the adiabatic index and U is the internal energy. Since the last term must be positive otherwise the configuration would be radially unstable we have

$$2K \leq |W| \qquad (1.3.14)$$

then

$$0 \leq \tau \leq 0.5 \qquad (1.3.15)$$

This parameter gives us a qualitative idea about the concept of slow and rapid rotation according to the inequalities

$$\tau \ll 1 \qquad \text{slow rotation} \qquad (1.3.16)$$

$$\tau \sim 0.5 \qquad \text{rapid rotation.} \qquad (1.3.17)$$

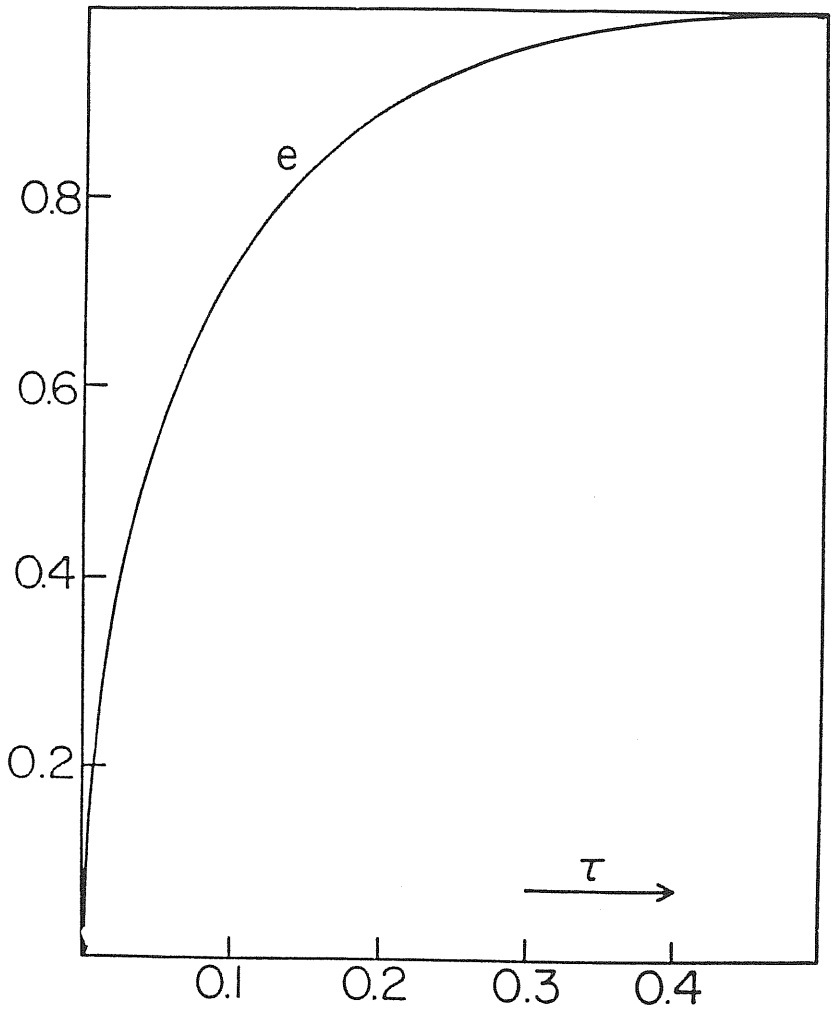

Fig. 1 - The eccentricity e along the MacLaurin sequence, as function of the ratio $\tau = K/|W|$.

1.4 Equilibrium configuration of ellipsoidal shape

Hydrostatic equilibrium of rotating stars has been studied using different approaches. As a first approximation we can assume that the configuration is incompressible and rotates with the simplest rotation law, e.g. uniform rotation. These models can be thought of as a particular case of the more general centrally condensed polytropic bodies, rotating with a differential law. Making this generalization we can divide the approaches used so far into four groups. The first one adopts models in which the equipotential surfaces are level surfaces of tractable coordinate systems. This is applied to homogeneous and uniformly rotating bodies no matter how rapid is the rotation. The second is a modification of the first and treats slowly rotating objects whose equipotential surfaces deviate only slightly from simple surfaces (Chandrashekar-Milne expansion). The third group uses a variational method in which the changes of the parameters describing the model are chosen among the ones which minimize the total energy (Roberts, 1962), The fourth group uses the most straightforward approach, that is the direct integration of the partial differential equations of equilibrium. This method has no limitations and can study as precisely as desired centrally condensed uniformly or differential rotating configurations.

Homogeneous uniformly rotating bodies share many properties with the differential polytropes. There are mainly two classes of such objects, the MacLaurin spheroids and the Jacobi ellipsoids. The former are axially symmetric, the latter are non-axisymmetric. Fig. 1 shows the eccentricity of such objects as a function of the parameter τ. Jacobi ellipsoids exists only for in the range $0.14 \leq \tau \leq 0.5$. This means that only rapidly rotating configurations can have triaxial symmetry. In Fig. 2 the dimensionless quantities

$$(1.4.1) \qquad \hat{\Omega}^2 = \frac{\Omega^2}{\pi\rho G}$$

$$(1.4.2) \qquad \hat{J} = \frac{J}{(GM^{9-}a)^{1/2}}$$

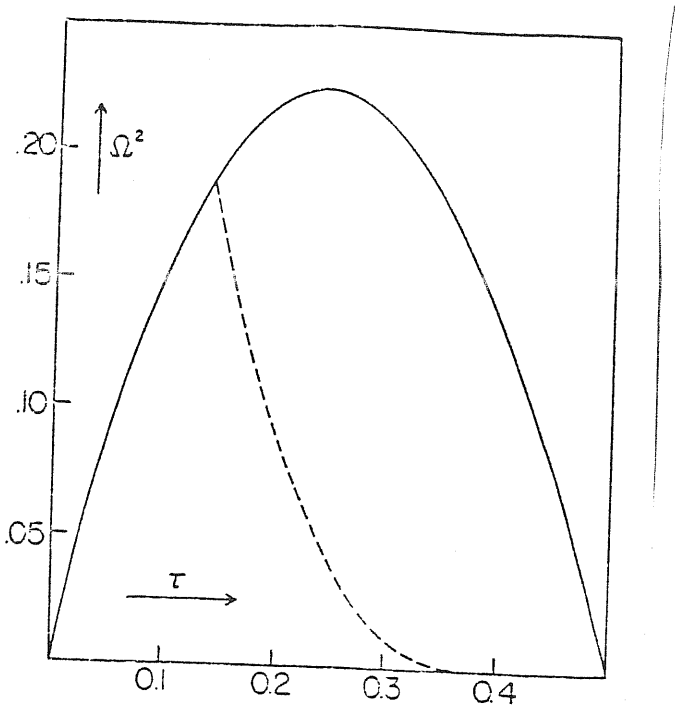

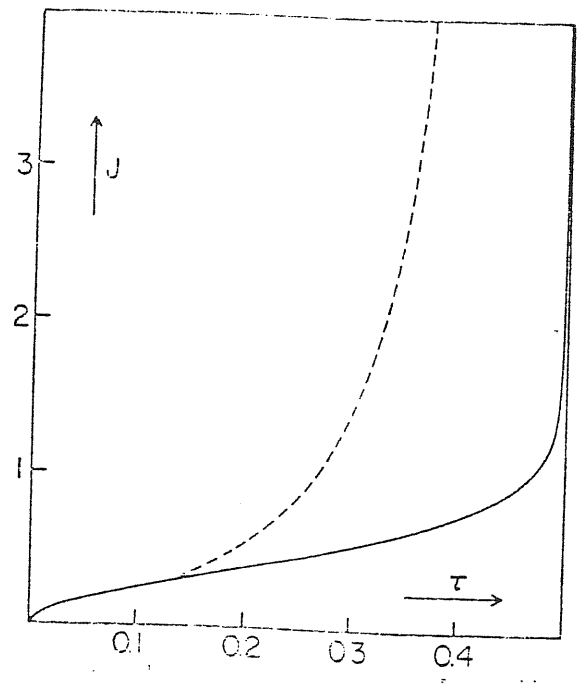

Fig. 2 - The squared angular velocity Ω^2 and the total angular momentum J along the MacLaurin (*solid line*) and the Jacobi (*dashed line*) sequences, as functions of τ.

where $\bar{a}=(a_1a_2a_3)^{1/2}$ and a_i are the axes of the configurations, are plotted. The full line refers to the MacLaurin sequence, whereas the dashed one refers to the Jacobi sequence.

If we consider a star contracting slowly J will increase monotonically as do τ and e, the object become progressively more oblate and it ends up as an infinitely thin disk. Moreover, for $0\leq\tau\leq0.14$ the MacLaurin spheroids are the only possible equilibrium configurations, whereas to each value of τ in the range $0.14\leq\tau\leq0.5$ there corresponds two figures of equilibrium. In Fig. 3 the total mechanical energy $K + W$ in units of $\frac{4}{5}\pi G\rho M\bar{a}^2$ is plotted against $\hat{J}$. The figure shows that a Jacobi ellipsoid has lower mechanical energy than the MacLaurin spheroid with the same M, J and volume V. If there is some dissipative mechanism a MacLaurin spheroid will evolve to a Jacobi ellipsoid beyond the point of bifurcation $\tau=\tau_b=0.14$. In order to check if this is the case one should solve the full set of hydrodynamical equations in which the dissipation is included. Press and Teukolsky (1978) integrating the second order virial equations with viscosity found that the MacLaurin spheroids slowly deform into stable Jacobi ellipsoids. An insight into the problem comes from the stability analysis. It can be shown that there is a neutral mode ($\omega=0$) at the bifurcation point τ_b, but $\omega^2>0$ on both sides of it. Moreover $\omega=0$ at $\tau=\tau_b$ is a double root and two sequences branch off the MacLaurin sequence at this point, namely, the Jacobi ellipsoids and the Dedekind sequence of triaxial ellipsoids whose overall shape is stationary relative to an inertial frame, although fluid circulates about the least axis . Now, if one includes viscous dissipation it can be shown that ω^2 becomes complex beyond τ_b, and the imaginary part is proportional to the viscosity. Then the perturbation increases slowly (on the viscous time scale) and the MacLaurin spheroid evolves into a Jacobi ellipsoid minimizing energy. This is a so-called *secular instability* because it is slow and needs dissipation to operate. Including dissipation by gravitational radiation instead of by viscosity, Chandrashekar (1970) has shown that there is again a secular instability driven by gravitational radiation reaction. The mode that is made unstable by gravitational radiation is not the same one that is made unstable

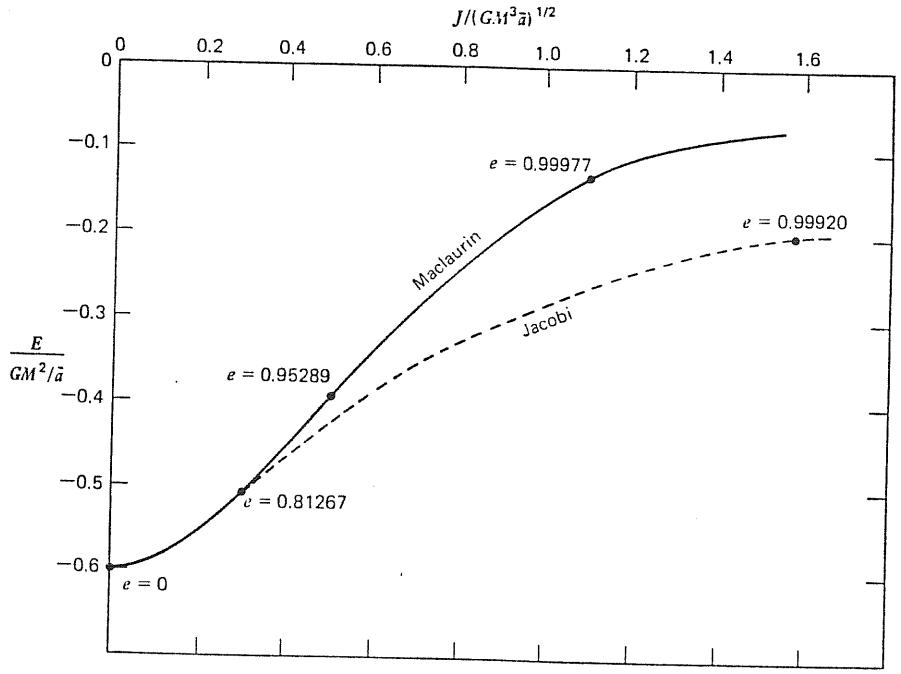

Fig. 3 - The total mechanical energy $E=K+W$ along the MacLaurin (*solid line*) and the Jacobi (*dashed line*) sequences, as functions of J.

by viscosity. For a discussion of such instability see the next section.

Another point of onset of instability occurs beyond τ_b at $\tau=\tau_i=0.2738$ along the MacLaurin sequence. At this point $\omega^2=0$, but ω^2 goes to negative values beyond τ_i no matter what physical process is going on. At this point the MacLaurin spheroids become *dynamically unstable*. This point can be reached when viscosity and gravitational radiation reaction work together or when dissipative effects are negligible.

James (1964) relaxed the hypothesis of homogeneity and solved numerically the equation of hydrodynamical equilibrium constructing sequences of uniformly rotating axisymmetric models with increasing rotation velocity, keeping constant the polytropic index n and the central density ρ_c. The range of polytropic index covered by his calculations was $0\leq n\leq 3$. According to these calculations all the sequences for $n\neq 0$ terminate for a value of the parameter τ, τ_{max}, which depends on the value of n. The sequences stop because of equatorial shedding, that is when the effective gravity at the equator becomes zero. For $n<0.808$, τ_{max} is greater than τ_b, therefore there is always a non-axisymmetric bar mode instability at $\tau=0.14$ irrespectively of n if the sequence extend that far. For $n\geq 0.808$, τ_{max} is smaller than τ_b, therefore the configurations are always stable up to the shedding point. This results suggests that uniformly rotating polytropes with $n\geq 0.808$ cannot store rotational energy to reach the point τ_b, they cannot rotate rapidly.

A different picture, which resembles the MacLaurin sequence more, comes out from considering differential rotating polytropes. Stoeckly (1965) solved numerically the relative set of equations and constructed self-consistent models of axisymmetric differential rotating polytropes with n=1.5. The results of this numerical integration indicate that for models whose rotation was nearly uniform the sequences terminate with models with zero effective gravity at the equator confirming the results of James. As the differential rotation increases the equidensity surfaces in the interior of the configuration assume a more elliptical form up to the case in which the models pass from a cusped interior

equidensity surface to a completely detached ring.

More general polytropic sequences with indices $0 \leq n \leq 3$ have been obtained by Bodenheimer and Ostriker (1973) using the self-consistent-field (SCF) method developed by Ostriker and Mark (1968). Analysis of stability (Ostriker and Bodenheimer, 1973) indicates that the instability points of the MacLaurin sequence (secular at $\tau_b=0.14$ and dynamical at $\tau \sim 0.27$) seem to be quite general (however see section 1.5). The method used did not allowed the authors to calculated configurations with high degree of flattening. A modification of the SCF method (Hachisu, 1986) removes those defects and enables to calculate structures such as ring, core-ring and very flat disk (see Chap. III).

Only very recently (Vandervoort, 1980, Vandervoort and Welty, 1981 and independently Ipser and Managan, 1981) study of non-axisymmetric inhomogeneous bodies has begun. In the past, efforts to generalize the axisymmetric configurations to non-axisymmetric ones, have been discouraged by the circumstances that, in the case of uniformly rotating polytropes, bifurcation occurs only for values of the polytropic index which are too low to be representative of the central concentrations of most real stars. On the other hand, it now appears that polytropes of a low polytropic index can model the structures of neutron stars. These studies are still in their infancy and only few cases have been considered. In particular Ipser and Managan under the assumptions of incompressible flow, absence of meridional motions and linear dependence of the motions upon the position, have constructed sequences for value of n in the range $0.5 \leq n \leq 0.7$. For larger n such configurations can exist only over a narrow range in angular velocity, since larger amounts of rotation yields outer regions in danger of succumbing to mass shedding. This result is in agreement with calculations made by James (1964), Vandervoort (1980) and Vandervoort and Welty (1981).

The problem of finding equilibrium configuration of rotating system in general relativity is far more complicated even in the simplest case of incompressible rigidly rotating fluid. The difficulty arise by the fact that no general solution is known for the exterior gravitational field. The Kerr solution can describe a

very restricted class of axisymmetric objects. So one must resort to approximated method or numerical methods. Here again we can divide in four different classes the lines of research which have been followed. The first one considers the effect of relativity fairly small (post-Newtonian approximation, hereafter PN) in which $GM/Rc^2 \ll 1$; the second one considers only slowly rotating objects for which $R^2\Omega^2 \ll GM/R$. The third and fourth ones apply to rapidly rotating fully relativistic models by using a variational principle method or by self-consistent-field calculations.

In a series of papers Chandrashekar (1965, 1967, 1971a,) used the PN approximation to study the effect of general relativity on the classic MacLaurin spheroids and Jacobi ellipsoids. The principal correction to such configurations is that the isobaric surfaces are pulled inwards at the equator and become less eccentric than predicted by Newtonian theory.

Bardeen (1971) reexamined the PN form of the MacLaurin spheroid using a different method. An interesting new axisymmetric instability point along the sequence of MacLaurin spheroids has been found by these PN analyses. The value of the eccentricity e at this point is 0.985. Bardeen suggested that a ringlike structure or a central bulge configuration may develop according to whether dissipation transfers angular momentum inwards or outwards. This is a subject which is not fully investigated yet.

When centrifugal effects are small compared with the gravitational ones, the rotation can be treated as a small perturbation on an already known non-rotating configuration. The field equations are then expanded in powers of the angular velocity . Hartle (1967) derived the structure equations correct to second order in Ω. These equations were solved by Hartle and Thorne (1968) for modelling rotating neutron stars and white dwarfs whose matter was assumed to obey either the Harrison-Weeler (1965) equation of state or Tsuruta and Cameron (1966) V_γ equation of state. They concluded that the effect of slow rotation on the determination of the mass limit is not very large.

Chandrashekar and Miller (1974) studied uniform slowly rotating configurations. Their aim was to mimic a quasi-stationary collapse through a sequence of models for different values of the

ratio of the radius R of the star to the Schwarzschild radius R_g. From this analysis appears a purely general relativistic effect on the behaviour of the ellipticity as function of the ratio R/R_g. As this ratio decreases (i.e. during contraction) the body becomes more and more oblate till reaches a maximum at $R/R_g \sim 2.3$ and then the ellipticity decreases again to zero. Non-linear relativistic effects enable the inward gravitational forces to overcome the outward forces.

For studying the effects of rapid rotation and of general relativity altogether, the methods described above cannot be applied anymore. Then one should use numerical techniques or variational principles. The aim of these latter is to find an expression which, when minimizing under some constraints, can lead to equations and conditions which determine the equilibrium structure of the body in consideration.

For axisymmetric configurations in uniform rotation which are barotropic, Hartle and Sharp (1965, 1967) developed a variational principle. They gave expressions for the total mass-energy M, angular momentum J and baryons number N in terms of the metric functions and density distribution. An equilibrium model is then found minimizing M under the constraints of specified J and N in all the configuration.

Abramowicz (1970) and Bardeen (1970) independently developed a rather more general variational principle for perfect fluid configurations which can be differentially rotating and non-barotropic. Again here the equilibrium configuration is calculated minimizing the total mass under the constrain that J and N are fixed for each ring of matter belonging to the body in consideration. This was used by Abramowicz and Wagoner (1976) to compute neutron star models.

Numerical relativistic calculations have been carried out first by Bardeen and Wagoner (1969, 1971) for disk configurations in which the pressure vanish (see later). Wilson (1972) considered differentially rotating polytropic models with n=3. He used a full 2-dimensional finite difference code for solving the field equations. Bonazzola and Schneider (1974) developed numerical methods for constructing rotating fluid bodies with various

pressure density relations and various amount of flattening. This method is a general relativistic version of Ostriker and Mark's one in which the Green function techniques for formulating the Einstein's equations in integral form is used. However, this paper together with that of Wilson are opened to a certain amount of criticisms. Wilson approximates the boundary conditions guaranteeing asymptotic flatness by certain *ad hoc* Newtonian-like conditions and this might lead to significant inaccuracy in highly relativistic models. Bonazzola and Schneider's method contains artificial restrictions that cause it to break down in highly relativistic situations before many interesting rotational effects may appear.

Very detailed sequences have been calculated by Butterworth and Ipser (1975, 1976) (hereafter referred to as BI), Butterworth (1976, 1979) using the general relativistic version of Stoeckly's method. In the first papers BI applied their method to construct sequences of uniformly homogeneous bodies which in certain cases exhibited interesting phenomena. Specifically, it was found that unlike the Newtonian sequences of MacLaurin spheroids, fully relativistic sequences terminate at points where centrifugal forces balance gravity at the equator (points marked *shed* in Fig. 4). Also, highly relativistic models with sufficient amount of rotation were found to develop regions within which observers must rotate with positive angular velocity relative to infinity (see Chap. II) (point marked *ergo* in Fig. 4). Fig 5 shows the eccentricity versus J/M_o^2, where M_o is the rest mass of the configuration. A body with $J/M_o^2 \leq 0.5$ reaches a maximum eccentricity ≤ 0.7 then moves downwards through states with smaller and smaller value of e. This confirm the result of Chandrashekar and Miller mentioned above.

In a further paper Butterworth (1976) considered uniformly rotating pseudo-polytropes ($p \propto \epsilon^{1+1/n}$). He did a comparison with the Newtonian computations made by James. In Fig. 6 we can see how close are the results between the Newtonian case and the relativistic case. The only difference is that for $n<2.5$ the relativistic objects are more spherical than their Newtonian counterparts of equal angular velocity and central rest mass

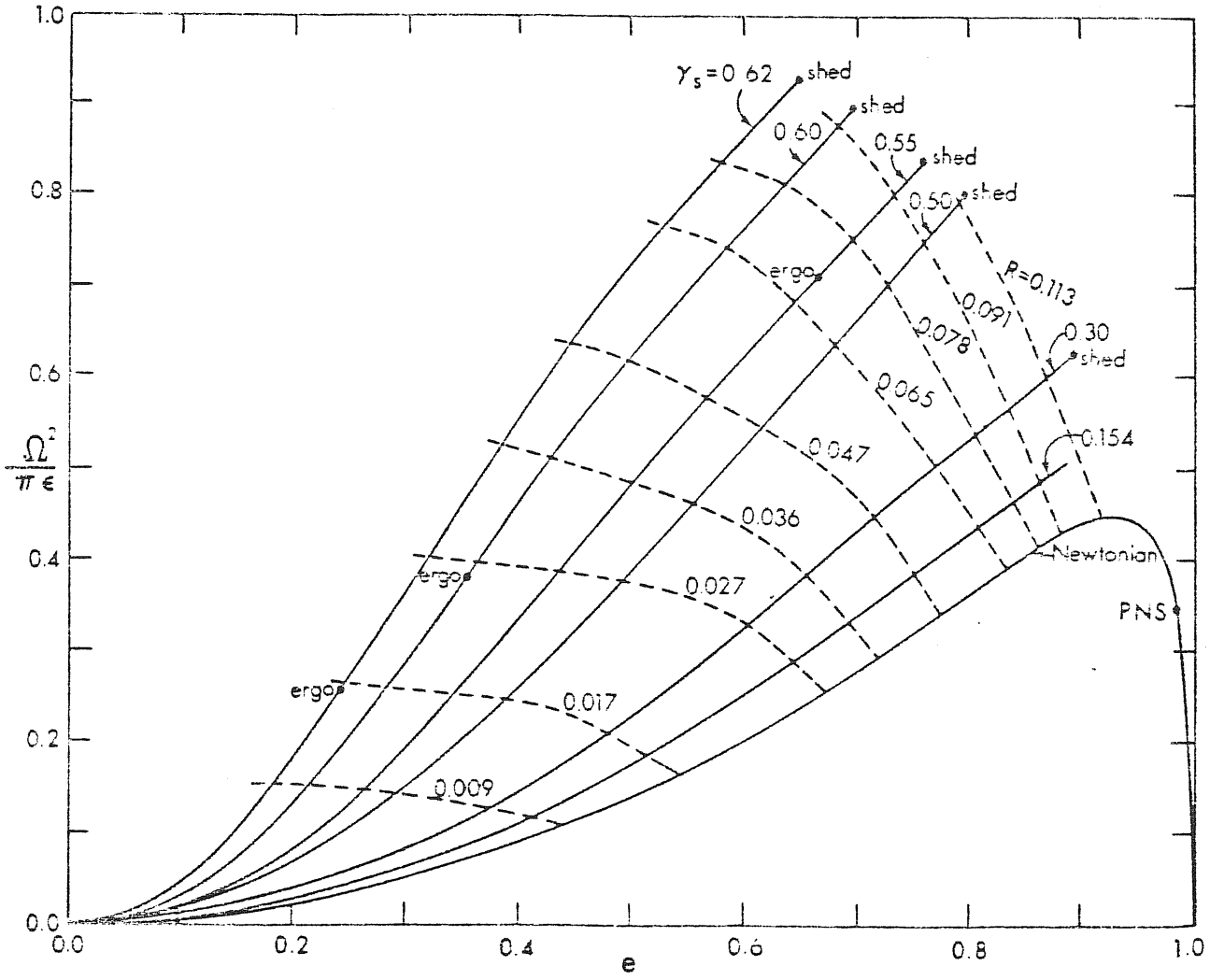

Fig. 4 - The angular velocity square in the unit π times the energy density ε (in the text e), versus the eccentricity for homogeneous bodies (from BI, 1976). See text for details.

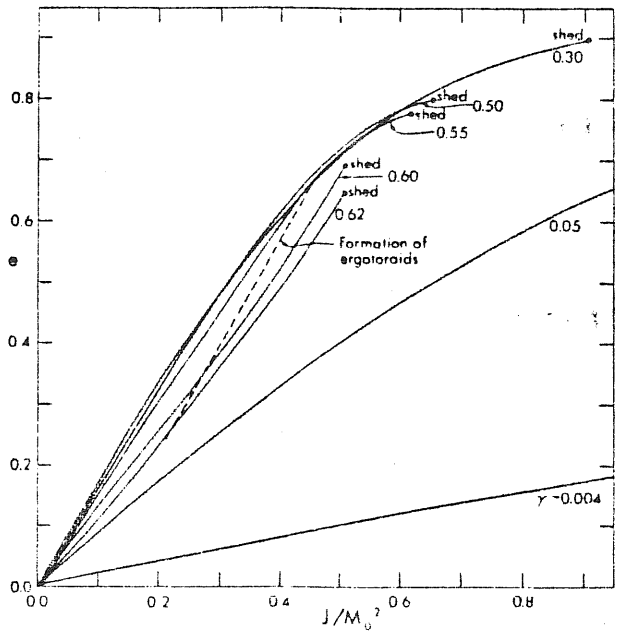

Fig. 5 - The eccentricity e versus J/M^2. For $\gamma \geq 0.004$, the dashed curve marks the points along the sequences of constant γ at which ergoregions appear (from BI, 1976).

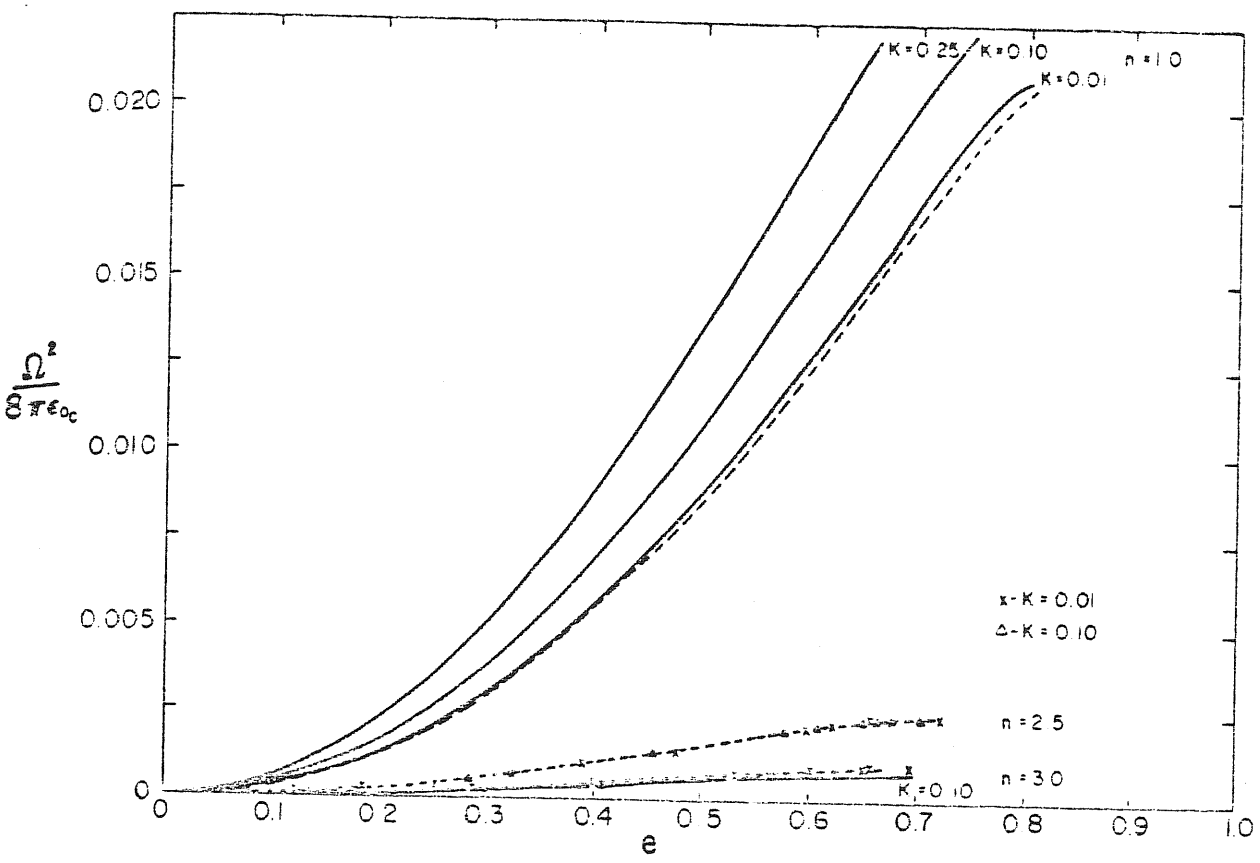

Fig. 6 - The squared angular velocity versus the eccentricity for pseudo-polytropes of index n (*solid curves*) and for Newtonian polytropes of index n as computed by James (1964) (*dashed curves*). From Butterworth, 1976.

density, while for n>2.5 they are more flattened. No ergoregions were found for these objects.

A modification of the numerical method allowed Butterworth (1979) to compute solutions with angular velocity decreasing as a function of the angular momentum (high eccentricity). These models are important not only to extend the relativistic sequence further, but also to investigate the association between the termination points on relativistic sequences with the first axisymmetric secular instability of the MacLaurin spheroids which occurs after the maximum in angular velocity.

Fig. 7 shows that sequences with $\gamma=1-e^{\nu}\leq 0.30$ have maxima in the angular velocity, whereas sequences with $\gamma\geq 0.30$ terminate at the mass-shedding instability point before a peak in the angular velocity is reached. The figure shows that these calculations are not very accurate since, for instance, the sequence with $\gamma=0.004$ does not pass very near to the three points of Newtonian instabilities (open circle).

Using a numerical code based on the program developed by BI, Friedman, Ipser and Parker (1984, 1986), Friedman and Ipser (1986) have studied the structure of rapidly rotating relativistic models, based on equations of state proposed for neutron star matter. Particular emphasis was given to establishing upper limit on rotation and mass. Figure 8 (from Friedman et al 1986) shows the relation between τ and Ω. The end-point of each sequence represents a star rotating sufficiently rapid that particles at the equator move at the Keplerian velocity Ω_k (angular velocity of a free particle in circular orbit). Because no uniformly rotating star can have $\Omega>\Omega_k$, the Keplerian frequency gives a definite upper limit on rotation (however see section 1.5). Table II (from Friedman et al., 1984) shows the effect of rotation on the upper mass limits for four equation of state with different stiffness.

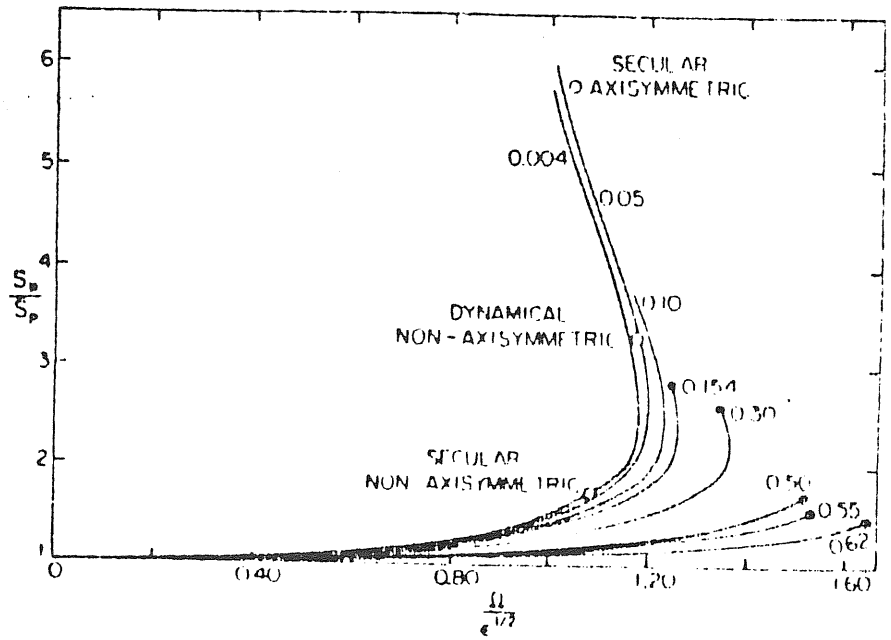

Fig. 7 - The ratio of proper equatorial radius to proper polar radius versus the angular velocity. Open circle indicate the location of instabilities of the MacLaurin spheroids. Full circle indicate the termination points. Curves are labeled by the corresponding value of γ. From Butterworth, 1979.

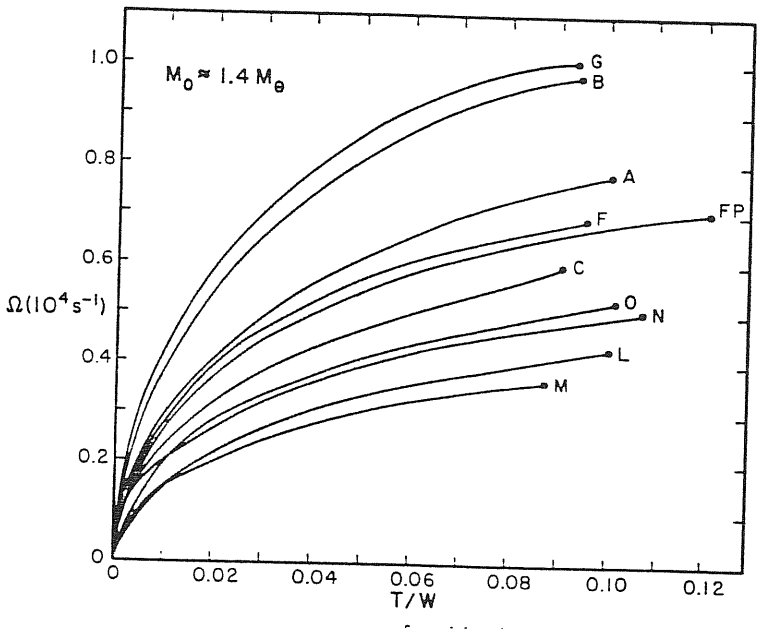

Fig. 8 - Angular velocity versus stability parameter τ for sequences of models with baryon mass $M_0 \sim 1.4 M_\odot$. The curves are labeled by letters denoting equations of state. The order from softest to stiffest is G, B, A, E, F, D, FP, C, O, N, L, M. From Friedman et. al., 1986.

TABLE II

Maximum mass models

Eq. of state	$M_{max}/M_{\odot}$	increase %	$M_{\odot}/M_{\odot}$	ρ_c (10^{15} g cm^{-3})	Ω (10^4 s^{-1})	T/W
L	3.53	30	3.68	0.84	0.69	0.108
C	2.16	17	2.47	2.7	1.11	0.108
F	1.72	17	1.96	3.9	1.23	0.091
G	1.55	14	1.73	5.5	1.53	0.101

Uniform rotation increases the maximum gravitational mass of a model by an amount ranging from ~14% for the softest to ~30% for the stiffest models (see Friedman et al. (1986) for the identification of the L,C,F and G equations of state which are in the order of decreasing stiffness). The table also provides the upper limit rotation rate . The softest equation of state permit the largest rotation rate.

The mass limit increases if the equation of state is only constraint by the energy condition $e \geq 0$, microstability condition $dp/de \geq o$ and causality condition $dp/de \leq 1$ (Friedman and Ipser, 1986). The maximum mass given for a uniformly rotating neutron star is then ~8.4 $M_{\odot}$. The motivation for the causality constraint is not completely obvious and if it is discarded then the upper mass limit increases to ~14 $M_{\odot}$.

Differentially rotating polytropes have been calculated by Komatsu et al. (1986). They used the generalization of Hachisu's method to calculated Newtonian equilibrium configurations (see Chap. III). The result which they obtained is that the mass increase due to rotation is much less for a differentially rotating configuration case than for a uniform rotating configuration, the increase being less than 1% in the differentially rotating case. This can be seen in Fig. 9 where the ratio of rest mass to non-rotating mass (M_s) is plotted against the axes ratio $1-r_p/r_e$.

1.5 Gravitational radiation instability.

The discovery of the millisecond pulsar PSR 1937+214 (Backer et al., 1982) has renewed interest in the study of the stability properties of rapidly rotating stars. The combination of the high density and high rotation rate of the millisecond pulsar makes it a likely candidate for an object where the gravitational radiation reaction-driven instability have played a physically important role in its formation and evolution.

Already in 1978, Papaloizou and Pringle predicted the possible existence of a class of rapidly rotating neutron stars, arising when old neutron stars (with weak magnetic fields) are spun up by accretion.

Since Chandrasekhar's (1970) discovery of gravitational radiation reaction secular instability, the understanding of such instability has greatly improved because the advances in Lagrangian variational techniques (Hunter 1977, Bardeen et al. 1977, Friedman and Schutz 1978a, 1978b). Using such techniques Friedman and Schutz (1978b) have shown that gravitational radiation makes all differential rotating, self-gravitating compressible perfect fluids unstable to non-axisymmetric perturbations. The eigenfunctions of the unstable modes have an $\exp(im\varphi)$ azimuthal dependence. Slowly rotating fluids are unstable only to modes with extremely long growth times and short wavelengths (large m). This instability time scales are function of the density of the fluid ρ and wave number m of the mode. They increase as ρ decreases and as m increases accordingly to the formulae (Comins, 1979b)

$$(1.5.1) \qquad t = \frac{(m-1)[(2m+1)!!]^2}{(m+1)(m+2)(1-e^2)^{1/2}} \left(\frac{e}{R\omega}\right)^{2m+1} \frac{\omega+(m-1)}{2\pi\rho G}\,\Omega$$

where R is the radius, e the eccentricity of the model and ω the frequency of the instability. As one spins up a perfect fluid model, it becomes unstable to modes with successively shorter growth times (and smaller value of m). For solar density, the t for all modes are much greater that all other relevant evolutionary time scales. Only for rapidly rotating white dwarfs

and neutron stars are the t small enough to make the instability physically important. For white dwarfs, only the m=2 modes grows quickly enough to be significant and only differentially rotating dwarfs can spin fast enough to be unstable to it.

Work by Detweiler and Lindblom (1977), Lindblom and Detweiler (1977) on the l=m=2 mode of the MacLaurin spheroids, by Comins (1979)and Baumgart and Friedman (1986) on all the l=m modes and by Lindblom and Hiscock (1983) on the general class of imperfect relativistic stars show that when dissipation due to viscosity is comparable to the loss of energy due to gravitational radiation, viscosity will damp out a gravitational-wave-driven instability. In the case of neutron stars, the instability can be expected to play a role only for old stars spun up by accretion or newly formed stars. In either case, because the star is hot, viscosity will be relatively small; viscous dissipation should stabilize modes with $m \geq 5$ for which the viscous damping time scale is shorter than the growth time of the instability in a corresponding perfect fluid model. Therefore the m=3 and 4 modes can be expected to set the limit on neutron stars rotation (Friedman, 1983, Wagoner, 1984).

Work on white dwarfs for calculating the instability points by Ostriker and co-workers (Tassoul and Ostriker, 1968, 1970, Ostriker and Bodenheimer, 1973, Ostriker and Mark, 1968, Ostriker and Tassoul, 1969) showed that the value $\tau=0.14$ at which the l=m=2 mode of MacLaurin becomes unstable was surprisingly insensitive to the compressibility and rotation law of the star. Although the tensor virial method they used, it turned out to provide neither a necessary (Hunter, 1977, Friedman and Schutz, 1975) nor sufficient (Friedman and Schutz, 1977b, Friedman, 1978) condition for stability, when Durisen and Inamura (1981) recomputed the instability points using a genuinely sufficient condition, they again found only small (<7%) departures from the MacLaurin values of τ. Inamura, Durisen and Friedman, (1985), and Managan (1985) have independently determined the gravitational-radiation instability points for polytropes in terms of the parameter τ. The adiabatic index governing the perturbations was assumed identical to the equilibrium value of $d(\log p)/d(\log \varepsilon)=1+1/n$ where n is the

polytropic index. As can be seen from table III the

TABLE III

Instability points of uniformly rotating polytropes

	n=0	n=0.5	n=1	n=1.5
τ_3	0.099	0.096	0.080	0.059
τ_4	0.077	0.074	0.058	0.049

critical values τ_3 and τ_4 of τ at which the m=3 and m=4 become unstable were found to increase with increasing stiffness, taking their maximum value for the incompressible (n=0) MacLaurin model.

In the calculations by Friedman, Ipser and Parker (1984, 1986) there is a second upper limit on rotation set by gravitational radiation instability. Using the results of Inamura et al. (1985) and Managan (1985) together with a numerical determination of the relation between τ and the angular velocity Ω, they found that all the sequences for different equations of state terminate before the ratio $T/|W|$ reached 0.14, therefore instability to a bar mode appears unlikely. Then the modes with the m=3 and m=4 are expected to set the upper limit on rotation for accreting neutron stars. Moreover, using two independent results of Lindblom (1985) and Managan (1985) they estimated the growth time of m=3 and m=4 modes finding that the growth times range from months to years.

These estimations, however, should be compared with the viscous damping time τ_ν. Because of the uncertainty in the viscosity ν, one cannot definitely decide when the gravitational radiation instability will be important. However, since in superfluid interior the viscosity is expected to go with the temperature as $\nu \propto T^{-2}$ for hot configurations the effect is small. Therefore, one can say that newly formed neutron stars which should be relatively hot ($T \sim 10^2$K) have their rotation limited by gravitational wave instability because in this case the viscous damping time is relatively long. Whereas, old accreting neutron stars with an expected temperature of $T \sim 10^7$ can have τ_ν of the order of months or years and the question remains still open.

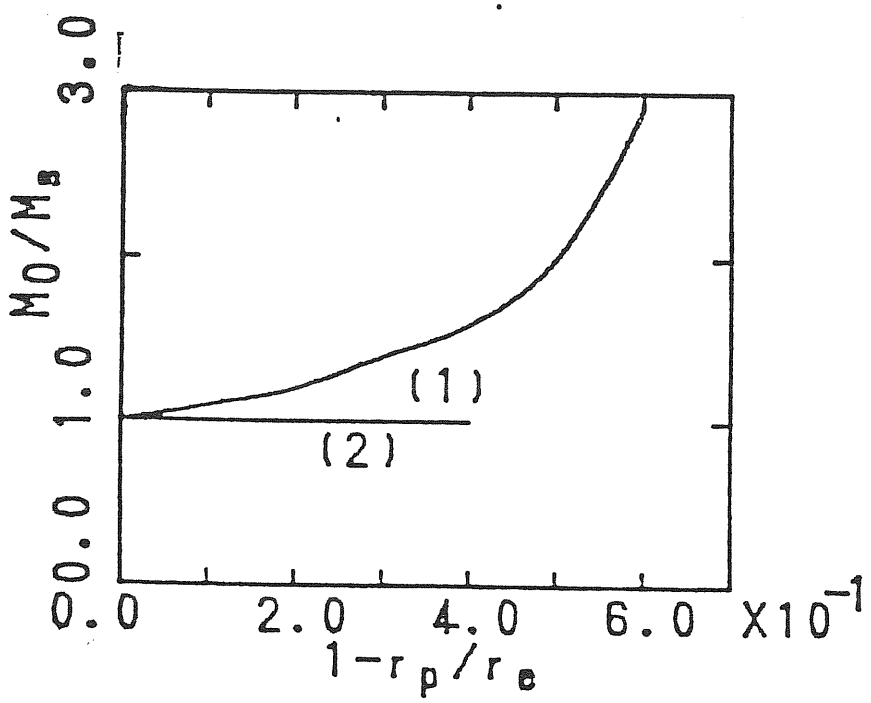

Fig. 9 - The ratio of the rest mass to the mass of corresponding non-rotating mass versus the axis ratio for a relativistic (1) and nearly Newtonian (2) sequences. From Komatsu et al. 1986.

1.6 Equilibrium configurations of self-gravitating tori with or without central body.

Spheroidal or ellipsoidal configurations are not the only axisymmetric equilibrium configurations that have been studied so far. Toroidal configurations have been considered partly because they are the next stage , in order of complexity, and partly for understanding astrophysical systems which surely have ring-shaped configurations like Saturn. Two groups of systems have been taken into account: rings with and without central bodies. Basic work on the subject includes contributions of Laplace (1789), Maxwell (1885), Poincare' (1891), Dyson (1893) and Randers (1942). These discussions of the equilibrium of rings have been restricted to those configurations which were slender (i.e. minor axis d $\ll$ major axis R), uniformly rotating and homogeneous. A remarkable step in the study of self-gravitating rings has been made by Ostriker (1964b) who considered slender uniformly rotating rings modelled by a polytropic equation of state. Using a perturbation technique, he was able to find a quite general solution of the Laplace equation which applies to any axisymmetric slender system. This method is quite similar to the Chandrashekar and Milne's method. Here the undistorted body is an infinite cylindrical polytrope whose structure was found in an early paper (Ostriker, 1964a). Treating the rotation, the curvature of the cylinder and the presence of a central body as perturbations then the equilibrium structure of the rings can be constructed. The main results can be summarized in the following statements. The equidensity surfaces of the ring are more distorted towards the center as the polytropic index increases (this seems obvious since as n increases the fluid becomes more compressible). The second result is that a central body forces the ring to rotate more rapidly. This is not surprising since if we put a body in the center of the ring the gravitational attraction will increase and only centrifugal forces which have opposite sign can compensate for it.

Toroidal figures of equilibrium without a central body have been reexamined after Dyson (1893) by Wong (1974). He was

motivated by the conjecture of Chandrashekar and Bardeen mentioned above that toroidal sequences of equilibrium could branch off from the MacLaurin sequence. Although these configurations have the stablest minimum-energy shape (Marcus et al., 1977) they do not departure from the MacLaurin spheroids directly (Wong, 1974), but through an intermediate sequence of very flattened objects called *MacLaurin hamburgers* by Eriguchi and Hachisu in a series of papers (Eriguchi and Hachisu, 1983, Eriguchi and Sugimoto, 1981, Hachisu and Eriguchi, 1983, Hachisu and Eriguchi, 1984 and Eriguchi and Hachisu , 1985) where they investigated bifurcation points of the MacLaurin sequence finding that many sequences with different shapes bifurcate from the spheroids.

Detailed numerical solutions of Einstein's equations for the structure of uniformly rotating infinitesimally thin disks have been considered by Bardeen and Wagoner (1969, 1971). In this approximation the Einstein equations outside the disk are those for vacuum and the matter source terms enter only as a discontinuity in the boundary conditions. With this simplification the general relativistic effects on the structure of the disk due to rotation were studied. Although these configurations are too unstable against fragmentation to be considered seriously as realistic astrophysical configurations, this work represent the starting point for the study of relativistic figures of equilibrium, since detailed techniques have been carried out for solving the stationary and axisymmetric Einstein equations. The relativistic generalization of the gravitational potential is expanded in powers of the relativistic parameter $\gamma=1-e^{\nu}$. The equilibrium configurations are characterized by the rest mass M_o and the total angular momentum J.

Figure 10 shows how the ratio J/M_o^2 decreases monotonically as γ increases. For a given angular momentum there is an upper limit to the rest mass or alternatively for fixed M_o, there exist a minimum angular momentum for which equilibrium is possible. Moreover, the fractional binding energy E_b/M_o is plotted against γ. The lack of a maximum suggests that uniformly rotating disks are stable against overall gravitational collapse.

Figure 11 shows how the angular velocity Ω increases to a

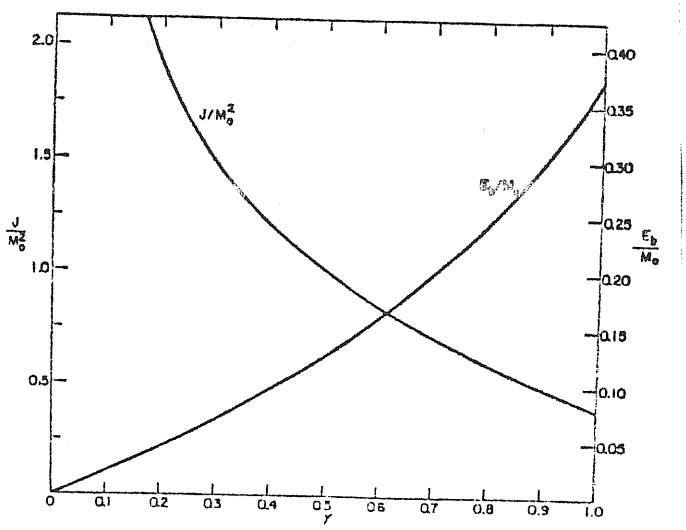

Fig. 10 - Angular momentum J and binding energy E_b as functions of γ. From Bardeen and Wagoner, 1971.

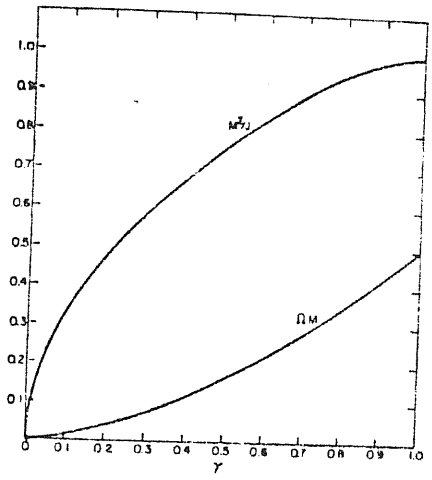

Fig. 11 - Angular velocity and the ratio M^2/J versus γ. From Bardeen and Wagoner, 1971.

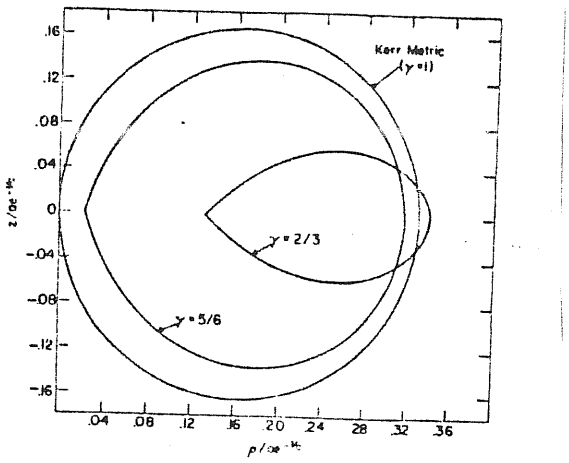

Fig. 12 - Curves of $g_{oo}=o$ for the indicated values of γ and for the Kerr metric in the plane described by the cylindrical coordinates (ρ,z). From Bardeen and Wagoner, 1971.

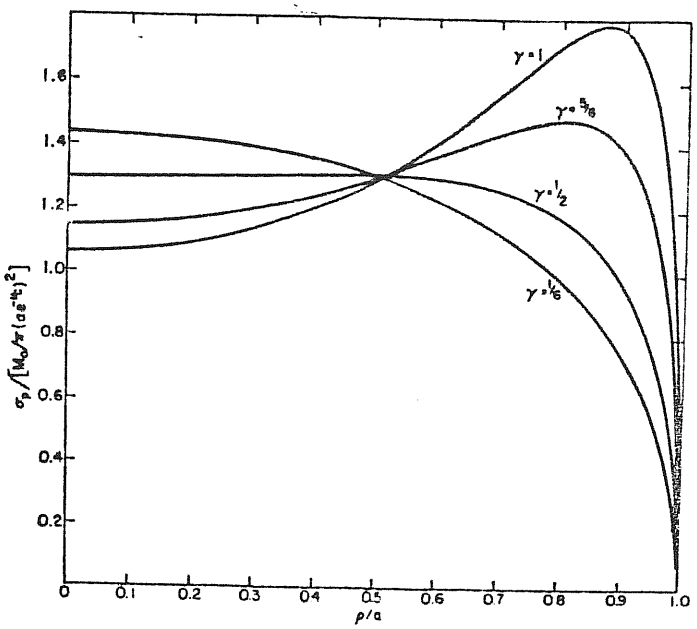

Fig. 13 - Surface density versus the fractional coordinate radius ρ/a (a is the coordinate radius of the rim of the disk). From Bardeen and Wagoner, 1971.

limiting finite value as $\gamma \longrightarrow \infty$. The same figure shows that the ratio $M^2/J \longrightarrow 1$ as $\gamma \longrightarrow 1$. Figure 12 shows the development of ergoregions. Such regions first appears at $\gamma \sim 0.6$. Figure 13 shows the surface density against the dimensionless radial coordinate. It can be seen that for $\gamma \geq 1/2$ the maximum is not longer at the center of the disk and surface density distribution becomes somewhat ring-like.

The authors generalized the Newtonian stability criterion against fragmentation to general relativity. The result is that the relativistic disks are more unstable than the Newtonian ones. The reason perhaps is that the former are more concentrated towards the rim of the disk. Since these configurations are unstable, it is important to consider differentially rotating disks. No computations have been done so far for such configurations.

Will (1974, 1976) considered the equilibrium configuration of a weakly self-gravitating ring of matter around a slowly rotating black hole. Considering the rotation of the black hole and the self-gravity of the ring as perturbations, he constructed sequences of equilibrium in terms of the quantity γ already used by Bardeen and Wagoner, and $\beta = h\omega_H$ where h is a parameter which characterize the size of the horizon and ω_H is the angular velocity of the black hole. To first order to the mass m of the ring and second order to ω_H, he obtained sequences of equilibrium configurations characterized by four parameters: the irreducible mass $M_{ir} = (A_H/16\pi)^{1/2}$ of the black hole, the mean proper circumference radius R, m and ω_H. In Fig. 14 the mass curve resulting from this model is plotted. The figure suggest that the *Penrose process* (by which energy can be extracted from a rotating black hole) may be different for a black hole-ring system than for Kerr black holes. This suggestion derives from the fact that the total mass for the black hole-ring configuration has a minimum for non-zero values of ω_H. for this reason the black hole still possesses an ergosphere in which particles can have negative energy as seen from infinity, and such energy can in principle be extracted. This situation is in contrast with the Kerr case, where the minimum energy configuration occurs precisely when the

ergosphere vanishes. Thus a Penrose process can in principle extract further energy from the system and this energy comes not only from the rotational energy of the hole but even from that of the ring.

In the case of vorticity free (constant angular momentum) self-gravitating ring around a black hole, Abramowicz (1982) has shown that the number of unknown metric functions reduce only to three.

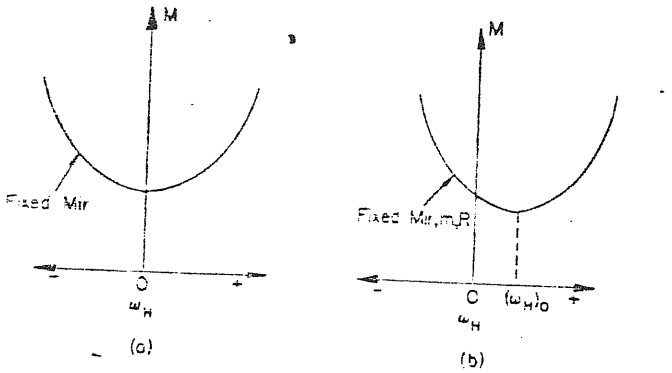

Fig. 14 - Mass curve for rotating black holes. (a) For a Kerr black hole. (b) For a slowly rotating black hole with a stationary axisymmetric ring of matter around it.

CHAPTER II

SELF-GRAVITATING TORI AROUND A RAPIDLY ROTATING BLACK HOLE: THE EQUATIONS.

This chapter is devoted to derive the set of equations which describe the equilibrium structure of tori around a black hole.

The theory of stationary and axisymmetric space-time is reviewed and the Einstein equations with the relative boundary conditions are derived. Not all the theorems involved are proved but only those which we believe are more relevant for our purpose. In particular many theorems about the Black holes equilibrium states are not included. The reader is referred to the book *Black Holes* and to the paper by Carter in *General Relativity - An Einstein Centenary Survey* for a complete treatment of that theory.

Prescriptions are given on how the matter configuration has to be specified consistently with the theory of equipotential surfaces in general relativity.

2.1 Stationary and axisymmetric space-times.

A space-time is said to be *stationary* if there exists a one parameter group of isometries whose orbits are timelike curves. These groups of isometries express the time translation symmetry of the space-time (i.e. the timelike coordinate t is cyclic, in the sense that we regain the same event if we change sign of it). Therefore a stationary space-time possesses a timelike Killing vector $\underline{\eta}$. Similarly, we call a space-time *axisymmetric* if there exists a one parameter group of isometries whose orbits are closed spacelike curves (i.e. there exist a spacelike coordinate ϕ which is cyclic). This implies that an axisymmetric space-time possesses a spacelike Killing vector $\underline{\xi}$. A space-time is *stationary and axisymmetric* if it possesses both these symmetries and, in addition, if the two killing vectors $\underline{\eta}$ and $\underline{\xi}$ commute

$$[\underline{\eta}, \underline{\xi}] = 0 \tag{2.1.1}$$

that is under simultaneous change of sign of ϕ and t we regain the

same event. In general the commutator of two Killing vectors is itself a Killing vector. We are considering asymptotically flat space-times in which property (2.1.1) holds. Since $\underline{\eta}$ and $\underline{\xi}$ commute, we can choose coordinates $(x^0 \equiv t, x^1 \equiv \phi, x^2, x^3)$ so that $\underline{\eta} \equiv \partial/\partial t$ and $\underline{\xi} \equiv \partial/\partial \phi$ are linearly independent and form a coordinate basis vector field. Moreover the space-time we are considering is associated with a body rotating around the $\underline{\xi}$ direction. Therefore the four-velocity of a fluid element u^α has the form

$$(2.1.2) \qquad \underline{u} = u^0 \underline{\eta} + u^1 \underline{\xi}$$

with

$$(2.1.3) \qquad u^0 \neq 0 \qquad u^1 = \Omega\, u^0 \neq 0 \qquad u^2 = u^3 = 0$$

where $\Omega = \Omega(x^1, x^2)$ is the angular velocity measured in coordinate time $\Omega \equiv u^1/u^0 = d\phi/dt$.

Because of the isometries, the components of the metric $g_{\alpha\beta}$ will be independent on t and ϕ, and so the line element takes the form

$$(2.1.4) \qquad ds^2 = \sum_{\alpha\beta} g_{\alpha\beta}(x^2, x^3)\, dx^\alpha dx^\beta$$

Now, let us consider a surface, Σ, spanned in each point by the vectors $\underline{\eta}$ and $\underline{\xi}$. This is the surface of orthogonal transitivity of the group of motions generated by the Killing vectors $\underline{\eta}$ and $\underline{\xi}$. On this surface we can define coordinates ρ and z such that the vector fields $\underline{\zeta} \equiv \partial/\partial \rho$ and $\underline{\chi} \equiv \partial/\partial z$ are orthogonal to both the vector fields $\underline{\eta}$ and $\underline{\xi}$, therefore,

$$(2.1.5) \qquad \begin{aligned} g_{\alpha\beta}\xi^\alpha \chi^\beta = 0 \qquad & g_{\alpha\beta}\xi^\alpha \zeta^\beta = 0 \\ g_{\alpha\beta}\eta^\alpha \chi^\beta = 0 \qquad & g_{\alpha\beta}\eta^\alpha \zeta^\beta = 0 \end{aligned}$$

from which we derive that

$$(2.1.6) \qquad g_{02} = g_{03} = g_{12} = g_{13} = 0$$

and the line element on the surface Σ is

$$(2.1.7) \qquad ds^2_\Sigma = g_{00} dt^2 + 2 g_{01} dt\, d\phi + g_{11} d\phi^2$$

Then, since this surface is orthogonal to the two-dimensional surface described by $\underline{\xi}$ and $\underline{\chi}$, the metric of the whole space-time can be written as

$$(2.1.8)\quad ds^2 = g_{00}dt^2 + 2g_{01}dt\,d\phi + g_{11}d\phi^2 + g_{ij}dx^i dx^j \qquad i,j=2,3$$

Any transformation of the form

$$(2.1.9)\quad x^i \longrightarrow x'^i = x'^i(x^2, x^3)$$

leaves (2.1.7) invariant. Therefore one has two degrees of freedom to express g_{ij}

The metric components g_{00}, g_{01} and g_{11} are invariant under any transformation of x^2 and x^3. This suggests that they must be geometric invariants associated with the symmetries of the space-time. Their invariance is elegantly expressed in terms of scalar products constructed out of the coordinate basis vectors $\underline{\eta}$ and $\underline{\xi}$ as follows

$$(2.1.10)\quad g_{00} = \eta^\alpha \eta_\alpha \qquad g_{01} = \eta^\alpha \xi_\alpha \qquad g_{11} = \xi^\alpha \xi_\alpha$$

Let us introduce now the quantities ν, ω and ψ by the following invariant definitions

$$(2.1.11)\quad e^{2\psi} = \xi^\alpha \xi_\alpha$$

$$(2.1.12)\quad \omega = -(\eta_\alpha \xi^\alpha)/(\xi^\beta \xi_\beta)$$

$$(2.1.13)\quad e^{2\nu} = -\eta^\alpha \eta_\alpha + (\eta^\alpha \xi_\alpha)^2/(\xi^\beta \xi_\beta)$$

Using these definitions the line element (2.1.8) takes the form

$$(2.1.14)\quad ds_\Sigma^2 = -e^{2\nu}dt^2 + e^{2\psi}(d\phi - \omega\,dt)^2 + g_{ij}dx^i dx^j$$

One degree of freedom can be used to reduce g_{ij} in diagonal form (see e.g. Chandrashekar, 1983)

$$(2.1.15)\quad ds^2 = -e^{2\nu}dt^2 + e^{2\psi}(d\phi - \omega\,dt)^2 + e^{2\mu_2}(dx^2)^2 + e^{2\mu_3}(dx^3)^2$$

and the other one can be used to relate μ_2 and μ_3. It is important to note that in the non-stationary case we do not have this freedom. Thus, if we should consider time dependent departures

from equilibrium of axisymmetric systems, we must allow that in consequence of the perturbations, the Eulerian changes in μ_2 and μ_3 will differ.

Because the behavior of the metric functions at spatially infinity it is much more transparent in spherical-polar coordinates, we will specialize the coordinates x^2 and x^3 accordingly

$$(2.1.16) \qquad x^2 = r \qquad\qquad x^3 = \vartheta$$

Making use of the freedom of gauge still left, we can define new functions

$$(2.1.17) \qquad e^{2\psi} = r^2 \sin^2\vartheta\, B^2 e^{-2\nu} \qquad e^{2\mu_2} = e^{2(\gamma-\nu)} \qquad e^{2\mu_3} = r^2 e^{2(\gamma-\nu)}$$

and the line element takes the form

$$(2.1.18) \quad ds^2 = -e^{2\nu}dt^2 + r^2\sin^2\vartheta B^2 e^{-2\nu}(d\phi - \omega\, dt)^2 + e^{2(\gamma-\nu)} \cdot (dr^2 + r^2 d\vartheta^2)$$

reducing the number of independent unknown metric functions only to four. This is the form used by Bardeen (1970) and Butterworth and Ipser (1976). We will use such a form as well.

There is a unique way to single out the physical interpretation of the components of the metric tensor which remains valid for rapid rotation and strong gravitational fields. In such cases an analysis based on static observers at rest as seen from infinity, is not appropriate because such observers may not even exist in certain regions of the space-time. Indeed

$$g_{oo} = -e^{2\nu} + r^2\sin^2\vartheta B^2 e^{-2\nu}\,\omega$$

can have either negative and positive sign. In the region where $g_{oo}>0$, the line (ϕ, r, ϑ)=const is not a timelike direction. In other words, no local observer with angular velocity $\Omega=0$ and $u^2=u^3=0$, that is an observer who would be stationary as seen from infinity can exist in such a region.

2.2 Locally non rotating frames and Einstein equations.

For any stationary axisymmetric, asymptotically space-time it is useful to introduce a set of local inertial frames in which the description of the physics is much simpler. The construction of such frames consists on replacing coordinate frames by orthonormal tetrads which are carried by locally non rotating observers.

An orthonormal tetrad is a set of four perpendicular unit vectors at a point in space-time, one timelike and three spacelike, which give the directions of the four axes of a locally Minkowskian coordinate system. The tetrad vectors can be used to express tensors in an arbitrary coordinate system in terms of physical quantities measured in this local reference frame. Associated with the metric (2.1.18) there is a uniquely sensible choice of observers and tetrads: the locally non rotating frames (LNRF) introduced by Bardeen (1970), for which the observers world lines are r=const, ϑ=const and $\phi = \omega t + \text{const}$. The orthonormal tetrad frame carried by such an observer is given by the following basis vectors (indices in parentheses will be used to denote components in the local orthonormal frame)

$$
\begin{aligned}
\underline{e}_{(0)} &= e^{\nu}\underline{dt} \\
\underline{e}_{(1)} &= -\omega\, r\sin\vartheta\, B e^{-\nu}\underline{dt} + r\sin\vartheta\, B e^{-\nu}\underline{d\phi} \\
\underline{e}_{(2)} &= e^{\gamma-\nu}\underline{dr} \\
\underline{e}_{(3)} &= r\, e^{\gamma-\nu}\underline{d\vartheta}
\end{aligned}
\qquad (2.2.1)
$$

The corresponding controvariant vectors are

$$
\begin{aligned}
\underline{e}_{(0)} &= e^{-\nu}(\partial/\partial t + \omega\, \partial/\partial\phi) \\
\underline{e}_{(1)} &= (r\sin\vartheta\, B e^{-\nu})^{-1}\partial/\partial\phi \\
\underline{e}_{(2)} &= e^{-\gamma+\nu}\partial/\partial r \\
\underline{e}_{(3)} &= r^{-1}e^{-\gamma+\nu}\partial/\partial\vartheta
\end{aligned}
\qquad (2.2.2)
$$

It is easy to verify that

$$(2.2.3) \qquad e^{i}_{(a)} e_{(b)i} = \eta_{(a)(b)} = \begin{vmatrix} -1 & 0 & 0 & 0 \\ 0 & 1 & 0 & 0 \\ 0 & 0 & 1 & 0 \\ 0 & 0 & 0 & 1 \end{vmatrix}$$

that is the chosen frame is Minkowskian, therefore represents locally an inertial frame. The rule for calculating the physical components of a tensor $T_{\alpha\beta}$ is

$$(2.2.4) \qquad T_{(a)(b)} = T_{\alpha\beta}\, e^{\alpha}_{(a)} e^{\beta}_{(b)}$$

and conversely

$$(2.2.5) \qquad T_{\alpha\beta} = T_{(a)(b)} e^{(a)}_{\alpha} e^{(b)}_{\beta}$$

Indices are raised and lowered by using the Minkowskian metric

$$(2.2.6) \qquad T_{(a)}{}^{(b)} = T_{(a)(c)} \eta^{(c)(b)}$$

At any instant in time, the local frame of any physical observer differs from the LNRF at the observer's location by a Lorentz transformation. We need only to know the velocity of an observer relative to the LNRF, and the transformation formulae of special relativity, to obtain any physical quantity in an arbitrary frame.

In this orthonormal frame the physical meaning of the metric functions is more transparent. Since ν, ω and ψ of (2.1.15) have invariant meaning, there exist a way to determine them by measurements. This can be done in the following way (Bardeen, 1970).

Consider an observer whose coordinate four-velocity is given by

$$(2.2.7) \qquad u^{0} = \frac{dt}{ds} = \frac{e^{-\nu}}{(1-v^{2})^{1/2}} \qquad u^{1} = \frac{d\phi}{ds} = \Omega u^{0} \qquad u^{i} = \frac{dx^{i}}{ds} = 0 \quad i=2,3$$

where $v=(\Omega-\omega)r\sin\theta B e^{-2\nu}$. In the local inertial frame, the same observer will have the four-velocity

$$(2.2.8)\qquad u^{(a)} = e^{(a)}_{\ i} u^{i} = \eta^{(a)(b)} e_{(b)i} u^{i}$$

or explicitly

$$(2.2.9)\qquad u^{(0)} = -\frac{1}{(1-v^2)^{1/2}} \qquad u^{(1)} = \frac{r\sin\vartheta B e^{-\nu}(\Omega-\omega)}{(1-v^2)^{1/2}} \qquad u^{(2)} = u^{(3)} = 0$$

The three-velocity relative to the LNRF has components

$$(2.2.10)\qquad v^{(a)} = \frac{u^{i} e_{i}^{\ (a)}}{u^{i} e_{i}^{\ (0)}} \qquad\qquad a = 1,2,3$$

In the case considered, the only component different then zero is

$$(2.2.11)\qquad v^{(1)} = v = r\sin\vartheta\, B\, e^{-2\nu}(\Omega - \omega)$$

and this is the velocity in the local inertial frame. Accordingly, a point which is considered at rest in the local inertial frame (i.e. $u^{(1)}=u^{(2)}=u^{(3)}=0$) will have an angular velocity ω as seen from infinity. Therefore the metric function $\omega(r,\vartheta)$ is referred to as the angular velocity measured at infinity of the locally non rotating observer and it is the angular velocity of any particle with zero angular momentum that is why these observers are called ZAMO (zero angular momentum observers). The non vanishing of ω is said to describe a *dragging* of the inertial frame.

The metric function ν can be considered as the general relativistic generalization of the Newtonian gravitational potential. In fact the ratio of the observed frequency at infinity to the emitted frequency in the locally non rotating frame is equal to e^{ν} for photons with zero angular momentum. Therefore $(e^{-\nu}-1)$ is identified as the gravitational red-shift. Moreover $r\sin\vartheta B e^{-\nu}$ is the proper circumferential radius of a circle around the axis of symmetry.

The physical simplicity of the locally non rotating frame is reflected into a mathematical simplicity of the Riemann and Ricci tensor components measured by the locally non rotating observer when expressed in terms of the metric functions (2.1.18). The Riemann tensor components projected onto this tetrad are given in Appendix A.

In the present study, we shall limit ourselves to the case in which the source of the gravitational field is a perfect fluid described by the energy momentum tensor

$$(2.2.12) \qquad T^{\alpha\beta} = (e + p)u^{\alpha}u^{\beta} + p\, g^{\alpha\beta}$$

where e and p denote the energy density and the pressure, respectively; these are considered to be functions of two independent thermodynamic variables through the equation of state

$$(2.2.13) \qquad p = p(e,s) \qquad \text{or} \qquad e = e(p,s)$$

where s is the specific entropy.

The Einstein field equations can be written

$$(2.2.14) \qquad G^{(\alpha)(b)} = R^{(\alpha)(b)} - \frac{1}{2}\, g^{(\alpha)(b)}R = 8\pi\, T^{(\alpha)(b)}$$

or, equivalently

$$(2.2.15) \qquad R^{(\alpha)(b)} = 8\pi \left[T^{(\alpha)(b)} - \frac{1}{2}\, g^{(\alpha)(b)}T \right]$$

where

$$(2.2.16) \qquad T = -(e - 3p)$$

is the trace of $T^{\alpha\beta}$. If the Ricci components are substituted in (2.2.15) then the $R_{(0)(0)}$ Einstein equations gives

$$(2.2.17) \qquad \nabla\cdot(B\,\nabla\nu) = \frac{1}{2}\, r^2 \sin^2\vartheta B^2 e^{-4\nu} \nabla\omega\cdot\nabla\omega + 4\pi\, e^{2y-2\nu}\left[(e+p)\frac{1+v^2}{1-v^2} + 2p\right]$$

where ∇ and $\nabla\cdot$ are the gradient and divergence operators in the Euclidean three-space. Equation (2.2.17) is the Raychaudhuri equation for the world lines of the ZAMO's. The acceleration four-vector a_α of a ZAMO has components

$$(2.2.18) \qquad a_t = a_\phi = 0 \qquad\qquad a_\alpha = \nu_{,\alpha} \qquad\qquad \alpha = r, \vartheta$$

The square of the shear of the world lines of the ZAMO's is

(2.2.19) $$\sigma^2 = \frac{1}{2}\,\sigma_{\alpha\beta}\sigma^{\alpha\beta} = \frac{1}{4}\,r^2\sin^2\vartheta B^2 e^{-4\nu}\nabla\omega\cdot\nabla\omega$$

therefore equation (2.2.17) can also be written

(2.2.20) $$a^{\alpha}{}_{;\alpha} = 2\,\sigma^2 + R_{(0)(0)}$$

In highly relativistic rapidly rotating stars the shear of the ZAMO world lines can predominate over the matter terms as source for the relativistic gravitational potential ν. This is important for numerical considerations.

The equation

(2.2.21) $$R_{(0)(1)} = 8\pi\, T_{(0)(1)}$$

gives

(2.2.22) $$\nabla\cdot(r^2\sin^2\vartheta B^3 e^{-4\nu}\nabla\omega) = -\,16\pi\, r\sin\vartheta B^2 e^{2\gamma-4\nu}\,\frac{e+p}{1-v^2}\,v$$

We will see later that the source for $\omega(r,\vartheta)$ is the angular momentum of the matter configuration since any axisymmetric field carries no angular momentum on its own.

The metric function B is obtained from the $R^{(0)}_{(0)} + R^{(1)}_{(1)}$ Einstein equation

(2.2.23) $$\nabla\cdot(r\sin\vartheta\nabla B) = 16\pi\, r\sin\vartheta B e^{2(\gamma-\nu)}p.$$

The remaining metric function y appears multiplying only matter source terms, and therefore it decouples from the other metric functions ν, ω and B in the vacuum. Once these components of the metric are known, y can be found by quadrature integrating the following linear equation

$$\gamma_{,\vartheta} = \left\{\sin^2\vartheta\left(1+r\,\frac{B_{,r}}{B}\right)^2+\left(\cos\vartheta+\sin\vartheta\,\frac{B_{,\vartheta}}{B}\right)^2\right\}^{-1}\cdot$$

$$\left[\left(\cos\vartheta+\sin\vartheta\,\frac{B_{,\vartheta}}{B}\right)\left\{\frac{9}{2}\,\frac{\sin\vartheta}{\cos\vartheta}\,\frac{B_{,\vartheta}}{B}-\left[r\left(\frac{X_{,r}}{X}\right)^2-\left(\frac{X_{,\vartheta}}{X}\right)^2\right]\right.\right.$$

$$\left.\left.-\,\frac{1}{2B}\left[r^2B_{,rr}-B_{,\vartheta\vartheta}+9\,\frac{\cos\vartheta}{\sin\vartheta}\,B_{,\vartheta}\right]\right\}+\frac{rB_{,r}}{B}\left[\cos\vartheta\left(\frac{1}{2}+r\,\frac{B_{,r}}{B}\right)\right.\right.$$

(2.2.24)

$$-\frac{1}{2}\frac{B_{,\vartheta}}{B}\Big] + r\sin\vartheta\Big[\frac{B_{,\vartheta r}}{B} + 2\frac{X_{,r}X_{,\vartheta}}{X^2}\Big]\Big(1+\frac{rB_{,r}}{B}\Big) + \sin^2\vartheta\cdot$$

$$\frac{B^2}{X^4}\Big\{\frac{1}{4}r^2(\cos\vartheta + \sin\vartheta\frac{B_{,\vartheta}}{B})\Big[r^2(\omega_{,r})^2 - (\omega_{,\vartheta})^2\Big] - \frac{1}{2}\sin\vartheta\cdot$$

$$r^3\Big(1+r\frac{B_{,r}}{B}\Big)\omega_{,\vartheta}\omega_{,r}\Big\}\Big]$$

which is the $R_{(2)(2)}-R_{(3)(3)}$ Einstein equation. In this equation we used $X=\ln\nu$ instead of ν. Equations (2.2.1), (2.2.22) and(2.2.23) are invariant under coordinate transformation as long as ∇ and $\nabla\cdot$ are reinterpreted accordingly, whereas equation (2.2.24) changes in a straightforward way.

Besides the Einstein equations for the four metric functions X, ω, B and y, we also have to impose the conservation condition

(2.2.25) $$T^{\alpha\beta}{}_{;\alpha} = 0 \ .$$

2.3. Equations governing the fluid configurations.

Since our space-time is axisymmetric and stationary equations (2.2.25) reduce to only one. This equation can be written explicitly (see Appendix B for a derivation of it) as

(2.3.1) $$a^i = \nabla^i(\ln u^t) - \frac{\ell\nabla^i\Omega}{1-\ell\Omega}$$

the four-acceleration is equal to

(2.3.2) $$a^i = \frac{\nabla^i p}{p+e}$$

and $\ell=(\xi^i u_i)/(\eta^k u_k)=u_\phi/u_t$ is the angular momentum per unit inertial mass. From the definitions of Ω and ℓ we can get the following relationships which will be useful later

(2.3.3) $$\ell = -\frac{g_{t\phi}+\Omega g_{\phi\phi}}{g_{tt}+\Omega g_{t\phi}} \qquad \Omega = -\frac{g_{t\phi}+\ell g_{tt}}{g_{\phi\phi}+\ell g_{t\phi}}$$

and for our metric these become

$$(2.3.4)\qquad \ell = \frac{r^2\sin^2\theta_B^2 e^{-2\nu}(\Omega-\omega)}{e^{2\nu}-\omega r^2\sin^2\theta_B^2 e^{-2\nu}(\Omega-\omega)} \quad \text{or} \quad \ell = \frac{r\sin\theta_B v}{e^{2\nu}+\omega r\sin\theta_B v}$$

and

$$(2.3.5)\qquad \Omega = \frac{v^2(1-\omega\ell)+\omega\ell}{\ell} \quad \text{or} \quad \Omega = \frac{\omega(1-\omega\ell)+\dfrac{\ell e^{2\nu}}{r^2\sin^2\theta_B^2}}{(1-\omega\ell)}$$

Following Thorne (1971) and Bardeen (1970) we next define some quantities of physical interest and some general characteristics of rotating equilibrium configurations. Some of these results are due to Abramowicz (1971a,b,c, 1974) and Steguin (1975).

The quantity e+p is the inertial mass per unit volume as measured in the rest frame of the fluid. It is this mass which determines how a fluid element responds to a force acting out it (see eq. (2.3.2)). The inertial mass per baryon is (e+p)/n, where n is the number baryon density. The quantities

$$(2.3.6)\qquad \phi = \frac{e+p}{n}(u^t)^{-1} = \frac{e+p}{n} e^{\nu}(1-v^2)^{1/2}$$

and

$$(2.3.7)\qquad j = \frac{e+p}{n} u_\alpha \xi^\alpha = \frac{e+p}{n} r\sin\theta_B e^{-\nu} v(1-v^2)^{-1/2}$$

are the energy required to inject a baryon into a star with zero angular momentum, and the angular momentum per baryon respectively. The energy required to inject a baryon into a ring with non-zero angular velocity Ω and bring it into equilibrium with its surrounding is (Thorne, 1971)

$$(2.3.8)\qquad \tilde{\varepsilon} = \phi + \Omega j = -\frac{e+p}{n}(u_\alpha \eta^\alpha)$$

The angular momentum per baryon j is conserved in any axisymmetric motions (but not necessarily stationary) inviscid, adiabatic motion (Bardeen, 1970, Abramowicz, 1971). This is a direct consequence of the equation of motion (2.2.25) and the equation for conservation of baryons

$$(2.3.9) \qquad (n\, u^{\alpha})_{;\alpha} = 0$$

However the quantity j is not conserved in non adiabatic motions (Steguin, 1975). The already introduced quantity ℓ can also be written

$$(2.3.10) \qquad \ell = \frac{j}{\mathcal{E}}$$

This quantity is a purely geometric object which does not depend on the thermodynamic properties of the fluid and it is conserved along the world line of the fluid element (Abramowicz, 1971). This property again can be derived from the equation of motion together with the conservation of baryon number.

Having defined such quantities the equation of motion can also be written as

$$(2.3.11) \qquad - T(u^{t})^{-1}\nabla s + \nabla\phi - j\nabla\Omega = 0$$

if we use the thermodynamic identity

$$(2.3.12) \qquad \frac{dp}{n} = d\left(\frac{e+p}{n}\right) - T\, ds$$

where T is the temperature of the fluid element defined by

$$(2.3.13) \qquad T = \left.\frac{\partial e}{\partial s}\right)_{n=const}$$

Also we rewrite here equation (2.3.1) as

$$(2.3.14) \qquad \frac{\nabla^{i} p}{e+p} = \nabla^{i}(\ln u^{t}) - \frac{\ell\nabla\Omega}{1-\Omega\ell}$$

From equations (2.3.11) and (2.3.14) we can derive a number of interesting theorems about the topology of rotating stars which apply to any configurations.

Hereafter we will assume that the fluid is governed by a barotropic equation of state for which the pressure is only function of the energy density

$$(2.3.15) \qquad p = p(e)$$

A straightforward consequence of this assumption is the possibility to write (2.3.2) as

$$(2.3.16) \qquad dW(p) = \frac{dp}{(e+p)}$$

where we put $dW=\alpha$. The surface of constant W are called level surfaces. In the Newtonian limit the level surfaces are those of constant potential (gravitational and centrifugal) therefore they are even called equipotential surfaces. From (2.3.16) we see that the surfaces of equal pressure coincide with the equipotential surfaces.

If the rotation is rigid a number of simplification permits to deduce some theorems. In this approximation equation (2.3.14) reduces to

$$(2.3.17) \qquad \frac{\nabla p}{e+p} = \nabla(\ln u^t)$$

Therefore the surface of constant pressure and constant redshift factor $1/u^t$ are parallel Boyer, (1965). Taking the curl (∇x) of both sides

$$(2.3.18) \qquad \frac{\nabla e \times \nabla p}{(e+p)^2} = 0$$

This results owed to Thorne (1971) can be interpreted saying: *In a rigidly rotating star the surface of constant pressure p and constant density e must coincide.*

From the equation of motion written as (2.3.11) we derive that: *In the case of rigid rotation the injection energy ϕ is constant inside the matter configuration if and only if $\nabla s=0$.* This result was first obtained by Boyer (1965, 1966).

We also see from equation (2.3.11) that: *The surface of constant angular velocity Ω and the surfaces of constant injection energy ϕ must coincide if the configuration is isentropic.*

For differentially rotating configurations Abramowicz generalize some of these theorems. Indeed taking the curl of equation (2.3.14) we obtain

$$(2.3.19) \qquad \frac{\nabla e \times \nabla p}{(e+p)^2} = \frac{\nabla \ell \times \nabla \Omega}{(1-\ell\Omega)^2}$$

From this equation we can state the following theorem: *The surfaces of constant specific angular momentum ℓ and the surfaces of constant angular velocity Ω, coincide if and only if the star is barotropic.*

Taking the curl of (2.3.11) we obtain

$$(2.3.20) \qquad \nabla T \times \left[\frac{\nabla s}{u^t} \right] + \nabla \left[\frac{1}{u^t} \right] \times (T \nabla s) = \nabla j \times \nabla \Omega$$

If the configuration is isentropic then

$$(2.3.21) \qquad \nabla j \times \nabla \Omega = 0$$

therefore: *The surface of constant angular momentum per baryon j and the surfaces of constant angular velocity Ω coincide each other if the star is isentropic.*

If the surfaces $\ell(r,\vartheta)=\text{const}$ and $\Omega(r,\vartheta)=\text{const}$ coincide, they then describe a surface whose equation can be written as

$$(2.3.22) \qquad F(\Omega, \ell) = 0$$

It can be shown (Abramowicz, 1974) that such surfaces have the topology of a cylinder and are called Von Zeipel's cylinders.

Such theorems do not tell us how to choose the rotation law of a relativistic configurations. Here the situation is the same as in the Newtonian theory. Constraint on the distribution of the specific angular momentum is provided by local stability analysis. Steguin (1975) has shown that *necessary conditions for stability for a rotating configuration in which the viscosity is negligible are that (i) the level surfaces of the pressure and the total energy density must coincide (ii) the gradient of the geometrical specific angular momentum ℓ must never point inward from a surface of constant ℓ:*

$$(2.3.23) \qquad \frac{d\ell}{dr} \geq 0$$

The generalization of the convection criterion for stability has been provided by Abramowicz (1971b) and Bardeen (1970) for the special case of isentropic perfect fluid configurations. A more general criterion was found by Steguin (1975). The result is

formally identically to that valid in Newtonian theory.

2.4. Relativistic tori around Black Holes.

Non-self-gravitating fluid disk configurations around a Schwarzschild and Kerr black holes have been studied by Fishbone and Moncrief (1976), Fishbone(1977), Abramowicz et al. (1978), Kozłowski et al. (1978) and Jaroszyński et al. (1980). Very recently Kuwahara et al. (1986) have extended the theory to a family of space-time with Tomimatsu-Sato metric. These are the fundamental papers about the structure of such disks in general relativity.

After the introduction by Paczyński and Wiita (1980) of a pseudo-Newtonian potential which mimics the circular orbits around a Schwarzschild black hole with an error of about 10%, a large number of papers have been written on accretion disks. This potential permits study of the physical properties of such configurations avoiding the complexity of using full general relativity. It is in this theory however, that new features appear in the theory of equipotential surfaces of a fluid around a black hole. Here we will give an account of this theory since we will specify our matter configuration accordingly. Following Abramowicz et al. (1978) we introduce the function

$$F(\ell) = \int_{\ell_{in}}^{\ell} \frac{\Omega \, d\ell}{1-\Omega\ell} \qquad (2.4.1)$$

which is called the Von Zeipel's formulae, where the subscript $_{in}$ refers to the inner edge of the disk. Using (2.4.1) the equation of motion of the fluid can be written as

$$W - W_{in} = \ln(u^t)_{in} - \ln(u^t) + F(\ell) \qquad (2.4.2)$$

Therefore, for a given gravitational field the equipotential surfaces can be found by specifying the function $\Omega=\Omega(\ell)$ or $\ell=\ell(\Omega)$.

Since the boundary of any perfect fluid barotropic stationary body has to be an equipotential surface (Boyer, 1965), from (2.4.2) we get

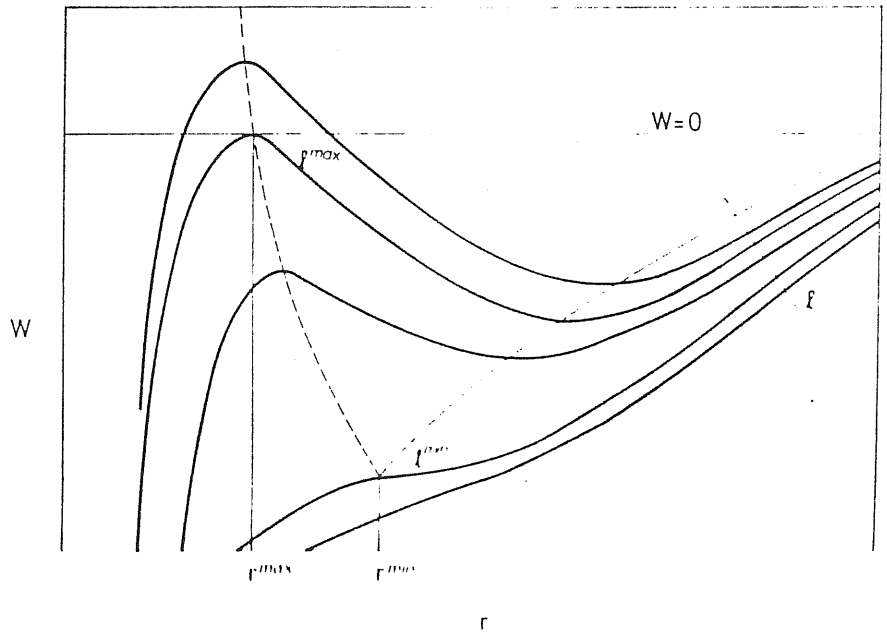

Fig. 15 - The potential W on the equatorial plane, for ℓ=const disks. The dashed line shows the loci of the minima (center) and maxima (cusp). From Kozłowski et al. 1978.

$$(2.4.3) \qquad \ln \frac{u^t_{out}}{u^t_{in}} = \int_{\ell_{in}}^{\ell_{out}} \frac{\Omega d\ell}{1-\Omega\ell}$$

For a known gravitational field this equation links r_{in} and r_{out}, the inner and outer edge of the disk. A particular simpler solution of this problem is given by the case in which the specific angular momentum is a constant ℓ_o. According to the condition of stability given by the equation (2.3.23) this corresponds to a marginally stable configuration. For such a case

$$(2.4.4) \qquad W(r,\vartheta) = \ln u^t$$

and from equation (2.4.3)

$$(2.4.5) \qquad u^t_{out} = u^t_{in}$$

The nature of such solutions can be understood by examining the behaviour of the potential W on the equatorial plane for a Kerr black hole. Figure 15 shows such a behaviour. For W<0 the equipotential surfaces are closed, for W>0 they are open. The minima and maxima correspond to places where the pressure gradient is zero (cfr. equation (2.3.16)). Figure 16 shows the topology of the equipotential surfaces around a Schwarzschild black hole. The topology of such surfaces around a Kerr black is the same. One of this surfaces has a cusp. In this point $\nabla W=0$ therefore $\nabla p=0$ and

$$(2.4.6) \qquad \ell_o = \ell_k(r) \qquad \text{at } \vartheta = \frac{\pi}{2}$$

since it is on the equatorial plane, where $\ell_k(r)$ is the angular momentum for Keplerian circular orbits. For a Kerr black hole the function ℓ_k can be calculated using (2.3.3) and the angular velocity in the equatorial plane for circular orbits

$$(2.4.7) \qquad \Omega = \Omega_k = \pm \frac{M^{1/2}}{(r^{3/2} \pm \alpha M^{1/2})}$$

where the upper sign is for direct orbits and the lower sign for retrograde orbits , α is the is the total angular momentum per unit mass M of the black hole. The behaviour of $\ell_k(r)$ is shown in Fig. 17. From this picture we can see that the cusp is located in

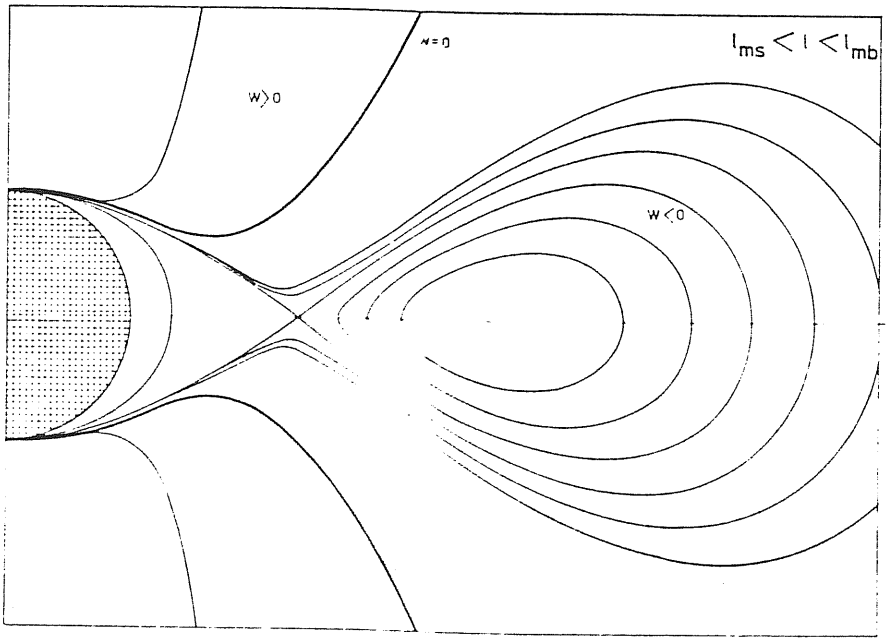

Fig. 16 - Equipotential surfaces for a disk orbiting the Schwarzschild black hole. From Abramowicz et al., 1978.

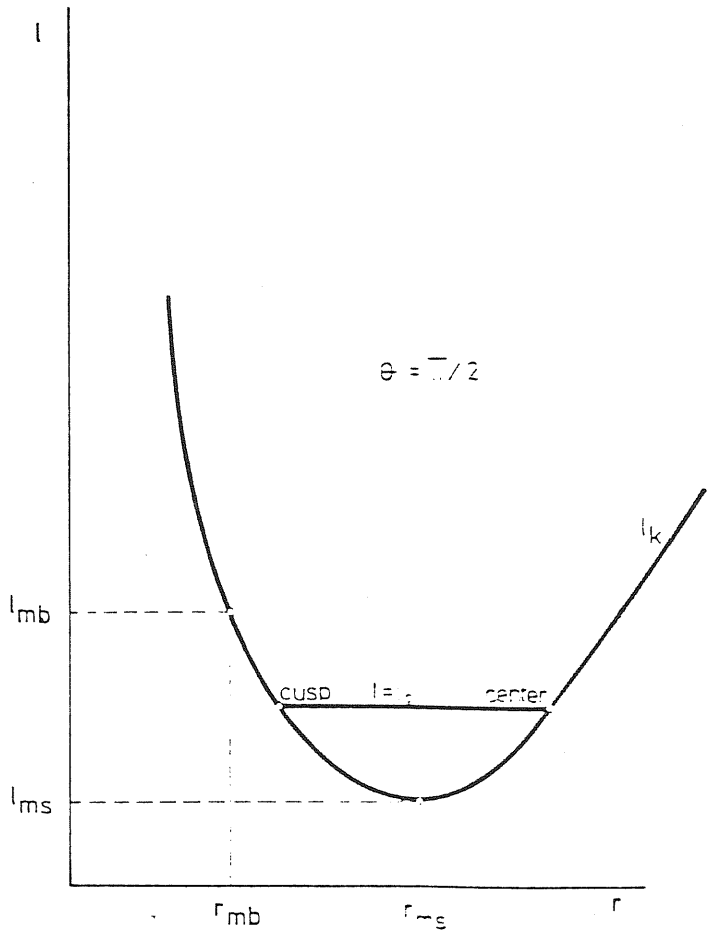

Fig. 17 - Location of disk's center and its cusp.

between the marginally bound orbit r_{mb} and the marginally stable orbit r_{ms}. The presence of the cusp is important for the accretion process. This point resembles the Lagrange L_1 point on the Roche lobe model in the close binary stars: due to the existence of the critical surface associated with it $W=W_{cusp}$ (for which W is maximum) a little deviation from hydrostatic equilibrium will drive matter to fall into the black hole without need of viscosity (Kozłowski et al., 1978).

Since in our case we are not interested in the accretion process, the radius of the inner edge of the torus is chosen to be slightly larger than the corresponding value of the cusp. The fluid is modelled by a polytropic equation of state

$$(2.4.8) \qquad p = k\,\rho^{\gamma} \quad \text{or} \quad p = (\gamma - 1)\rho\varepsilon \quad \text{and} \quad e = \rho(1+\varepsilon)$$

where $\gamma=4/3$ is the adiabatic index, ε is the specific internal energy and k is a constant which in general depends on the entropy. In this case the equation of hydrostatic equilibrium can be integrated giving (see Appendix C)

$$(2.4.9) \qquad p = \left[\frac{\gamma-1}{\gamma k^{1/\gamma}} \left(\frac{u^t_{in} - u^t}{u^t} \right) \right]^{\frac{\gamma}{\gamma-1}}$$

To get this equation we have imposed the condition that at the boundary p=0. Once the equation of state (2.4.8), the rotation law

$$(2.4.10) \qquad \ell = \text{const} \qquad\qquad \ell_{mb} \leq \ell \leq \ell_{ms}$$

and a value for the radius of the inner edge of the torus are specified, the value of the radius of the outer edge and its surface are determined by solving alternately the Einstein equations for the field and (2.4.9) for the matter consistently.

2.5 Boundary conditions.

Einstein's equations (2.2.17), (2.2.22)-(2.2.24) and (2.4.8)-(2.4.10) form a complete set. However, to solve them we need boundary conditions. The boundary condition p=0 for the hydrostatic equilibrium equation was already imposed. For the

Einstein equations we must impose boundary conditions on the event horizon of the black hole, at asymptotically flat infinity and on the axis of symmetry.

On the axis of symmetry ν, ω and B must be regular functions with zero gradients normal to the axis

$$\nu_{,\vartheta} = \omega_{,\vartheta} = B_{,\vartheta} = 0 \qquad \text{at } \vartheta = 0 \tag{2.5.1}$$

Integration of equation (2.2.24) then guarantees that the same is true for the function y. The constant of integration is determined by the requirement of local flatness on the axis: The linear radius of a circle around the axis of symmetry $r\sin\vartheta e^{y-\nu}$ must be equal to the circumferential radius $r\sin\vartheta B e^{-\nu}$, then

$$e^{y} = B \tag{2.5.2}$$

Reflection symmetry about the equatorial plane implies

$$\nu_{,\vartheta} = \omega_{,\vartheta} = B_{,\vartheta} = 0 \qquad \text{at } \vartheta = \frac{\pi}{2}\,. \tag{2.5.3}$$

To get the boundary conditions at infinity we suppose that our configuration is an isolated system, that is we ignore the influence of distant matter and cosmological curvature on the system, therefore at infinity the space-time can be considered flat. Thus asymptotically flat space-times represent ideally isolated systems in general relativity. Unlike Maxwell theory of electromagnetism, the structure of an isolated system in general relativity is no longer straightforward. The asymptotic form of the gravitational field in terms of an infinite set of multipole coefficients which are related in a simple way to the source of the field is no more possible. This difficulty arises since in general relativity there is no longer a background flat metric $\eta_{\alpha\beta}$ in terms of which the fall off rates of the curvature of the space-time metric $g_{\alpha\beta}$ can be specified. Therefore there is no unique way of specifying how the limit $r \longrightarrow \infty$ has to be taken. One way of doing it is to define a space-time to be asymptotically flat if there exists a system of coordinates such that the metric components in these coordinates behave in an appropriate way at

large coordinate values e.g. $g_{\alpha\beta} = \eta_{\alpha\beta} + O(1/r)$ as $r \longrightarrow \infty$ along either spatial or null directions. Another way which is coordinates independent is to use the concept of conformal infinity (see e.g. Wald, 1984). In either case there is no simple relation between the distant gravitational field and the matter distribution since the non-linearity of Einstein's equations allows the geometry to be also a source for them. We will follow the coordinate dependent way to settle down the asymptotic behaviour of the gravitational field since it is more transparent for the application we have in mind.

According to our definition of asymptotic flat space-time the metric functions ν, ω, B and y have the following values at infinity

$$(2.5.4) \qquad \nu,\ \omega,\ y \longrightarrow \infty \qquad \text{and} \quad B \longrightarrow 1$$

so that at infinity the metric (2.1.18) reduces to the flat one in spherical coordinates. At infinity one has e=p=0, the equation (2.2.23) becomes

$$(2.5.5) \qquad \nabla\cdot(r\sin\vartheta\nabla B) = 0 \quad .$$

As $r \longrightarrow \infty$ then

$$(2.5.6) \qquad B = 1 + O(r^{-2}) \quad .$$

Also, as we shall show below ω is $O(r^{-3})$ as $r \longrightarrow \infty$, therefore the term $r^2\nabla\omega\cdot\nabla\omega$ in (2.2.17) is $O(r^{-6})$, and this is an order higher than any that we shall retain in our analysis. Then equation (2.2.17) reduces to

$$(2.5.7) \qquad \nabla^2\nu = 0$$

therefore

$$(2.5.8) \qquad \nu \sim -\frac{M}{r} + O(r^{-2})$$

where M is a constant whose physical meaning will be explained in the next section. The behaviour of ω as $r \longrightarrow \infty$ is determined by the equation

$$(2.5.9) \qquad \nabla\cdot(r^2\sin^2\vartheta B^2 e^{-4\nu}\nabla\omega) = 0$$

or, in view of (2.5.6) and (2.5.8)

$$(2.5.10) \qquad \nabla\cdot\left[\left(1 + 4\frac{M}{r}\right)r^2\sin\vartheta\nabla\omega\right] = 0 \ .$$

The solution of this equation in *zeroth* order is of the form (Hartle, 1967)

$$(2.5.11) \qquad \omega = \sum_{l=1}^{\infty} \omega^{(0)}_l(r)\frac{dP_l}{d\mu} = 2\sum_{l=1}^{\infty}\frac{J_l}{r^{l+2}}\frac{dP_l}{d\mu} \qquad (\mu = \cos\vartheta)$$

where a factor 2 has been introduced in the definition of the constant J_l for later convenience; also P_l denotes a Legendre polynomial of order l.

The solution for ω including the *first-order* term $4M/r$ in equation (2.5.10) can be obtained by substitution

$$(2.5.12) \qquad \omega = \sum_{l=1}^{\infty}\left[\omega^{(0)}_l + 4\frac{M}{r}\omega^{(1)}_l\right]\frac{dP_l}{d\mu}$$

Equation (2.5.10) then gives

$$(2.5.13) \qquad \frac{1}{r^4}\frac{d}{dr}\left[r^4\frac{d\omega^{(1)}_l}{dr}\right] - \frac{(l-1)(l+2)}{r^2}\omega^{(1)}_l = -2\frac{l+2}{r^{l+5}}J_l$$

A particular solution is

$$(2.5.14) \qquad \omega^{(1)}_l = -\frac{l+2}{l+1}\frac{J_l}{r^{l+3}}$$

Therefore the solution for ω to $O(r^{-4})$ is given by

$$(2.5.15) \qquad \omega = \frac{2J_1}{r^3} - \frac{6J_1M}{r^4} + O(r^{-5})$$

More terms in the expansions can be computed in a way similar to BI (1976).

These conditions define the total gravitational mass and total angular momentum as we will see in the next section.

The remaining boundary conditions on the functions ν, ω and B are to be imposed at the inner boundary of the configuration that

is the event horizon.

The event horizon can be defined as a smooth two-dimensional null surface, spanned by the Killing vectors ξ and η of the space-time. Let the equation of the event horizon be

$$F(r,\vartheta) = 0. \tag{2.5.16}$$

The condition to be a null surface is

$$g^{ij}F_{,i}F_{,j} = 0 \qquad (i,j = r,\vartheta). \tag{2.5.17}$$

For the metric (2.1.15) the condition is

$$e^{2(\mu_2-\mu_3)}\left[(F_{,2})^2 + (F_{,3})^2\right] = 0 \tag{2.5.18}$$

Using the gauge freedom we can set

$$e^{2(\mu_2-\mu_3)} = f(r) \tag{2.5.19}$$

where f is a function only of r (see (2.1.17)). From equation (2.5.18) it then follows that the equation of the null surface is given by

$$f(r) = 0. \tag{2.5.20}$$

This means that without loss of generality the coordinate locus of the horizon can be made a sphere of constant radius. Moreover, the value of the coordinate radius of the horizon is

$$r = \frac{h}{2} \tag{2.5.21}$$

where h is a free parameter of the black hole therefore the coordinate radius can be rescaled by this value. (This is very useful for the numerical calculations since it avoids the problem of calculating the change in the coordinate radius of the horizon induced by the self-gravity of the matter around the black hole (see Chap. IV)).

The second condition that the null surface is spanned by the Killing vectors requires that the determinant of the metric of the subspace (t,ϕ), vanishes on $f(r)=0$

(2.5.22) $e^{2\nu} = 0$ on $f(r) = 0$.

The metric coefficients $Be^{-\nu}$ and $r^2e^{\gamma-\nu}$ must be a regular positive function in order that the intersection of the horizon with a space-like hypersurface have regular geometry. Therefore

(2.5.23) $B = 0$ at $r = h/2$.

Immediately outside the horizon the space must be vacuum, since any stationary matter configuration would have to resist an infinite gravitational acceleration on the horizon (see (2.2.18) and (2.5.22)). The general vacuum solution for B consistent with equation (2.5.23) is (Bardeen, 1973)

$$(2.5.24) \quad B(r,\theta) = \sum_{l=0}^{\infty} b_l r^l \left[1-(h^2/4r^2)^{l+1}\right] T_l^{1/2}(\cos\theta)$$

where $T_l^{1/2}(\cos\theta)$ are Gegenbauer polynomials. If there is no matter between the horizon and infinity, the boundary condition at infinity gives $b_0=1$ and $b_l=0$ for $l>0$. However, if a source for B is present outside the horizon the b_l should be adjusted to compensate for it. We will not make use of the general solution (2.5.24), but rather we solve equation (2.2.23) numerically together with the other field equations.

Carter (1973) has shown that certain quantities are constant on the horizon. Indeed, if the horizon is spanned by the Killing vectors $\underline{\xi}$ and $\underline{\eta}$ it is possible to define a null tangent vector $\underline{\lambda}$ by

(2.5.25) $\underline{\lambda} = \underline{\eta} + \Omega_H\underline{\xi}$

where Ω_H is a scalar which is a constant on the horizon and represent the local angular velocity of the horizon. Let's now prove that it is a constant (*rigidity theorem*). Contracting (2.5.25) with ξ^α we get

(2.5.26) $(\underline{\xi},\underline{\xi})\,\Omega_H = -(\underline{\xi},\underline{\eta})$ with $(\underline{\xi},\underline{\xi}) = \xi^\alpha\xi_\alpha$

since $\underline{\xi}$ is orthogonal to $\underline{\lambda}$. Taking the gradient of (2.5.26) and

using the relations

$$(2.5.27)\qquad \xi^{\alpha}\nabla_{\alpha}\eta^{\beta} = -\frac{1}{2}\nabla^{\beta}(\underline{\xi}.\underline{\eta})$$

$$(2.5.28)\qquad \xi^{\alpha}\nabla_{\alpha}\xi^{\beta} = -\frac{1}{2}\nabla^{\beta}(\underline{\xi}.\underline{\xi})$$

$$(2.5.29)\qquad \xi^{\alpha}\nabla_{\alpha}\eta^{\beta} = \eta^{\alpha}\nabla_{\alpha}\xi^{\beta}$$

holding for the Killing vectors $\underline{\xi}$ and $\underline{\eta}$ and using (2.5.26) we obtain

$$(2.5.30)\qquad (\underline{\xi}.\underline{\xi})^{2}\nabla^{\beta}\Omega_{H} = \left[(\underline{\xi}.\underline{\xi})\eta^{\alpha} - (\underline{\xi}.\underline{\eta})\xi^{\alpha}\right]\nabla_{\alpha}\xi^{\beta}$$

Making use of the definition of (2.5.25) and (2.5.26) equation (2.5.30) can be written

$$(2.5.31)\qquad (\underline{\xi}.\underline{\xi})\nabla^{\beta}\Omega_{H} = 2\lambda^{\alpha}\nabla_{\alpha}\xi^{\beta}.$$

By using the property (2.5.27) we get

$$(2.5.32)\qquad (\underline{\xi}.\underline{\xi})\nabla^{\beta}\Omega_{H} = -\nabla^{\beta}(\underline{\lambda}.\underline{\xi}) = 0$$

since $\underline{\lambda}$ and $\underline{\xi}$ are orthogonal. From (2.1.12) and (2.5.26) then follows that on the horizon $\omega=\Omega_{H}$ which is a constant.

Summarizing, a complete set of boundary conditions on the horizon, one for each of the equations (2.2.17), (2.2.22) and (2.2.23) is

$$(2.5.33)\qquad e^{2\nu} = 0$$

$$(2.5.34)\qquad \omega = \Omega_{H}$$

$$(2.5.35)\qquad B = 0.$$

These boundary conditions ensure the regularity of the solution on the horizon.

2.6 Total mass and angular momentum.

The angular momentum and gravitational mass of the system as

whole are defined by the asymptotic behaviour of the geometry at infinity. We will now obtain explicit integral expressions for these quantities.

The approach (Komar, 1959) we will follow uses the fact that the contraction of the Ricci tensor with a Killing vector is a pure divergence in a stationary and axisymmetric space-time. For the angular momentum the relevant Killing vector is ξ^{α}, while for the gravitational mass is η^{α}. Consider an integral over a t=constant spacelike hypersurface whose surface element is $d\Sigma_{\beta}$

$$(2.6.1) \qquad \int R^{\beta}{}_{\alpha}\xi^{\alpha}d\Sigma_{\beta} = \int R^{t}{}_{\phi}\,(-g)^{1/2}d^{3}x = 8\pi\int T^{t}{}_{\phi}(-g)^{1/2}d^{3}x$$

where g is the determinant of the metric. This is equivalent to integrate equation (2.2.22)

$$(2.6.2) \qquad \iint r^{2}\sin\vartheta\,dr\,d\vartheta\;\nabla\cdot\left[r^{2}\sin^{2}\vartheta B^{3}e^{-4\nu}\nabla\omega\right] =$$

$$-\,16\pi\iint r^{2}\sin^{2}\vartheta B^{2}e^{2\gamma-4\nu}\,\frac{e+p}{1-v^{2}}v\;dr\,d\vartheta$$

The volume integral over the divergence (on the left hand side) is converted into two surface integrals using Gauss's theorem, one at infinity and one on the horizon, of the form

$$(2.6.3) \qquad J = \int d\vartheta\; r^{4}\sin^{3}\vartheta B^{3}e^{-4\nu}\,\frac{\partial\omega}{\partial r}$$

At infinity, $e^{-4\nu}=1$, B=1 and

$$(2.6.4) \qquad \frac{\partial\omega}{\partial r} \simeq -\,6\,J_{1}\,r^{-4}$$

therefore

$$(2.6.5) \qquad J = -\,8\,J_{1}$$

The volume integral of the left hand side of equation (2.6.2) is then equal to $-8J_{M}$ where J_{M} is the angular momentum of the matter outside the black hole. It is then natural to define the angular momentum of the black hole from the surface integral on the

horizon such that

$$(2.6.6)\qquad J_H = J - J_H = \frac{1}{8}\int_0^{\pi} d\vartheta\, r^4 \sin^3\vartheta B^3 e^{-4\nu}\frac{\partial\omega}{\partial r}$$

therefore the total angular momentum is

$$(2.6.7)\qquad J = J_H + 2\pi\iint r^3 \sin\vartheta dr d\vartheta\left[B^2 e^{2\gamma-4\nu}\frac{e+p}{1-v^2}v\right]$$

For the gravitational mass we have the relation

$$(2.6.8)\qquad \int R^{\beta}{}_{\alpha}\eta^{\alpha}d\Sigma_{\beta} = \int R^{t}{}_{t}(-g)^{1/2}d^3x = 8\pi\int(T^{t}{}_{t} - \frac{1}{2}T)(-g)^{1/2}d^3x$$

This involves a combination of equations (2.2.17) and (2.2.22)

$$(2.6.9)\qquad \iint r^2\sin\vartheta dr d\vartheta\ \nabla\cdot\left[B\nabla\nu - \frac{1}{2}r^2\sin^2\vartheta B^3 e^{-4\nu}\omega\nabla\omega\right] =$$

$$4\pi\iint r^2\sin\vartheta dr d\vartheta\left\{Be^{2(\gamma-\nu)}\left[(e+p)\frac{1-v^2}{1-v^2} + 2p\right] + 2r\sin\vartheta\omega B^2 e^{2\gamma-4\nu}\frac{e+p}{1-v^2}v\right\}$$

Now the surface integral has the form

$$(2.6.10)\qquad S = \int_0^{\pi}\sin\vartheta d\vartheta\left[r^2 B\frac{\partial\nu}{\partial r} - \frac{1}{2}r^4\sin^2\vartheta B^3 e^{-4\nu}\omega\frac{\partial\omega}{\partial r}\right]$$

which can be represented as the sum of two parts, S_1 and S_2. At infinity the $\partial\omega/\partial r$ term is negligible compared with the $\partial\nu/\partial r$ term, therefore S_2 can be neglected with respect to S_1; from the asymptotic expansion (2.5.8) we have

$$(2.6.11)\qquad \frac{\partial\nu}{\partial r} \simeq Mr^{-2}$$

then

$$(2.6.12)\qquad S_{\infty} = S_1 = 2M$$

Taking into account the boundary conditions at r=h/2 and

equation (2.6.6), the surface integral at the horizon becomes

$$(2.6.13) \qquad S_H = \int_0^{\pi} r^2 \sin\vartheta d\vartheta \; B \; \frac{\partial \nu}{\partial r} + 2 \Omega_H J_H$$

The integral can be written as

$$(2.6.14) \qquad \int_0^{\pi} r^2 \sin\vartheta d\vartheta \; B \; \frac{\partial \nu}{\partial r} = \frac{\varkappa_H}{2\pi} \int_0^{\pi} 2\pi \, d\vartheta (r \sin\vartheta B e^{-\nu})(r e^{\gamma-\nu}) = \varkappa_H \mathcal{A}_H$$

where $\mathcal{A}_H$ is the area of the two-surface describing the horizon and $\varkappa_H$ is the rescaled gravitational acceleration of the ZAMO on the horizon. The physical acceleration felt by a ZAMO is (see (2.1.18))

$$(2.6.15) \qquad (a_\alpha a^\alpha)^{1/2} = e^{-(\gamma-\nu)} \left[(\nu_{,r})^2 + r^{-2} (\nu_{,\vartheta})^2 \right]$$

This is for unit proper time; when it is rescaled to per unit coordinate time (proper time at infinity) by a factor e^{ν}, the limit on the horizon is

$$(2.6.16) \qquad \varkappa_H = (e^{\nu})_{,r} \, e^{-(\gamma-\nu)}.$$

Carter (1973) showed that this is another quantity which is constant on the horizon.

Thus the total gravitational mass is given by

$$(2.6.17) \qquad M = M_H + 2\pi \iint r^2 \sin\vartheta dr d\vartheta \left\{ B e^{2(\gamma-\nu)} \left[(e+p) \frac{1-v^2}{1-v^2} + 2p \right] + 2r \sin\vartheta \omega B^2 e^{2\gamma-4\nu} \frac{e+p}{1-v^2} v \right\}$$

here M_H is the mass of the black hole

$$(2.6.18) \qquad M_H = \frac{1}{4\pi} \varkappa_H \mathcal{A}_H + \Omega_H J_H .$$

Smarr (1973) first showed that the mass of a Kerr black hole could be put in this form. Equation (2.6.17) was derived by Bardeen, Carter and Hawking (1973) and generalized to include electromagnetic fields by Carter (1979).

CHAPTER III

NUMERICAL METHODS

The Einstein equations derived in the previous chapter for an axisymmetric and stationary space-time are a complicated coupled system of non-linear partial differential equations and, as for most non-linear partial differential equations, there exist no general analytical methods for obtaining all solutions. Indeed, aside from the Kerr solution very few solutions of physical interest have been found. The way of obtaining other solutions of physical interest is to solve the set of non-linear partial differential equations using numerical techniques. This chapter describes a few methods which have been used in the past by other authors and the Multigrid method which will be applied for solving the Einstein equations for our configuration. This is not the first application of Multigrid to general relativity since very recently Choptuik and Unruh (1986) applied the method to obtain initial data for already solved axisymmetric problems in the vacuum for boosted and spinning black holes, but the first application for a more realistic and without any doubt much more difficult problem from the numerical point of view. Indeed in their case they had to solve only one non-linear equation (the Hamiltonian constraint equation) for the conformal factor (see Choptuik and Unruh, 1986) through which the determination of the initial data for the space-times analyzed is done via the Bowen and York's (1980) formalism. In our case we have a set of non-linear equations and among other difficulty an interface (the surface of the torus) to treat consistently.

3.1 Discretization of elliptical type partial differential equations.

The stationary and axisymmetric Einstein equations are non-linear elliptic type partial differential equations. The numerical techniques developed to solve them are all based on a self-consistent iterative method. The aim of these methods is to

give a tool for solving the field equations consistent with a given distribution of matter. The method consists of two steps: the *potential step*, in which the field equations are solved for a given distribution of density and the *equilibrium step*, in which a new distribution of density is computed from the previously computed potential.

These two steps involve the discretizations of the corresponding equations. The general approach is that of using a finite difference scheme transforming the partial differential equations into finite algebraic ones. Another way of discretizing partial differential equations is that of using the finite element methods (for an application of this method to general relativity see Mann (1982, 1983, 1985)). Since we will use finite difference schemes we will give here some general concepts on them.

Using finite difference a function is transformed into a vector of finite dimensions, a differential operator into a matrix operator and differential equations into matrix equations.

To construct a difference approximation to a given elliptic problem we must first select a discrete subdivision of the domain of integration. Consider a two-dimensional problem and suppose we divide the plane x-y into sets of equal squares of sides h, by equally spaced grid lines parallel to the y-axis, defined by $x_i = ih$, $i=1,..,n$ where n-1 is the number of squares and equally spaced grid lines parallel to the x-axis defined by $y_j = jh$ $j=1,..,n$. For any function u which is continuous and has continuous derivatives we can write the Taylor expansions

$$(3.1.1) \qquad u(x+h,y) \simeq u(x,y) + h\frac{\partial u}{\partial x} + \frac{1}{2}h^2\frac{\partial^2 u}{\partial x^2} + \frac{1}{6}h^3\frac{\partial^3 u}{\partial x^3} + \ldots.$$

$$(3.1.2) \qquad u(x-h,y) \simeq u(x,y) - h\frac{\partial u}{\partial x} + \frac{1}{2}h^2\frac{\partial^2 u}{\partial x^2} - \frac{1}{6}h^3\frac{\partial^3 u}{\partial x^3} + \ldots.$$

Addition of these expansions gives

$$(3.1.3) \qquad u(x+h,y) + u(x-h,y) = 2u(x,y) + h^2\frac{\partial^2 u}{\partial x^2} + O(h^4)$$

neglecting terms of order higher then h^2 it follows

$$(3.1.4) \qquad \frac{\partial^2 u}{\partial x^2} \simeq \frac{u(x+h,y)-2u(x,y)+u(x-h,y)}{h^2} + K\frac{h^2}{12}$$

where $|K| \leq \max |u_{xxxx}(x,y)|$. Similar formulae can be derived for derivatives with respect to y. The leading error of formula (3.1.4) is $O(h^2)$ this error is called *truncation error* resulting from the truncation of the Taylor's series. Equation (3.1.4) is called *central difference formula* since for calculating the derivative at the point (x,y) uses the values of u at points immediately before and after which lie on the same grid line. Subtracting equation (3.1.3) from equation (3.1.2) and neglecting terms of order h^3 we get

$$(3.1.5) \qquad \frac{\partial u}{\partial x} \simeq \frac{u(x+h,y)-u(x-h,y)}{2h} + O(h^2)$$

This is the central difference approximation of the first derivative. Less accurate formulae (first order in h) can be obtained directly from (3.1.2) and (3.1.3) neglecting terms of second or higher order in h. Equation (3.1.2) gives the *forward-difference* formula

$$(3.1.6) \qquad \frac{\partial u}{\partial x} \simeq \frac{u(x+h,y)-u(x,y)}{h}$$

Equation (3.1.3) gives the *backward-difference* formula

$$(3.1.7) \qquad \frac{\partial u}{\partial x} \simeq \frac{u(x,y)-u(x-h,y)}{h}$$

From now on we will denote the value of any function at the point $P(ih, jh)$ by $u_{i,j}$.

Using the formulae derived above it is straightforward to approximate the Laplacian by finite approximation. The result is the following

$$(3.1.8) \qquad \nabla^2 u \simeq (4u_{i,j} - u_{i-1,j} - u_{i,j-1} - u_{i+1,j} - u_{i,j+1})/h^2$$

This formula is the so called *5-point stars* approximation for the Laplacian. The particular form (3.1.8) holds in the case when the mesh-sizes in the directions are the same. This formulae is approximated to the second order in h. Higher order formulae can

obtained just retaining more terms in the expansions. However second order difference formulae are probably the most commonly used approximation in finite differencing since higher order schemes generally requires more work numerically.

As another example of differencing techniques we consider the expression $\nabla\cdot[f(x,y)\nabla u]$ which will be useful later. The discretization of this expression is made applying central differences directly to the divergence obtaining

$$(3.1.10)\quad \nabla\cdot[f(x,y)\nabla u] \sim$$

$$\sim [f_{i+1/2,j}(u_{i+1,j}-u_{i,j})+f_{i-1/2,j}(u_{i-1,j}-u_{i,j})]/h^2$$

$$+ [f_{i,j+1/2}(u_{i,j+1}-u_{i,j})+f_{i,j-1/2}(u_{i,j-1}-u_{i,j})]/h^2$$

This form is convenient because it is conservative (expression (3.1.10) usually appears in integrals which express some conservative law) therefore it will preserve the properties of the differential equations.

The treatment of the boundary conditions depends on the type and on the method (see later). There are three different type of boundary conditions in elliptic problems: 1) Dirichlet conditions, where the value of the unknown function is given on the boundary, 2) Neumann conditions, where the normal derivative is specified, and 3)Robbins or mixed conditions where some combination of the function and its first derivative on the boundary are given. Dirichlet type of boundary conditions present no difficulty when formulating finite difference scheme. The other two type need particular care. Usually extra grid lines are introduced in a such a way that the derivatives can be approximated to the accuracy desired and then they can be imposed on the interior equations either including them or treating them separately (see later)

The problem of solving an elliptic equation of the Laplace type ($\nabla^2 u=0$) or Poisson type ($\nabla^2 u=f$) reduces on solving the set of algebraic equations obtained after a discretization of the type (3.1.8) is used. There are several methods for solving those equations and the choice depends on the problem at hand.

3.2 Numerical methods for solving set of algebraic equations.

When the system of equations to solve is linear then the discretized system of n equations will also be linear and may be written in the form

$$(3.2.1) \qquad A\underline{u} = \underline{b}$$

where A is a nxn matrix and $\underline{u}$ and $\underline{b}$ are n-components vectors. Broadly speaking there are two classes of methods for solving equations of the type (3.2.1): *direct methods*, which solve the problem in a given number of steps and *iterative or relaxation methods* which compute an infinite sequence of better and better approximation.

Direct methods usually involve the decomposition of the matrix A into lower and upper triangular matrices accomplished by the *Gaussian elimination* (for an account of this method see any textbook on numerical analysis, e.g. *Numerical Recipes* by Press et al. 1986). These methods, in general, require large computing time ($O(n^3)$) and large storage ($O(n^3)$) so even with today's large computer it is prohibitive to use them for complicated problems like the one we have to solve. Therefore we remand the interest reader to those books which describe them in an extensive way (e.g. *Numerical Solution of Elliptic Problems* by Birchoff and Linch, 1984) since we will not use them.

In contrast with direct methods which, neglecting the machine precision, can give the exact solution in a finite number of steps, iterative methods require, theoretically, an infinite number of operations to determine the solution. In practice, the solution process is in general stopped, after some number of iterations, when some criterion of convergence is satisfied. Because these methods are widely used to solve the system of equations resulting from the discretization of boundary value problem and because these relaxations play an important role in Multigrid (see later this chapter) we will give a brief review here.

Consider the following boundary value problem in a two-dimensional domain Ω

(3.2.2) $L\,u = f$

(3.2.3) $B\,u = g$

where L and B are differential operators corresponding to the interior and boundary equations for the unknown. Suppose that L is a second order, elliptic operator and B can be the identity or normal derivative or a combination of both operators. Suppose next, that the discretization of the problem is the following

(3.2.4) $L^h \underline{u}^h = \underline{f}^h$

(3.2.5) $B^h \underline{u}^h = \underline{g}^h$.

For simplicity suppose that the boundary conditions have been already imposed into the interior equation so the equation to be solved can be thought to be only (3.2.4). With iterative methods, equation (3.2.4) is solved starting with an initial approximation $\underset{\sim}{u}^h$ and then the new iterate approximation is calculated from previous iterates getting thus a sequence of iterates $\underline{u}^{(k)}$ such that

(3.2.6) $\lim_{k \to \infty} \underline{u}^{(k)} = \underline{u}^h$

For *one-step stationary* iterative method the k+1-th iteration is obtained by the formula

(3.2.7) $\underline{u}^{(k+1)} = G\,\underline{u}^{(k)} + \underline{b}$

where $G = I - \omega D^{-1} L$ and $\underline{b} = \omega D^{-1} \underline{f}$ (D is the diagonal of the matrix L^h and I is the identity matrix and ω is a parameter in the range (0,1) which is used to accelerate the process of getting the solution). It is *one-step* because it generates $\underline{u}^{(k+1)}$ from the single estimate $\underline{u}^{(k)}$ and *stationary* because G does not depend on k. The condition for convergence of such methods is provided by the following theorem: *An iterative method is convergent if and only if the spectral radius $\rho(G)$ of the matrix G, defined as the largest in magnitude of the eigenvalues of G, is less than 1.*

To this class belongs the commonly called Jacobi iteration which consists on changing the value of the unknown using the required neighboring values from the previous iteration such that the local difference equations are satisfied. In this case we do not need to store the matrix G, all it is required is sufficient information to evaluate the difference equations in each point. This is characteristic of any iterative method and it is the primary reason why they have been extensively used in the past. For the particular case of Jacobi iteration only two vectors containing the current and previous iterations are needed to be stored. An improvement to this iteration can achieved using the newly calculated quantities whenever possible in the course of an iteration. In terms of components this can be written as follows

$$(3.2.8) \qquad u_i^{(k+1)} = \sum_{j<i} c_{i,j} u_j^{(k+1)} + \sum_{j>i} c_{i,j} u_j^{(k)} + b_i$$

where

$$(3.2.9) \qquad c_{i,j} = -a_{i,j}/a_{i,i} \qquad\qquad b_i = f_i/a_{i,i}$$

being $a_{i,j}$ the element of the matrix L^h. This is the Gauss-Seidel iteration which has the advantage of requiring storage for a single vector to maintain the estimate of the grid function.

Since these methods solve for one value of the grid function at a time, they are often referred to as *point relaxation* methods. Another class of iterative methods involves the simultaneous replacement of those values which belongs to a given grid lines and that simultaneously satisfy the equations on that line. This process is called *line relaxation*. The simultaneous replacement is easy and inexpensive to do, since the system of equations to be solved for each line is tridiagonal (see e.g. Press et al. 1986).

The above briefly described methods tend to have asymptotic slow convergence. This can be seen through a simple example.

Consider the one-dimensional boundary value problem

$$(3.2.10) \qquad -u''(x) = f(x) \qquad 0 \le x \le 1 \qquad\qquad u(0)=u(1)=0$$

whose discretization is the following

(3.2.11) $$\frac{-u_{i+1}+2u_i-u_{i-1}}{h^2} = f_i \qquad i=1, \quad ,N$$

where N-1 is the number of intervals in which the domain is divided. The discretization can also be put in the general form (3.2.4). Suppose we solve the equation using the iterative method in (3.2.7) which can also be written as

(3.2.12) $$\underline{u}^{(k+1)} = \underline{u}^{(k)} - D^{-1}(L^h\underline{u}^{(k)} - \underline{f}^h) = \underline{u}^{(k)} + D^{-1}\underline{r}^{(k)}$$

where the $\underline{r}^{(k)}$ is the *residual* vector given by

(3.2.13) $$\underline{r}^{(k)} = \underline{f}^h - L^h\underline{u}^{(k)}.$$

Using (3.2.12), this gives

(3.2.14) $$r^{(k+1)} = G\, r^{(k)}$$

Clearly

(3.2.15) $$r^{(k)} = G^k\, r^{(0)}$$

where G^k is the k-th power of the matrix G and $r^{(0)}$ is the residual corresponding to the initial solution estimate. This residual can then be expressed as combination of the eigenvectors ϕ_m of G as

(3.2.16) $$r^{(0)} = \sum_{m=1}^{N-1} c_m\phi_m.$$

It then follows from (3.2.15) that

(3.2.17) $$r^{(k)} = \sum_{m=1}^{N-1} c_m(\lambda_m)^k\phi_m$$

where λ_m are the eigenvalues of the matrix G. Now the eigenvalues and eigenvectors of the matrix G are given by (supposing $\omega=1/2$)

(3.2.18) $$\phi_m = [\sin(\pi mh), \sin(2\pi mh), \quad ,\sin((N-1)\pi mh)]$$

(3.2.19) $$\lambda_m = \cos^2(\pi mh/2) \qquad m=1,\ldots,N-1.$$

Therefore the spectral radius of the matrix G is

(3.2.20) $$\cos^2 \frac{\pi h}{2} \sim 1 - \frac{\pi^2 h^2}{2} + O(h^4)$$

For small h, this spectral radius will be of order 1 resulting in very slow convergence rate. This slowness is due to the lowest frequency components (*smooth components*) of the residuals. On the other hand the spectral radius is much less than 1 for those high frequencies (*non-smooth components*) for which $\cos^2(\pi mh/2)$ is much less than unity.

For a given approximation $\tilde{u}^{(k)}$ of the problem we can define the error as

(3.2.21) $$e^{(k)} = u^{(k)} - \tilde{u}^{(k)}$$

Therefore the iteration equation can also be written as

(3.2.22) $$e^{(k+1)} = G\, e^{(k)}$$

The analysis made for the residuals holds even for the errors. Thus we can conclude, with the help of Fig. 18 that those error components which are not visible on a given grid are the ones responsible for slow convergence, whereas high frequency errors are very efficiently smoothed by relaxation. The situation is that of Fig. 18 in which typical error smoothing behaviour is shown.

3.3 Methods used to solve stationary and axisymmetric Einstein's equations.

As already mentioned in Chap. I several numerical techniques have been developed to solve the Einstein equations for stationary and axisymmetric systems (Bardeen and Wagoner, 1971, Wilson, 1972, Bonazzola and Scheneider, 1974, Butterworth and Ipser, 1976, Eriguchi, 1980, Komatsu et al., 1986). Among these the most promising are the ones developed by Butterworth and Ipser and Komatsu et al.. Here we give an outline of these methods and explain why we will not use them.

Butterworth and Ipser generalized Stoeckley's (1965) method on rotating Newtonian polytropes to general relativity. Briefly,

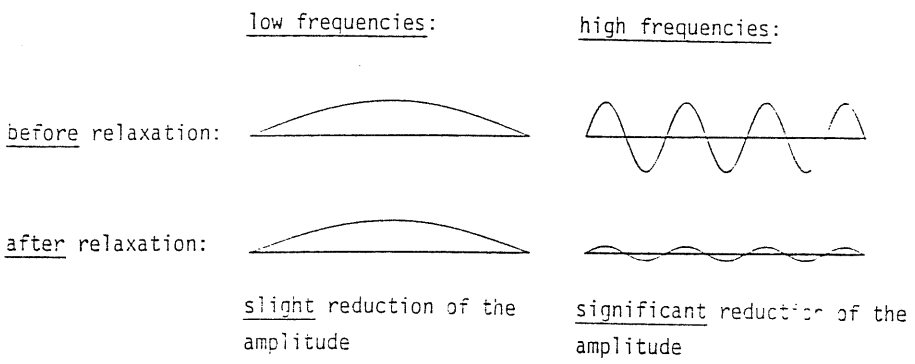
low frequencies:
high frequencies:
before relaxation:
after relaxation:
slight reduction of the amplitude
significant reduction of the amplitude

Fig. 18.

they used the Newton-Raphson method to approximate the solution $(g_{\alpha\beta},p)$ of Einstein's equations

$$(3.3.1) \qquad G_{\alpha\beta} = 8\pi\, T_{\alpha\beta}$$

As a zeroth approximation they took a previously constructed model $(g^{0}_{\alpha\beta},p^{0})$ close to the one to be computed. Then after slightly increasing the rotation parameter, the pressure p^{1} was recomputed using the hydrostatic equilibrium equation and the following perturbation equations were solved

$$(3.3.2) \qquad \delta G_{\alpha\beta} - 8\pi\, \delta T_{\alpha\beta} = G_{\alpha\beta}(g^{0}) - 8\pi\, T_{\alpha\beta}(g^{0},p^{1})$$

for the perturbed $\delta g_{\alpha\beta}$ obtaining a first order approximation $(g^{1}_{\alpha\beta},p^{1})$. The (n+1)-st approximation is obtained from the n-th by first solving the hydrostatic equilibrium equation to find p^{n+1} in terms of $g^{n}_{\alpha\beta}$ and then solve (3.3.2) to find $g^{n+1}_{\alpha\beta}=g^{n}_{\alpha\beta}+\delta g_{\alpha\beta}$ in terms of p^{n+1} and $g^{n}_{\alpha\beta}$. This process is continued until convergence is reached. A sequence was constructed for a succession of increasing values of the rotation parameter.Equations (3.3.2) involves a global linearization. Actually they do not linearize the equations globally, but for each of them (regarded as an equation for each metric function) the linearization is done with respect one metric function only. The discretization is made on a finite grid which consists of a chosen number of radial spokes emanating from the origin at the Gauss-Legendre quadrature values and a chosen number of equally spaced radial intervals along each spoke. The choice of Gauss-Legendre quadrature values is dictated by the fact that each function is expressed in terms of Legendre polynomials for the angular part. The radial derivatives are approximated using central difference formulae. This method allows to use a few points in the angular direction and still have good accuracy. The drawback is that since the spokes emanating from the origin of the domain of integration the resolution of external configurations which do not contain the origin cannot be controlled in an easy way. Thus, although this way of discretization gives a good accuracy for systems of elliptical shapes, it is not adequate for body with toroidal shape or for very flattened objects in general.

More adequate, for this purpose, is the method used by Eriguchi (1986, GR11) to constructed relativistic sequence of polytropic spheroidal and toroidal (without central body) bodies. The method is not yet published in detail, and only a brief sketch is contained in a very recent preprint (Komatsu et al., 1986). They divide the Einstein equations into three parts: a linear part, a non-linear part and the matter source term. Then by introducing a Green's function for the linear part they reduce the equation to an integro-differential problem. This seems to be a procedure which it can only be followed if the non-linear term is thought to have little contribution. Therefore the method in principle might not be able to treat a strong gravitational field. Their claims, to be able to compute highly relativistic configurations, are questionable since their strength of relativity parameter is only the ratio of the pressure to the energy density and they do not give any information about the strength of the gravitational field. One advantage of using an integral formulation of Einstein's equations is that the boundary conditions are already imposed on the equations and so nothing special needs to be done to treat them. in contrast Butterworth and Ipser had to calculate asymptotic expansions of the metric functions up to higher orders than those of Chap. II in order to impose the conditions at a finite distance (two zones outside the surface of the configuration considered). The expansion of the metric functions to higher order introduces a formidable difficulty, namely the calculation of the multipole moments, since in general relativity their source is not only the matter but also the geometry (see Chap. II). A generally covariant integral formulation of Einstein's equations was made by Sciama et al. (1969). This formulation gives a better representation of the mathematical structure of Einstein's equations (regarding only the source terms as contributing linearly to the potential $g^{\alpha\beta}$) and so a similar form would be suitable to solve numerically the equations.

3.4 Multigrid Methods.

In the previous section we have seen that the standard iterative methods in some situations can be very slow since the local nature of a relaxation sweep which is efficient on smoothing those modes with very short wavelengths that interact at short distance and are not influenced by distant boundaries. Brandt (1973) used this property to construct the Multigrid method which solves a system of discrete equations using a collection of grids with different mesh-sizes taking advantage of the relation between different discretizations of the same continuous problem. In order to have a good convergence rate one should be able to reduce as many error components possible. The use of different grids with different mesh-sizes provides a good tool for this, since a large spectrum of frequencies can then be represented. The idea of the method is very simple and can be stated as follows.

a) coarse grid correction.

For ease of exposition we suppose that the differential problem to be solved is

$$(3.4.1) \qquad L\,u = f \qquad \text{with b.c.} \qquad B\,u = g$$

where L is a linear operator. Suppose that the discretization of equation (3.4.1) on a grid with mesh-size h is

$$(3.4.2) \qquad L^h u^h = f^h \qquad\qquad B^h u^h = g^h$$

After applying any iterative procedure suppose we have an approximate solution $\tilde{u}^h$. The error $v^h = u^h - \tilde{u}^h$ then satisfies

$$(3.4.3) \qquad L^h v^h = r^h \qquad \text{where} \qquad r^h = f^h - L^h\tilde{u}^h$$

Since relaxation reduces only high frequency components, the only modes left after few sweeps are the smooth ones therefore v^h is a smooth function and can be approximated by a coarser grid function v^H which satisfies

$$(3.4.4) \qquad L^H v^H = r^H \qquad \text{where} \qquad r^H = I_h^H r^h.$$

Here L^H is a coarse grid approximation of L^h and I_h^H is the fine to

coarse grid transfer operator. Note that since the grid H has much less points than the grid h (one quarter of points in two dimensions, if H = 2h), it is much easier to solve (3.4.4) than to solve (3.4.3). Having obtained an approximate solution $\tilde{v}^H$ of equation (3.4.4) we use it as correction to accelerate the convergence of the fine grid

$$\tilde{u}^h \longleftarrow \tilde{u}^h + I_H^h \tilde{v}^H \qquad (3.4.5)$$

where I_H^h is a coarse to fine grid interpolation operator. This process is called *coarse grid correction*.

b) Full Multi-Grid.

To solve efficiently the equation (3.4.4) we can employ a coarse grid correction recursively; i.e., equation (3.4.4) is itself solved by relaxation sweeps combined with a still coarser grid correction. We thus have a sequence of grids with mesh-sizes $h_1 > h_2 > \ldots > h_M$, where $h_M \equiv h$ and $h_j = 2h_{j+1}$. In the *Full Multi-Grid* (FMG) algorithm, the first approximation is obtained by interpolating from a solution on the next coarser level, which itself has been calculated by a similar (FMG) algorithm. From the differences between the final solutions at different mesh-sizes, we can directly calculate the rate of convergence to the differential solution (see Fig. 19).

Independently, Hackbusch in 1975/76 developed the fundamental elements of multigrid methods without knowing the existing literature. His major contribution consists of presenting a general convergence theory of Multigrid methods (Hackbusch, 1980, 1981, 1985). For a large class of problems the theory predicts that the number of operations needed for solving the problem to the level of truncation error is less than $C \cdot n$ (see for instance Hackbusch, 1985) where C is a constant and n is the number of grid points of the finest grid used. Usually the theory gives quite large values of C and so on this basis one might not choose to use the Multigrid method. However practical experiments give a different answer. For example for problems with singularities it is not possible to have a rigorous proof of convergence. However in practice these problems are solved with the same efficiency as

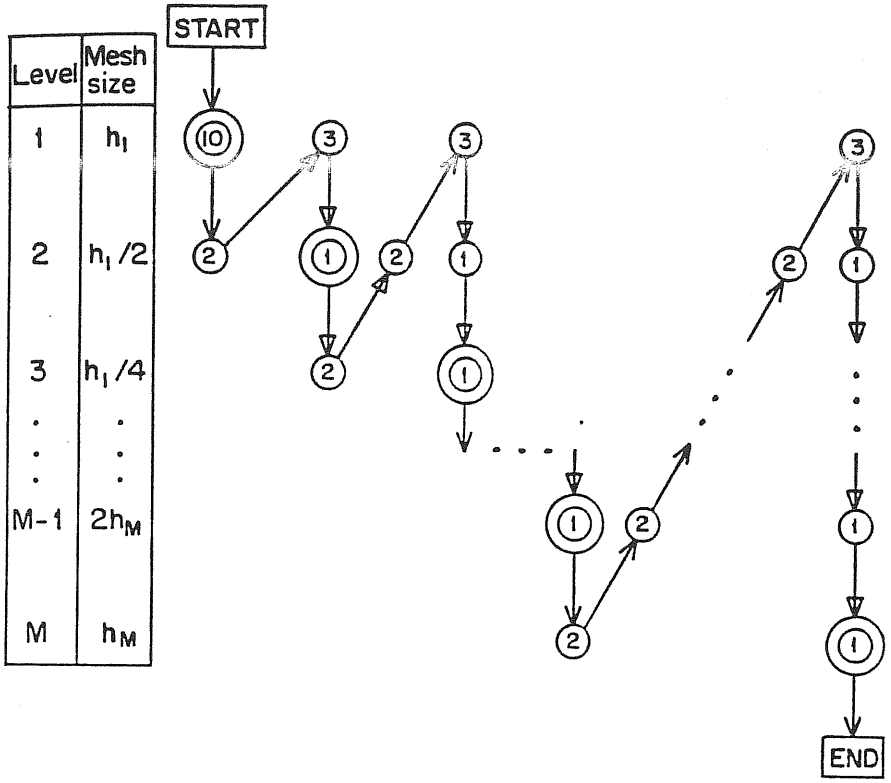

= Higher order interpolation

= Linear interpolation of corrections

= Transfer to coarser level

= Transfer to coarser level where τ-extrapolation can be made

(r) = r relaxation sweeps

= The stage in the algorithm where the error is smaller than the discretization error of that level

Fig. 19 - Fixed Full Multi-Grid (FMG) algorithm.

regular problem (see e.g. Brandt, 1981 and Brandt and Ta'asan, 1985).

c) Full Approximation Scheme.

The correction scheme is not applicable to non-linear problems since equation (3.4.4) is valid only for linear L^h. In this case we should use the *Full Approximation Scheme* (FAS) performing the same steps but in terms of another coarse grid variable. Instead of v^H we use

$$\hat{u}^H \equiv \hat{I}_h^H \tilde{u}^h + v^H \qquad (3.4.6)$$

as the coarse grid unknown variable. This function approximates the full solution represented on the coarse grid. Using (3.4.6) the coarse grid equation (3.4.4) becomes

$$L^H \hat{u}^H \equiv \hat{f}^H \qquad \text{where} \qquad \hat{f}^H \equiv L^H(\hat{I}_h^H \tilde{u}^h) + I_h^H r^h \qquad (3.4.7)$$

Then the coarse grid correction equivalent to (3.4.5) becomes

$$\tilde{u}^h \longleftarrow \tilde{u}^h + I_H^h(\tilde{u}^H - \hat{I}_h^H \tilde{u}^h) \qquad (3.4.8)$$

One important advantage of FAS is its direct application to non-linear problems without linearizing the equations. The correction equation (3.4.3) in the case L^h is non-linear, can be written in the form

$$L^h(\tilde{u}^h + v^h) - L^h(\hat{u}^h) \equiv r^h \qquad (3.4.9)$$

Transferring this equation to the coarse grid (replacing L^h by L^H, $\tilde{u}^h$ by $\hat{I}_h^H \tilde{u}^h$, v^h by v^H and r^h by $I_h^H r^h$) we get the FAS equation (3.4.7).

d) Dual point of view.

We may write equation (3.4.7) also as

$$L^H \hat{u}^H = f^H + \tau_h^H \qquad (3.4.10)$$

where

$$\tau_h^H = L^H(\hat{I}_h^H \tilde{u}^h) - I_h^H(L^h \tilde{u}^h) \qquad (3.4.11)$$

and

$$(3.4.13) \qquad f^H = I_h^H f^h$$

Equation (3.4.10) without τ_h^H is the usual coarse grid equation and τ_h^H is the fine-to-coarse defect correction.

We can now reverse our point of view of the entire multigrid process: instead of regarding the coarse grid as a device for accelerating convergence on the fine grid, we can view the fine grid as a device to calculate the correction τ_h^H to the coarse grid equation visiting a finer grid. This is the so called *dual point of view.*

e) τ - extrapolation.

The defect τ_h^H can serve as an estimation of the *local truncation error* τ^H

$$(3.4.14) \qquad \tau^H = L^H(\hat{I}^H u) - I^H(L\,u)$$

where u is the true solution of the differential solution and $\hat{I}^H$, I^H are continuum-to-H-grid interpolation operators. Note the analogy between (3.4.11) and (3.4.14). The term τ^H is the correction for the right hand side of the equation

$$(3.4.15) \qquad L^H u^H = f^H$$

in order u^H coincides with the true solution $\hat{I}^H u$ at the grid H, whereas τ_h^H is the correction in order that u^H will coincide at convergence with the fine grid solution $I_h^H u^h$. It is then clear that at convergence

$$(3.4.16) \qquad \tau^H \approx \tau^h + \tau_h^H$$

where $\tau^h = L^h(\hat{I}^h u) - I^h(Lu)$. This relation is very important since it allows to raise the approximation order. Indeed, suppose that the local approximation order is p, i.e.

$$(3.4.17) \qquad \tau^h(x) \approx c(x)\, h^p \qquad c(x) \text{ independent on } h$$

then for the next coarse grid (H=2h) we can write

(3.4.18) $\tau^H(x) \approx 2^p\, c(x)\, h^p$

therefore equation (3.4.16) becomes

(3.4.19) $\tau_h^H(x) \approx (2^p-1)\, c(x)\, h^p$

using then (3.4.18)

(3.4.20) $\tau^H(x) \approx 2^p(2^p-1)^{-1}\tau_h^H(x)$

Then the approximation order of grid-H can be raised by just multiplying the truncation error τ_h^H by the factor $2^p(2^p-1)^{-1}$ and using equation (3.4.10) as a coarse grid equation. This operation is called τ *extrapolation* and it is a by-product of FAS.

f) Local grid refinement.

In most practical problems non-uniform resolution is needed. Finer grids are needed near singularity, non-smooth boundaries, boundary layers, shock, etc. In our problem the solutions is characterized by three different lengthscales: the horizon size, the scale corresponding to the structure of the torus and infinity. The FAS algorithm can deal with these needs in an automatic way, using local grid refinements and/or local coordinates transformation.

Non-uniformity in multigrid methods is reached, realizing that finer grids can extend only in subdomains. Allowing for grid contraction or extension the FAS scheme with τ-extrapolation technique will give a very efficient solution process. The idea is that τ will tell us where further resolution is needed in the domain. If in some subdomain the local truncation error is far below the average, a finer grid is introduced in that subdomain and a local multigrid cycle will be applied till the truncation error will be below the level desired. This can be done automatically selecting the mesh-size h in an optimal way trying to minimize the work invested to obtain a given accuracy. This is a typical optimization problem.

When a proper multigrid algorithm is used, the amount of invested work W, is proportional to the number of grid points in

the domain, and can therefore be approximated by

$$(3.4.21) \qquad W \approx \int \frac{w}{h^d} dx$$

where d is the dimension of the problem's domain, h^{-d} is the local number of grid points and w is the work per grid point, which is generally proportional to the complexity of the finite difference formulae.

The solution error E can always be approximated by a functional of the form

$$(3.4.22) \qquad E \approx \int G\tau dx$$

where τ is the local truncation error. The *error weighting function* G is chosen according to the problem. Equation (3.4.22) states that the error made at one point affects the solution error, and its measure E, independently of that made at another point.

The Euler equation for optimizing h by minimizing E under fixed W is

$$(3.4.23) \qquad \frac{\partial E}{\partial h} + \lambda \frac{\partial W}{\partial h} = 0$$

or by using (3.4.21) and (3.4.22)

$$(3.4.24) \qquad G\frac{\partial \tau}{\partial h} = \lambda d w h^{-d-1}$$

where λ is a constant independent of the position of the grid, expressing the rate of exchange optimal accuracy for work. Equation (3.4.24) can be used either calculating with FAS the estimation of the truncation error and then when the left hand side is larger than the right hand side a fine grid is introduced or alternatively if an estimation of the truncation error is known in advance then equation (3.4.24) is used to constructed the set of grids to use in the Multigrid (for an application of the latter case see Bai and Brandt, 1985 and Dendy, 1984).

CHAPTER IV

MULTIGRID IN GENERAL RELATIVITY: VACUUM SPACE-TIMES.

The multitude of features (non-linearity, Neumann-like boundary conditions, unbounded domain or, in general, different lengthscales, etc) characteristic of our problem require a thorough understanding of their implications in terms of the Multigrid process. Mistreating just one of them may cause the solution time to increase very significantly. Therefore it is a good strategy to proceed step by step, introducing one new feature at a time. For this reason, we have started with the simplest models connected with our problem for which analytic solutions are known.

We start with specializing our system consider the vacuum case, then we neglect rotation. Therefore the first experiment done is for getting numerically the Schwarzschild solution. Next the rotation is included so the corresponding analytic solution is that of the Kerr metric. The experiments done concern only the equations for the metric functions B, ν and ω. The equation for y does not presents large difficulties being a linear first order differential equation.

4.1 The Schwarzschild case.

When outside the horizon of the black hole no matter is present then the right hand sides of the equations (2.2.17), (2.2.22) and (2.2.23) go to zero. Moreover if the black hole is supposed to be non-rotating then the metric becomes spherically symmetric and the metric function ω is identically zero in all the space-time. Therefore the equations reduces to

$$\nabla\cdot(B\nabla\nu) = 0 \qquad (4.1.1)$$

$$\nabla\cdot(r\sin\theta\nabla B) = 0 \qquad (4.1.2)$$

with the following boundary conditions

(4.1.3) $\nu_{,\vartheta} = B_{,\vartheta} = 0$ at $\vartheta = 0,\ \pi/2$

(4.1.4) $e^{\nu} = 0 \qquad B = 0$ at $r = h/2$

(4.1.5) $\nu \sim -\frac{M}{r} \qquad B = 1$ at large r.

Since the boundary condition for the ν metric function at the horizon it is more convenient to work with the variable $X=e^{\nu}$ instead of ν. Moreover, the radial coordinate can be rescaled using the value of the coordinate radius of the horizon. Therefore the system of equations to solve in this case is

(4.1.6) $\nabla\cdot(\frac{B}{X}\nabla X) = 0$

(4.1.7) $\nabla\cdot(r\sin\vartheta\nabla B) = 0$

with the boundary conditions

(4.1.8) $X = 0 \qquad B = 0 \qquad \frac{B}{X}$ regular at $r = 1$

(4.1.9) $X = 1 - \frac{2}{r} \qquad B = 1$ at large r

(4.1.10) $X_{,\vartheta} = B_{,\vartheta} = 0$ at $\vartheta = 0,\ \pi/2$

Although we know that in this case the solution does not depend on the angular coordinate we still retain the angular part of the above system in our numerical experiments. It easy to verify (see Appendix C) that the solution in this case is given by

(4.1.11) $X = \frac{r-1}{r+1}$ and $B = 1 - \frac{1}{r^2}$

As we can see from the Appendix, it is very crucial to use the regularity condition in order to determine the solution analytically. We will see that is crucial numerically as well.

In order to solve numerically our equations using the Multigrid it is important to chose first a good discretization scheme and then an efficient relaxation algorithm. To analyze

different discretizations and relaxation methods let's concentrate our attention, for the moment, to the equation for the metric function B which, being linear, is much simpler to analyze.

Since the equation is in divergence form it is natural to discretize it in a conservative form. Before doing that we have to chose our grid. We chose r=R=50 as outer edge of the domain where the boundary condition at infinity should be imposed. Note that this approximation introduces a lower limit on the error we can obtain, unless an adaptive Multigrid scheme is used. This lower limit is easily calculated from the difference between the value of B given by the analytic solution for r=50 and one. Chosen the outer edge of the grid we have now a finite domain which can be subdivided using a finite number of meshes in both directions. Suppose, that the resulting mesh-size in the r-direction is h_r and the one in the ϑ-direction is h_ϑ. In selecting the discretization scheme we should keep in mind the local property of relaxation, therefore we can confine our considerations only to those terms which are locally important. For a linear equation the locally important terms are those which contain the higher derivatives. The locally important part (*principal part*) of equation (4.1.7) is

$$r\,B_{,rr} + \frac{B_{,\vartheta\vartheta}}{r} = 0 \qquad (4.1.12)$$

the discretization of such an equation is

$$r_i \frac{B_{i+1,j} - 2B_{i,j} + B_{i-1,j}}{h_r^2} + \frac{1}{r_i} \frac{B_{i,j+1} - 2B_{i,j} + B_{i,j-1}}{h_\vartheta^2} = 0 \qquad (4.1.13)$$

In the Gauss-Seidel relaxation scheme the points (i,j) are scanned one by one in some prescribed order. Given an approximation $\tilde{B}_{i,j}$, at each point this value is replaced by a new value, $\bar{B}_{i,j}$, such that equation (4.1.13) is satisfied. That is, $\bar{B}_{i,j}$ satisfies

$$r_i \frac{\tilde{B}_{i+1,j} - 2\bar{B}_{i,j} + \bar{B}_{i-1,j}}{h_r^2} + \frac{1}{r_i} \frac{\tilde{B}_{i,j+1} - 2\bar{B}_{i,j} + \bar{B}_{i,j-1}}{h_\vartheta^2} = 0 \qquad (4.1.14)$$

where the new values $\bar{B}_{i-1,j}$, $\bar{B}_{i,j-1}$ are used since, in the order chosen (lexicographic), by the time (i,j) is scanned new values

have already replaced old ones at $(i-1,j)$ and $(i,j-1)$. The new approximation $\bar{B}_{i,j}$ does not satisfies (4.1.13) and further relaxation sweeps may be required to improve it. It is therefore important to define the *convergence factor* as

$$(4.1.15) \qquad \mu = \|\bar{v}\| / \|v\| \quad \text{where} \quad v_{i,j} = B_{i,j} - \tilde{B}_{i,j}, \quad \bar{v}_{i,j} = B_{i,j} - \bar{B}_{i,j}$$

and $\|\cdot\|$ being a suitable norm. An analysis of the smoothing effect can be done expanding the errors v and $\bar{v}$ in Fourier series

$$(4.1.16) \qquad v_{i,j} = \sum A_{\underline{\vartheta}} e^{i(\vartheta_1 i + \vartheta_2 j)} \qquad \bar{v}_{i,j} = \sum \bar{A}_{\underline{\vartheta}} e^{i(\vartheta_1 i + \vartheta_2 j)}$$

where $\underline{\vartheta} = (\vartheta_1, \vartheta_2)$ and the summations are extended over a subset of the square $|\underline{\vartheta}| = \max(|\vartheta_1|, |\vartheta_2|) \leq \pi/2$. Subtracting (4.1.13) from (4.1.14) and substituting (4.1.16) we get

$$(4.1.17) \qquad (ae^{i\vartheta_1} + ce^{i\vartheta_2})A_{\underline{\vartheta}} + (ae^{-i\vartheta_1} + ce^{-i\vartheta_2} - 2a - 2c)A_{\underline{\vartheta}} = 0$$

where $a = (h_{\vartheta} r_i)/h_r$ and $c = h_r/(h_{\vartheta} r_i)$. Hence the *amplification factor* of the $\underline{\vartheta}$ component due to one relaxation sweep is

$$(4.1.18) \qquad \mu(\vartheta) = \left| \frac{\bar{A}_{\underline{\vartheta}}}{A_{\underline{\vartheta}}} \right| = \left| \frac{ae^{i\vartheta_1} + ce^{i\vartheta_2}}{2a + 2c - ae^{-i\vartheta_1} - ce^{-i\vartheta_2}} \right|$$

Among all components we are interested only in those which cannot be represented on a coarser grid. These are the components for which $(h/H)\pi \leq |\underline{\vartheta}| \leq \pi$, where H is the mesh-size of the next coarser grid. Since we will assume from here on that $H/h = 2$ we will be interested in those components for which $\pi/2 \leq |\underline{\vartheta}| \leq \pi$. From (4.1.18) we see that as $\underline{\vartheta} \longrightarrow (0,0)$, $\mu(\underline{\vartheta}) \longrightarrow 1$, which explains why smooth components are slow to converge. We can then define the *smoothing factor* as the largest convergence factor for all components not represented at coarser level

$$(4.1.19) \qquad \bar{\mu}(\vartheta) = \max_{\pi/2 \leq |\vartheta| \leq \pi} \mu(\vartheta)$$

This factor gives the relaxation convergence factor for those components which converge on grid h; others will converge on grid

H. Now, provided that $a/c \sim 1$ the function defined in (4.1.18) has a maximum for the pair $(\pi/2, \arccos 4/5)$ and the value of it for this value of $\underline{\theta}$ is $\bar{\mu}=.5$, which means that as long as $a \sim c$ point relaxation needs only three sweeps to reduce the high-frequency error components by almost an order of magnitude. The situation is different when $a \ll c$ (or $a \gg c$). For instance

$$(4.1.20) \qquad \mu\left(\frac{\pi}{2}, o\right) = \left[\frac{a^2+c^2}{a^2+(c+2a)^2}\right]$$

which approaches 1 as $a \to 0$. In such cases there are other kind of relaxation methods that one should use, namely line relaxation which can give a good smoothing factor as the point relaxation. The line to be simultaneous updated in the course of a sweep depend on which condition is meet: $a \ll c$ or $a \gg c$. In the first case, being the coefficient of the r-derivative term in the principal part more important than the other term, the discrete operator has strong connection in the r direction therefore only in that direction we can have smoothing of the error and the line to relax simultaneous is the r-line; vice versa for the other case, the line to relax simultaneous is the θ-direction. In our case the three conditions $a \sim c$, $a \ll c$ or $a \gg c$ will be meet depending on how far we are from the inner edge of the grid (see definitions of a and c). Therefore in such coordinates, the relaxation method used will depend on the value of r. This may be quite expensive in terms of computational work since during a sweep we should check which of the above three conditions is satisfied. Not only this, but line relaxation can be very expensive if it has to be employed for a system of equations. A way out of this problem is to use a different coordinate.

A quite natural change of coordinate is to use $s=\ln r$ instead of r. The reason is that this will provide a natural non-uniform grid in the radial coordinate giving more resolution in r near the horizon, where the metric functions have most of their variations in terms of the radial coordinate. Moreover using s instead of r equation (4.1.12), assumes the form

$$(4.1.21) \qquad \frac{B_{,rr}}{r} + \frac{B_{,\vartheta\vartheta}}{r} = 0$$

whose discretization, provided that $h_\vartheta \simeq h_r$ satisfies the condition a≃c. Therefore using s as independent radial variable we can still use the point relaxation which is the most inexpensive relaxation technique.

Another important piece of the Multigrid mosaic is the transfer of the residuals. This transfer serves, essentially to calculate the right hand side of the coarser grid equation after few relaxation sweeps have been made on the fine-grid to smooth the high-frequency error components. The choice of the proper operator I_h^H applied to the residuals, depends on the type of equation we are dealing with. For constant coefficient equations like the Poisson's equation in Cartesian rectangular coordinates it is enough to *inject* the value of the residuals at a given point in the fine-grid to the corresponding point in the coarse-grid (see Fig. 20).

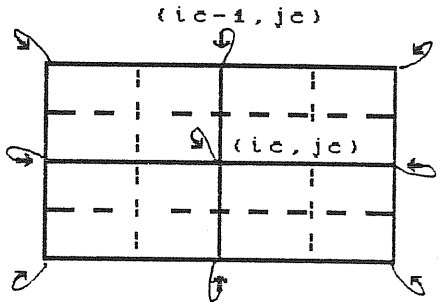

$$(I_h^H r^h)_{ic,jc} = r^h_{2ic-1,\,2ic-1}$$

Fig. 20

For equations with rapidly varying coefficients or for non-linear equations the simple injection is not a good transfer. The reason is that when the coefficients vary rapidly in two contiguous meshes then even the residuals change rapidly. To have a good representation of them in the coarse grid we should use *full residual weighting*. There are several ways to construct such transfers, one of those is that of requiring that the integral of the residuals on the fine grid should be equal to the integral extended on the coarse grid of the transferred residuals

$$(4.1.22) \qquad \int I_h^H r^h dxdy \approx \int r^h dxdy$$

for a rectangular grid with coordinates x and y. Then discretizing such an expression we get

$$(4.1.23) \qquad H_x H_y \sum I_h^H r^h(x^H) = h_x h_y \sum r^h(x^h)$$

For each point in the coarse grid the summation is limited to a subset of neighboring fine grid points for reducing the computational work. On the other hand the number of points should be large enough to give a good averaging of the residuals. An optimal subset is the one made of those nine grid points just around the coarse grid point considered. Using these nine points full weighting can be done through the formula

$$(4.1.24) \qquad (I_h^H r^h)_{ic,jc} = \frac{1}{4} r^h_{if,jf} + \frac{1}{8}\left[r^h_{if+1,jf} + r^h_{if,jf+1} + r^h_{if-1,jf} + r^h_{if,jf-1}\right] + \frac{1}{16}\left[r^h_{if+1,jf+1} + r^h_{if-1,jf+1} + r^h_{if+1,jf-1} + r^h_{if-1,jf-1}\right]$$

where $if=2ic-1$ and $jf=2jc-1$. Equation (4.1.24) is the transfer operator generally used for equation with variable coefficients like Navier-Stokes equations (Brandt, 1984). However for diffusion equations (Alcouffe et al. 1981) with discontinuous coefficients a better operator needs to be constructed. A way is to construct it by using the diffusion coefficients itself as weights in a fashion that we will explain. The operation of transferring the residuals from fine to coarse grid can be regarded as a process of distribution of the calculated residuals in the fine grid to nearby coarse grid points in a such a way that the right hand side of the coarse

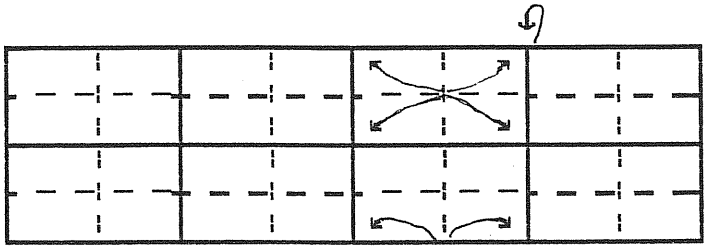

Fig. 21

grid equation still preserve the smoothing properties of the fine grid residuals. Now, consider two grids with mesh-sizes ratio H/h=2 (see Fig. 21). Each coarse grid cell contains four fine grid cells and therefore nine fine grid points. These can be divided in three classes: those which coincide with the coarse grid points, those which lie on coarse grid lines but do not coincide with the coarse grid points and the ones at the center of the coarse grid cell. Each point belonging to different class contributes differently to the nearby coarse grid point. The residuals at the point at the center of the cell will contribute to the residuals of the four vertices of the coarse grid cell, whereas the residuals relative to the finer grid points bracketed by two coarse grid points will contribute only to the residuals relative to the bracketing coarse grid points. Those residuals relative to the fine grid points which coincide with the coarse grid points will give direct contributions to the residuals of those coarse grid points taking into account the presence of the contiguous cells. The proportion of these splitting of the residuals are dictated by the weights chosen. A way for choosing these is to reverse our point of view and think how we would interpolate the residuals to the fine grid points given those at the coarse grid points for each of the above classes. This process is equivalent to construct the inverse coarse-to-fine interpolation operator which is used in the process of Multigrid to interpolated the coarse grid corrections.

The choice we have done is that of taking as weights the diffusion coefficients which appear in the equations. With the use of s as coordinates, equation (4.1.2) can be written

$$(4.1.25)\qquad \partial_s(r^2\sin^2\vartheta B_{,s}) + \partial_\vartheta(r^2\sin^2\vartheta B_{,\vartheta}) = 0$$

the discretization of it is

$$(4.1.26)\qquad \sin^2\vartheta_j \frac{h_\vartheta}{h_r}\left[r^2_{i+1/2}(B_{i+1,j}-B_{i,j})+r^2_{i-1/2}(B_{i-1,j}-B_{i,j})\right]$$
$$+\ r_i^2 \frac{h_r}{h_\vartheta}\left[\sin^2\vartheta_{j+1/2}(B_{i,j+1}-B_{i,j})+\sin^2\vartheta_{j-1/2}(B_{i,j-1}-B_{i,j})\right]$$

Using the coefficients of (4.1.26) with the above prescriptions

the residuals transfer operator is

$$(4.1.27)\qquad (I_h^H r^h)_{ic,jc} = \frac{1}{4} r^h_{if,jf}$$
$$+ \frac{1}{4}\Big[A^{--}_{if-1/2,jf-1/2} r^h_{if-1,jf-1} + B^{-}_{if-1/2} r^h_{if-1,jf}$$
$$+ A^{-+}_{if-1/2,jf+1/2} r^h_{if-1,jf+1} + C^{-}_{jf-1/2} r^h_{if,jf-1}$$
$$+ C^{+}_{jf+1/2} r^h_{if,jf+1} + A^{+-}_{if+1/2,jf-1/2} r^h_{if+1,jf-1}$$
$$+ B^{+}_{if+1/2} r^h_{if+1,jf} + A^{++}_{if+1/2,jf+1/2} r^h_{if+1,jf+1}\Big]$$

where $A^{\pm\pm}_{if,jf}$, $B^{\pm}_{if,jf}$ and $C^{\pm}_{if,jf}$ are defined as follows

$$A^{\pm\pm}_{if,jf} = B^{\pm}_{if,jf} C^{\pm}_{if,jf}$$

$$(4.1.28)\qquad B^{-}_{if} = \frac{r^2_{if}}{r^2_{if}+r^2_{if-1}} \qquad B^{+}_{if} = \frac{r^2_{if}}{r^2_{if}+r^2_{if+1}}$$

$$C^{-}_{jf} = \frac{\sin^2\theta_{jf}}{\sin^2\theta_{jf}+\sin^2\theta_{jf-1}} \qquad C^{+}_{jf} = \frac{\sin^2\theta_{jf}}{\sin^2\theta_{jf}+\sin^2\theta_{jf+1}}$$

It is then clear that the interpolation of the coarse grid corrections should be done using the formulae

$$(4.1.29)\qquad v^h_{if+1,jf} = \frac{r^2_{if-1/2} B^H_{ic,jc} + r^2_{if+1/2} B^H_{ic+1,jc}}{r^2_{if-1/2}+r^2_{if+1/2}}$$

for those points which lie on the horizontal lines,

$$(4.1.30)\qquad v^h_{if,jf+1} = \frac{\sin^2\theta_{jf-1/2} B^H_{ic,jc} + \sin^2\theta_{jf+1/2} B^H_{ic,jc+1}}{\sin^2\theta_{jf-1/2}+\sin^2\theta_{jf+1/2}}$$

for those lying in the vertical lines, and

$$v^{h}_{if+1,jf+1} = \left[r^{2}_{if-1/2} (\sin^{2}\theta_{jf-1/2} B^{H}_{ic,jc} + \sin^{2}\theta_{jf+1/2} B^{H}_{ic,jc+1}) \right.$$

(4.1.31) $$\left. + r^{2}_{if+1/2} (\sin^{2}\theta_{jf-1/2} B^{H}_{ic+1,jc} + \sin^{2}\theta_{jf+1/2} B^{H}_{ic+1,jf}) \right] /$$

$$(r^{2}_{if-1/2} + r^{2}_{if+1/2})(\sin^{2}\theta_{jf-1/2} + \sin^{2}\theta_{jf+1/2})$$

for fine grid points centered in coarse grid squares. A good test to see if this operators transfer the residuals of our equation in a proper way is the following. Consider the following problem on a grid with mesh-size h

(4.1.32) $$L^{h} u^{h} = \delta^{h}(\underline{\xi}) = \begin{cases} 1 & \underline{x} = \underline{\xi} \\ 0 & \underline{x} \neq \underline{\xi} \end{cases} \qquad \underline{x} \equiv (r, \theta)$$

with the boundary conditions

(4.1.33) $$u^{h} = 0 \qquad \text{on the four edges of the grid,}$$

where L^{h} is the discretized operator (4.1.26) of equation (4.1.25). Consider now the same problem on a grid with mesh-size $H=2h$ whose right hand side is calculated using the operator I^{H}_{h} of equation (4.1.27)

(4.1.34) $$L^{H} u^{H} = I^{H}_{h} \delta^{h}(\underline{\xi})$$

This problem together with (4.1.32) should be the same discrete representation of the differential equation $Lu=\delta(\underline{\xi})$ whose solution is the Green's function. Then choosing $\underline{\xi}$ on grid h we solve equation (4.1.32) by doing a certain number of relaxation sweeps (until convergence) getting a solution u^{h}_{a}. Separately, we transfer the right hand side of equation (4.1.32) on grid H using the operator (4.1.28) and solve equation (4.1.33) till convergence by relaxation. The solution u^{H} then it is interpolated using (4.1.29)-(4.1.32) to the fine grid obtaining another fine grid solution u^{h}_{b}. Far from ξ these two solutions should coincide and their ratio be near to one. In table IV the results of such an experiment for two grids in which the coarsest grid has 8x4 grid points, are shown for different grid points. We see that there is

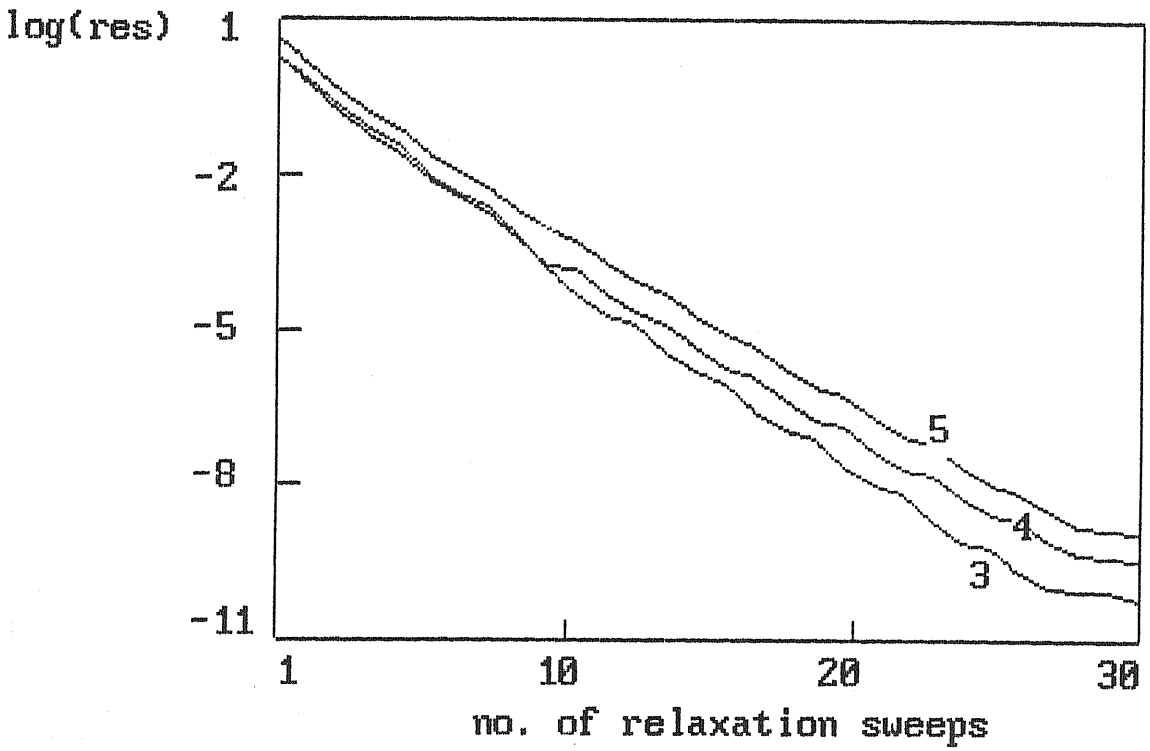

Fig. 22 - Residuals versus number of relaxations for the B-equation with Dirichlet boundary conditions. Multigrid with 5 levels is used.

a good agreement between the two solutions.

TABLE IV

The position of a grid point is referred to the finer grid

grid point	(2,2)	(3,2)	(3,3)	(4,4)	(2,8)
u_a^h / u_b^h	0.7	0.7	0.8	0.8	0.9

Using the relaxation scheme and the transfer operators described above we have implemented a Multigrid method for solving equation (4.1.26). The algorithm used is FMG with fixed FAS. The number of grids (levels) used was 5 and the coarsest grid had 4x2 grid points. We choose this pair of grid points because for it the ratio of the two mesh-sizes is nearly one (h_r/h_ϑ=1.24 for R=50). An optimal pair would be 8x3 which gives h_r/h_ϑ=.93 but this would require more computational work on the coarsest grid. In order to separate any possible interferences of the boundary conditions (see later) with the interior equations we have done the first experiment using Dirichlet boundary conditions on the axis of symmetry and on the equatorial plane. This can be done since we know the analytic solution. Figure 22 shows the behaviour of the logarithm of the Euclidean norm of the residuals ($\|r^h\| = \left(\sum |r_{i,j}|^2 h_r h_\vartheta\right)^{1/2}$) with the number of relaxations sweeps made on the finest grid for each level. We show here the results for level 3, 4, and 5. These plots show the asymptotic algebraic convergence. The residuals decrease by several order of magnitude in a small number of relaxation. Here we used fixed algorithm. It is enough to make two relaxation sweeps before going to the next coarse grid. After a coarse grid correction another relaxation sweep if made in order to smooth those high frequency components that the interpolation could introduce. Therefore for each level, in every cycle we make three relaxation sweeps on the finest grid. Then in Fig. 22, for each level 30 relaxation sweeps correspond to ten Multigrid cycles. The results are very good, the residuals decrease with a more or less constant rate. This is a completely different situation with respect the standard iterative methods in

which the convergence rate is not constant and tends to slow down after a certain number of iterations.

To include the Neumann type of boundary conditions is not an easy task. The efficiency of the Multigrid is easily destroyed if these boundary conditions are not treated properly. The problem being that the interior equations are of an order higher than the boundary conditions. This can be seen as follow. Consider the usual model problem Lu=f with boundary conditions Bu=g. Suppose that L is an m-order differential operator and B is an ℓ-order one, with $\ell<m$. For those interior points close to the boundary the solution error v^h satisfies the discretized m-order interior equation

$$(4.1.35) \qquad L^h v^h_\alpha = h^{-m} \sum_\beta a_{\alpha\beta} v^h_\beta = r^h_\alpha$$

as well as the ℓ-order boundary conditions

$$(4.1.36) \qquad B^h v^h_\gamma = h^{-\ell} \sum_\beta a_{\gamma\beta} v^h_\beta = r^h_\gamma$$

Combining the two equations and solving with respect to the interior residuals r^h_α we get an expression whose leading term is $O(h^{\ell-m})$ for smooth errors ($v^h \sim O(1)$, therefore r^h_α, $r^h_\gamma \sim O(1)$), for non smooth error that term should be multiplied by the magnitude of the residuals. This means that if the boundary conditions are mixed with the interior equations then the interior residuals will change by an $O(h^{\ell-m})$ and since $\ell<m$ the smoothness of the interior residuals after relaxation will be destroyed, being usually $h<1$.

Following Brandt, a way around this difficulty is to relax the equation $\nabla^2_s B = \nabla^2_s g$ instead of Bu=g, where ∇^2_s is the Laplacian operator along the boundary and s is the boundary arclength. This increases ℓ by 2, making the perturbation to the interior smoothness negligible. In practice, this means that, instead of satisfying the given conditions at each boundary points, we only change its error to be equal to an average of the errors at neighboring boundary points. In case the boundary smoothing factor is not as good as the interior one, a couple of boundary sweeps may be done per each interior one. In our coordinates the operator ∇^2 corresponds to take the second partial derivatives with respect

to r along the boundary. This operator can be applied to the discretized version of the boundary conditions. We use second order central differences for approximate the derivatives at the boundary. This introduces extra grid points at which the value of the unknown variables can be extrapolated using a certain number of interior grid points. We used a three points interpolation formulae and the final discrete version of the boundary conditions is

$$(4.1.37) \qquad \frac{1.5B_{i,J}-2B_{i,J-1}+0.5B_{i,J-2}}{h_\vartheta} = g_{i,J} \qquad \text{at } \vartheta=\pi/2$$

$$(4.1.38) \qquad \frac{-1.5B_{i,1}+2B_{i,2}-0.5B_{i,3}}{h_\vartheta} = g_{i,1} \qquad \text{at } \vartheta=0$$

Taking the second derivative with respect to r of both sides of equation (4.1.37), the variation $\delta B_{i,J}=B^{new}_{i,J}-B^{old}_{i,J}$ due to a relaxation sweep is given by

$$(4.1.39) \qquad \delta B_{i,J}= \left[r_{i,J}- \frac{1}{2}(r_{i+1,J}+r_{i-1,J})\right]h_\vartheta/1.5$$

where

$$(4.1.40) \qquad r_{i,J}= g_{i,J}+\frac{1.5B_{i,J}-2B_{i,J-1}+0.5B_{i,J-2}}{h_\vartheta}$$

Similar relations would hold for the boundary condition at $\vartheta=0$ if this boundary conditions had to be treated in the same way. At this boundary, however, the situation is different. For $\vartheta\longrightarrow 0$ the left hand side of equation (4.1.25) goes to zero. Therefore the residuals relative to interior points near that boundary are very small and the changes on the residuals are very small so we do not need to treat this boundary conditions separately and we impose them.

Near the boundaries the residual transfer should be modified.

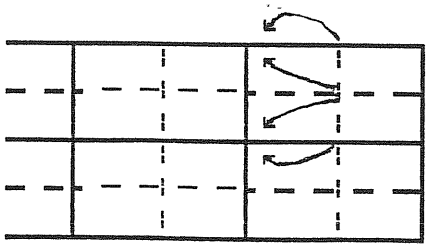

Fig. 23

This is because the influence of the residuals on the solution depend on the distance from the boundary. Therefore the residuals relative to the fine grid points close to the boundary should be represented differently as (4.1.27) in the coarse grid. We will not write the formulae here because they are easily constructed from (4.1.27) taking into account that the residuals of the fine grid points near the boundary should be distributed according to the scheme of Fig.23.

Figure 24 shows the history of the residuals versus the number of relaxation sweeps for each level when the Neumann boundary conditions (4.1.10) are implemented in the Multigrid scheme described above. Comparing these graphs with those relative to the experiment made with Dirichlet boundary conditions, we see that the efficiency is not anymore the same, but in comparison with standard iterative methods is still very good (see Fig. 25). Moreover we see that for each level a Multigrid cycle is not as efficient as it should be, in fact the wobbling showed in Fig 24 is not an effect of the graphics, but a real oscillation perhaps due to the intermixed residuals of the boundary with interior ones. After all their treatment is not trivial and it is significant Dendy's opinion (1982) about it: *Something special .... must be done at the boundary. This is easy in principle - especially if Brandt is nearby to advise - but it is a pain in practice.* In any case, this does not effect the relative solution error $\|B\|$ defined as

$$(4.1.40) \qquad \|B\| = \max_{i,j} \frac{|B^{computed} - B^{exact}|}{B^{exact}}$$

which is of the order 10^{-4} already at level 3. This is the minimum error we could expect since the approximation of applying the asymptotic boundary condition at r=50; the accuracy cannot be improved by going to finer grids.

Consider now the non-linear equation for the metric function X. This equation using the s coordinate can be written

$$(4.1.41) \qquad \partial_s(r\sin\vartheta \frac{B}{X} X_{,s}) + \partial_\vartheta(r\sin\vartheta \frac{B}{X} X_{,\vartheta}) = 0$$

We discretize this equation in conservative form, obtaining

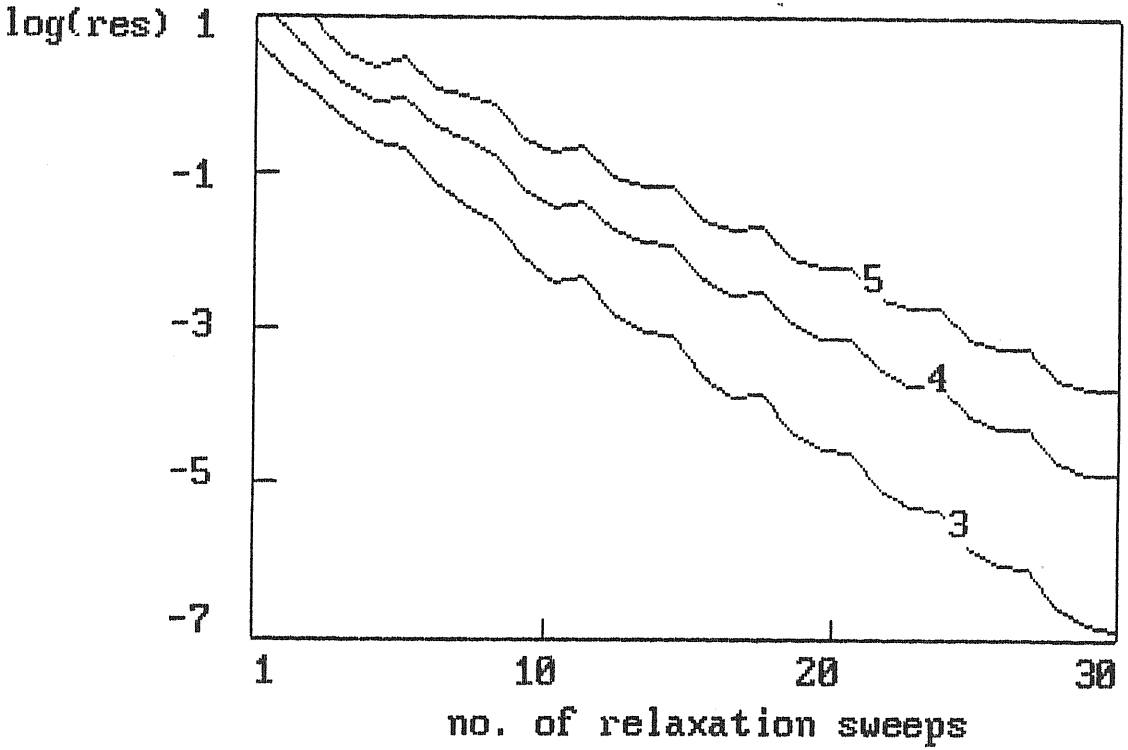

Fig. 24 - Residuals versus number of relaxations for the B-equation with Neumann boundary conditions. Multigrid with 5 levels is used.

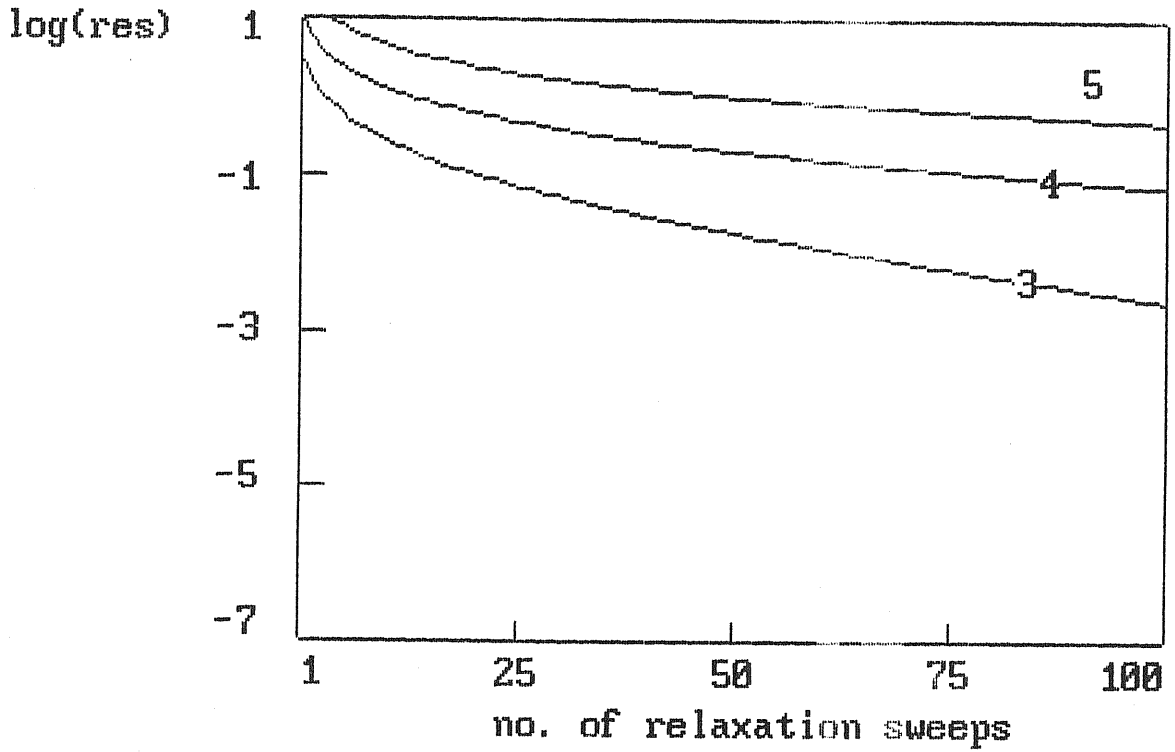

Fig. 25 - Residuals versus number of relaxation for the B-equation for three different grids when one-grid iteration method is used.

$$(4.1.42)\quad \frac{h_\vartheta}{h_s}\sin\vartheta_j\left[r_{i+1/2}\left(\frac{B}{X}\right)^h_{i+1/2,j}\left(X^h_{i+1/2,j}-X^h_{i,j}\right)+\right.$$

$$\left.r_{i-1/2}\left(\frac{B}{X}\right)^h_{i-1/2,j}\left(X^h_{i-1/2,j}-X^h_{i,j}\right)\right]+\frac{h_s}{h_\vartheta}r_i\left[\sin\vartheta_{j+1/2}\left(\frac{B}{X}\right)^h_{i,j+1/2}\cdot\right.$$

$$\left.\left(X^h_{i,j+1/2}-X^h_{i,j}\right)+\sin\vartheta_{j-1/2}\left(\frac{B}{X}\right)^h_{i,j-1/2}\left(X^h_{i,j-1/2}-X^h_{i,j}\right)\right]=0.$$

The resulting discretized equation is a non-linear algebraic equation since the values of B/X at mid-points are functions of X at full grid points. However relaxation in Multigrid is used to smooth the error and not for solving the equations, then it is enough to relax a non-linear equation through an approximate linearization. Thus, for example, if the equation has a term of the type uu_r and the current approximation just before relaxing at some point is $\tilde{u}$, then the relaxation at that point will involve only the term $\tilde{u}u_r$. A full linearization would in addition include the term $(u-\tilde{u})\tilde{u}_r$, but on local scale this term is negligible as long as the differences of $\tilde{u}$ at adjacent grid points are small compared with $\tilde{u}$ itself. Now, it is easy to verify that this is the case for large values of r, but not near the horizon where the metric functions have their most variations. In view of this considerations we have decided to construct a relaxation routine for equation (4.1.42) making one Newton step for the two nearest radial grid lines and apply Gauss-Seidel point relaxation, in the rest of the grid, to the approximated (as described above) discretized equations. The full Newton step require a full linearization of equation (4.1.42) and this depends on how X is evaluated at mid-points.

Since the metric functions are defined at full grid points their values at mid-points need to interpolated from those at full grid points. This can be done in several ways, using linear interpolation averaging the values at two adjacent grid points or using higher order interpolation which involve more points, in general the number of points (minus one) is the order of the interpolation. In our case we need to know the values of the ratio B/X at mid-points which lie on r=const or on ϑ=const grid lines. We could interpolate separately the two functions and then take

the ratio but since the ratio B/X is close to one far from the horizon we decide to interpolate the value of the ratio itself calculated at full grid points. Referring to Fig. 26, those points marked with the symbol ■ or ■■ are interpolated linearly. After a few experiments we found that 3-point polynomial interpolation is needed to recover $O(h^2)$ accuracy, for those points marked by ⧗ near the horizon. Any interpolation formula would require the value of the function at a grid point whose position for a given line precedes the position of the point in consideration. For evaluating $(B_{3/2,j}/X_{3/2,j})$ we cannot use the value of B/X at i=1 since on the horizon X=0. However the function B/X is regular at

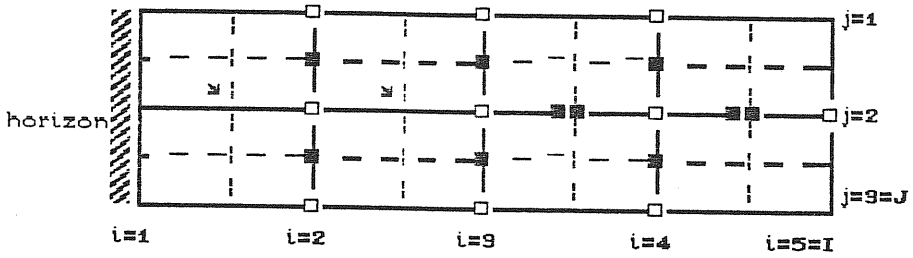

Fig. 26

the horizon therefore we can extrapolate backward the value of $(B/X)_{3/2}$ using the next three interior points for each value of j. Then for i=2 the formulae used to interpolate the function B/X at mid-points are

$$(4.1.43)\qquad \left(\frac{B}{X}\right)^h_{i-1/2,j} = \frac{1}{4}\left[\frac{15}{2}\left(\frac{B}{X}\right)^h_{i,j} - 5\left(\frac{B}{X}\right)^h_{i+1,j} + \frac{3}{2}\left(\frac{B}{X}\right)^h_{i+2,j}\right]$$

$$(4.1.44)\qquad \left(\frac{B}{X}\right)^h_{i+1/2,j} = \frac{1}{4}\left[\frac{3}{2}\left(\frac{B}{X}\right)^h_{i,j} + 3\left(\frac{B}{X}\right)^h_{i+1,j} - \frac{1}{2}\left(\frac{B}{X}\right)^h_{i+2,j}\right]$$

For i=3 we use

$$(4.1.45)\qquad \left(\frac{B}{X}\right)^h_{i-1/2,j} = \frac{1}{4}\left[\frac{3}{2}\left(\frac{B}{X}\right)^h_{i-1,j} + 3\left(\frac{B}{X}\right)^h_{i,j} - \frac{1}{2}\left(\frac{B}{X}\right)^h_{i+1,j}\right]$$

$$(4.1.46)\qquad \left(\frac{B}{X}\right)^h_{i+1/2,j} = \frac{1}{4}\left[-\frac{1}{2}\left(\frac{B}{X}\right)^h_{i-1,j} + 3\left(\frac{B}{X}\right)^h_{i,j} + \frac{3}{2}\left(\frac{B}{X}\right)^h_{i+1,j}\right]$$

For those points lying on ϑ=const grid lines we use

$$(4.1.47)\qquad \left(\frac{B}{X}\right)^h_{i,j-1/2} = \frac{1}{2}\left[\left(\frac{B}{X}\right)^h_{i,j-1} + \left(\frac{B}{X}\right)^h_{i,j}\right]$$

$$(4.1.48)\qquad \left(\frac{B}{X}\right)^h_{i,j+1/2} = \frac{1}{2}\left[\left(\frac{B}{X}\right)^h_{i,j+1} + \left(\frac{B}{X}\right)^h_{i,j}\right]$$

When these expressions are put in (4.1.42) we get a non-linear equation in $X_{i,j}$. We solve it by using the Newton method (see any textbook on numerical analysis, e.g. Press et al. 1986) on the two nearest grid lines to the horizon and the approximate relaxation on the rest of the grid. Let $\tilde{X}^h_{i,j}$ be the current approximation of the solution. After a Newton step the change $\delta X^h_{i,j}$ due to the iteration can be written symbolically as

$$(4.1.49)\qquad \delta X^h_{i,j} = - \frac{r^h(\tilde{X}^h_{i,j})}{\text{first derivative of (4.1.42) w.r.t. } X^h_{i,j}}$$

where r^h is the residual function. Putting the expressions for B/X calculated in mid-points in (4.1.42) and taking the first derivative of it the result is, for i=2

$$(4.1.50)\qquad \delta X^h_{2,j} = - r^h(\tilde{X}^h_{2,j}) \Big/ \left[q^h_{2,j} + \frac{B^h_{2,j}}{2(X^h_{2,j})^2}\left\{\frac{9}{4}(e^h_{2,j}X^h_{3,j} + 5w^h_{2,j}X^h_{1,j}) + n^h_{2,j}X^h_{2,j+1} + s^h_{2,j}X^h_{2,j-1} - X^h_{2,j}\left[\frac{9}{4}(e^h_{2,j}+5w^h_{2,j}) + n^h_{2,j} + s^h_{2,j}\right]\right\}\right]$$

and for i=3

$$(4.1.51)\qquad \delta X^h_{3,j} = - r^h(\tilde{X}^h_{3,j}) \Big/ \left[q^h_{3,j} + \frac{B^h_{3,j}}{2(X^h_{3,j})^2}\left\{\frac{9}{2}(e^h_{3,j}X^h_{4,j} + w^h_{3,j}X^h_{2,j}) + n^h_{3,j}X^h_{3,j+1} + s^h_{i,j}X^h_{3,j-1} - X^h_{3,j}\left[\frac{9}{2}(e^h_{3,j}+w^h_{3,j}) + n^h_{3,j} + s^h_{3,j}\right]\right\}\right]$$

where $e_{i,j}$, $w_{i,j}$, $n_{i,j}$, $s_{i,j}$ and $q_{i,j}$ are given by

$$e^h_{i,j} = \frac{h_\vartheta}{h_s} r_{i+1/2}\sin\vartheta_j$$

$$w^h_{i,j} = \frac{h_\vartheta}{h_s} r_{i-1/2}\sin\vartheta_j$$

(4.1.52)
$$n^h_{i,j} = \frac{h_s}{h_\vartheta} r_i \sin\vartheta_{j+1/2}$$

$$s^h_{i,j} = \frac{h_s}{h_\vartheta} r_i \sin\vartheta_{j-1/2}$$

$$q^h_{i,j} = e^h_{i,j}\left(\frac{B}{X}\right)^h_{i+1/2,j} + w^h_{i,j}\left(\frac{B}{X}\right)^h_{i-1/2,j} +$$

$$n^h_{i,j}\left(\frac{B}{X}\right)^h_{i,j+1/2} + s^h_{i,j}\left(\frac{B}{X}\right)^h_{i,j-1/2}$$

The transfer operators are constructed again using the diffusion coefficients of the original equation. In this case we should even include the ratio B/X, but this would require an unacceptable computational time to compute the residual transfer therefore we decide to use as weights only the function $r\sin\vartheta$. This is not bad, since the ratio B/X is close to one except near the horizon where in any case a much better relaxation is used. We will not write here the expressions for these operators since they can be obtained from those used for the B equation replacing r^2 with r and $\sin^2\vartheta$ with $\sin\vartheta$.

Using the recipes described above we solved the equation for X using the same algorithm (FMG with fixed FAS) used for the B equation. The first experiments were made trying to separate several features which when present together would make it difficult to decide which in particular was the cause for any possible trouble. The way in which we proceeded was the following. First we fixed the analytic value of B avoiding having to solve its equation at the same time and for the non-linear term we similarly used the analytic value of X, in order to see the performance of the relaxation routine neglecting the non-linearity. When we got a satisfactory answer we started trying several interpolation choices in the two nearest grid lines on the horizon. As we already mentioned the best answer was given using three points interpolation formulae. These experiments were done using Dirichlet boundary conditions as for the B equation. Then we introduced the Neumann boundary conditions and finally we considered the full problem. The two equations are solved separately using Gauss-Seidel point relaxation as described above.

In Fig. 27 the behaviour of an average of the residuals relative to the two equations versus the number of relaxation sweeps in successively finer grids is shown. The figure shows how the residuals decrease rapidly in a small number of relaxations. For comparison in Fig. 28 the same quantities are plotted when only one grid is used with different meshes. The result of this comparison is that Multigrid needs only a few iterations to reduce the residuals by several order of magnitude whereas for the fixed grid even a hundred iterations do not decrease the residuals to those values. Moreover for a given grid, we can compare the slope of the curve. In the Multigrid case the slope is more or less constant whereas in the one-grid case it tends asymptotically towards a horizontal line. As noted previously, this is due to the fact that smooth components are not reduced and therefore convergence slows down.

In table V the relative errors for the metric functions B and X, calculated using L_∞ norms (see definition in (4.1.40)), are

TABLE V

level	grid	$\|B\|$	$\|X\|$
2	8x4	$4.\times10^{-4}$	7.9×10^{-2}
3	16x8	$4.\times10^{-4}$	2.9×10^{-2}
4	32x16	$4.\times10^{-4}$	4.5×10^{-3}
5	64x32	$4.\times10^{-4}$	8.9×10^{-4}

shown. Notice that the equation for B is already solved on grid 2 up to the approximation of applying the asymptotic boundary condition at r=50 M. This approximation (used even for the X metric function) sets a lower limit on the error; the accuracy cannot be improved by going to finer grids. For the non-linear equation in X we need to use five levels to reach the lower limit on the accuracy.

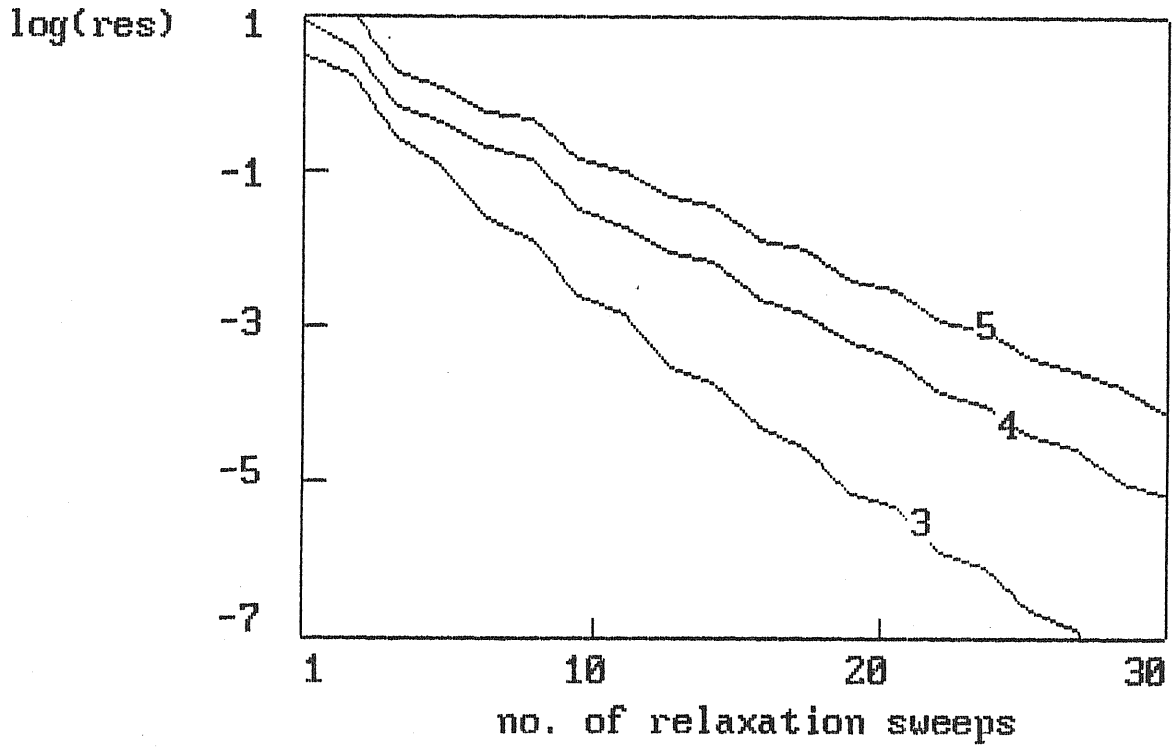

Fig. 27 - Residuals versus number of relaxations for the Schwarzschild case. Multigrid with 5 levels is used.

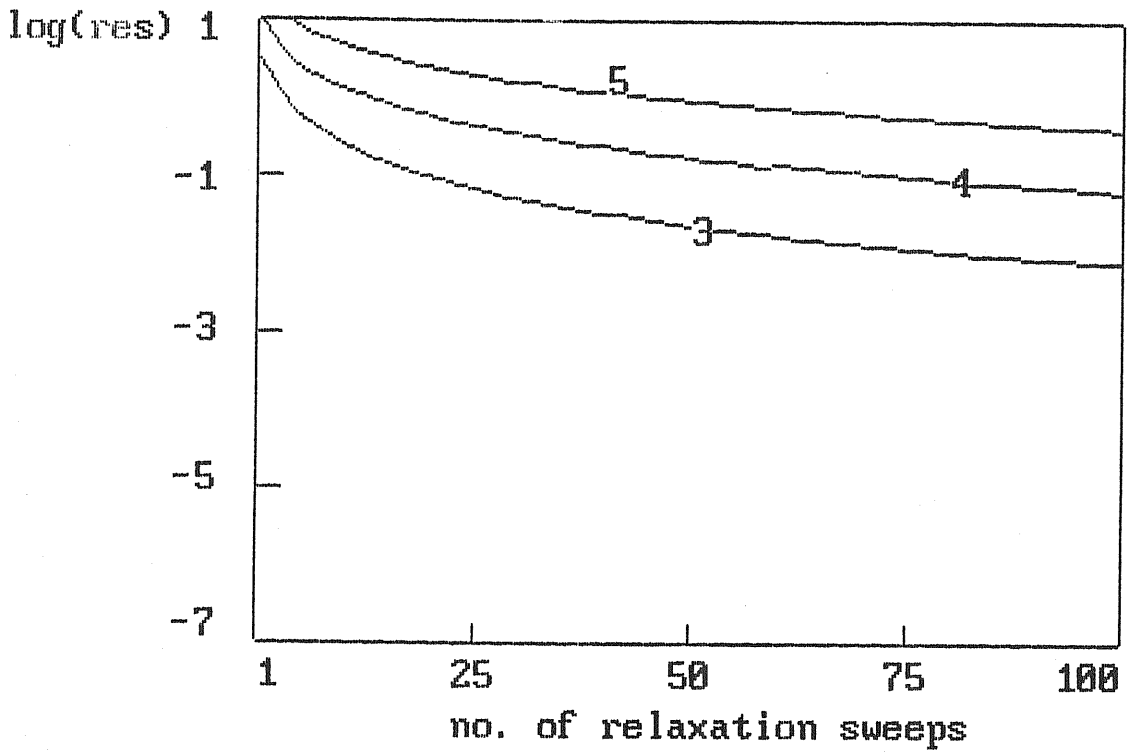

Fig. 28 - Residuals versus number of relaxations for the Schwarzschild case for three different grids when one-grid iteration method is used.

4.2 The Kerr case.

We now turn our attention to the Kerr solution for a stationary and axisymmetric vacuum space-time. This solution is generally expressed in terms of Boyer and Lindquist (BL) (1967) coordinates which are different than the ones used in this thesis. In BL coordinates the metric is written (here M=1) as

$$(4.2.1)\qquad ds^2 = -\left(1-\frac{2R}{\Sigma}\right)dt'^2 - 4\frac{\alpha R\sin^2\vartheta}{\Sigma}\,dt'd\phi' + \frac{\Sigma}{\Delta}\,dR^2 + \Sigma d\vartheta'^2 + \left(R^2+\alpha^2+2\alpha^2R\frac{\sin^2\vartheta}{\Sigma}\right)\sin^2\vartheta\, d\phi'^2$$

Where α is the specific angular momentum and Σ and Δ are defined as follows

$$(4.2.2)\qquad \Sigma = R^2 + \alpha^2\cos^2\vartheta$$

$$(4.2.3)\qquad \Delta = R^2 - 2R + \alpha^2$$

we define here another quantity A which will be used after

$$(4.2.4)\qquad A = (R^2+\alpha^2)^2 - \alpha^2\Delta\sin^2\vartheta.$$

Since the radial coordinate appearing in the metric (2.1.18) is different of the BL radial coordinate R, we need to know a relation between them that is a function r(R). Comparison of corresponding differentials yields five relations for the eight quantities X, ω, B, y, t, r, ϑ and ϕ in terms of BL coordinates. We impose three additional relations on the coordinates to make the problem determinate

$$(4.2.5)\qquad t = t' \qquad \vartheta = \vartheta' \qquad \phi = \phi'.$$

Then, equations (2.1.18), (4.2.1) and (4.2.5) imply

$$(4.2.6)\qquad e^{-2\nu}(-1 + r^2\sin^2\vartheta B^2\omega^2 e^{-2\nu}) = 1 - 2R/\Sigma$$

$$(4.2.7)\qquad r^2B^2\omega\, e^{-2\nu} = 4\alpha R/\Sigma$$

$$(4.2.8)\qquad e^{2y-2\nu}dr^2 = (\Sigma/\Delta)dR^2$$

$$(4.2.9)\qquad e^{2y-2\nu} = \Sigma/r^2$$

$$r^2 B^2 e^{-2\nu} = R^2 + \alpha^2 + 2\alpha^2 R\sin^2\vartheta/\Sigma \qquad (4.2.10)$$

Substituting the expression (4.2.9), equation (4.2.8) becomes

$$\frac{dr}{r} = \frac{dR}{\Delta^{1/2}} \qquad (4.2.11)$$

which, if we impose the condition

$$\lim_{R\to\infty} \frac{r}{R} = 1 \qquad (4.2.12)$$

may be integrated directly giving

$$r = \frac{1}{2}\left[\sqrt{R^2 - 2R + \alpha^2} + R - 1\right] \qquad (4.2.13)$$

or inverting,

$$R = \left[(2r+1)^2 - \alpha^2\right]/4r. \qquad (4.2.14)$$

Then combining the other equations we get finally

$$e^{2\nu} = \Sigma\Delta/A \qquad (4.2.15)$$

$$\omega = 2\alpha R/A \qquad (4.2.16)$$

$$e^{2\gamma} = \Sigma^2\Delta/r^2 A \qquad (4.2.17)$$

$$B^2 = \Delta/r^2 \qquad (4.2.18)$$

The parameter h of the horizon in our coordinate then is

$$h = (1 - \alpha^2)^{1/2} \qquad (4.2.19)$$

This quantity divided by 2 is used to rescale the radial coordinate as in Schwarzschild case. Equations (4.2.15)-(4.2.18) represent the analytic solution of the present test problem and this is used as initial approximation as well.

For stationary and axisymmetric space-times, in addition to the equation for B (which will not be considered in the present discussion because this equation is treated as described in the previous section), we have

$$\nabla\cdot\left(\frac{B}{X}\nabla X\right) - \frac{1}{2} r^2\sin^2\vartheta\,\frac{B^3}{X^4}\,\nabla\omega\cdot\nabla\omega = 0 \qquad (4.2.20)$$

$$\nabla\cdot(r^2\sin^2\vartheta\,\frac{B^3}{X^4}\,\nabla\omega) = 0$$

with the boundary conditions

(4.2.21) $X = 0 \qquad \omega = \Omega_H = \alpha(1-\alpha^2)^{1/2}/2\left[1+(1-\alpha^2)^{1/2}\right]$ at $r=1$

(4.2.22) $X = 1 - \frac{2}{r} \qquad \omega = \frac{8\alpha}{(1-\alpha^2)r^3}\left[1-\frac{\sigma}{(1-\alpha^2)^{1/2}r}\right]$ at $r=50$

(4.2.23) $X_{,\vartheta} = \omega_{,\vartheta} = 0$ at $\vartheta = 0, \pi/2.$

Note that the equations have already been rescaled by $h/2$. The metric function ω is not dimensionless, so doing the rescaling we need to multiply it by $h/2$. In these units the solution is determined by two parameters Ω_H and α. For our experiments we choose Ω_H to be given by the Kerr solution as (4.2.21), then it will be enough actually to specify a value for α. The range allowed for α is $0\le\alpha<1$.

Equations (4.2.20) are strongly non-linear and coupled each other. To relax them we apply the same idea of doing a Newton step on the two nearest grid lines to the horizon and make relaxation of the approximate equations on the rest of the grid. The divergence terms are discretized in conservative form. The extra term in the first equation (4.2.20), which will be referred to as the equation for X, is discretized as follows

(4.2.24) $$-\frac{1}{2}r_i^3\sin^3\vartheta_j\left[\frac{h_\vartheta}{h_r}(\omega_{i+1,j}-\omega_{i,j})(\omega_{i,j}-\omega_{i-1,j}) + \frac{h_r}{h_\vartheta}(\omega_{i,j+1}-\omega_{i,j})(\omega_{i,j}-\omega_{i,j-1})\right]$$

The second equation (4.2.20) is discretized as

(4.2.25) $$\frac{h_\vartheta}{h_s}\sin^3\vartheta_j\left[r^3_{i+1/2}\left(\frac{B^3}{X^4}\right)^h_{i+1/2,j}(\omega^h_{i+1/2,j}-\omega^h_{i,j}) + r^3_{i-1/2}\left(\frac{B^3}{X^4}\right)^h_{i-1/2,j}(\omega^h_{i-1/2,j}-\omega^h_{i,j})\right] + \frac{h_s}{h_\vartheta}r_i^3\left[\sin^3\vartheta_{j+1/2}\left(\frac{B^3}{X^4}\right)^h_{i,j+1/2}\right.$$

$$(\omega^{h}_{i,j+1/2}-\omega^{h}_{i,j}) + \sin^{9}\vartheta_{j-1/2}\left[\left(\frac{B^{3}}{X^{4}}\right)^{h}_{i,j-1/2}(\omega^{h}_{i,j-1/2}-\omega^{h}_{i,j})\right] = 0.$$

These two equations form a set of non-linear algebraic equations which are solved as we already said using the Newton method only in the first two grid lines. For a system of equation

(4.2.26) $$F^{1}(x^{1},x^{2}) = 0 \qquad F^{2}(x^{1},x^{2}) = 0$$

the method gives the solutions in the form

(4.2.27) $$x^{n}_{k+1}=x^{n}_{k} - \frac{1}{D}\begin{bmatrix} \frac{\partial F^{2}}{\partial x^{2}} & -\frac{\partial F^{1}}{\partial x^{2}} \\ -\frac{\partial F^{2}}{\partial x^{1}} & \frac{\partial F^{1}}{\partial x^{1}} \end{bmatrix}\begin{bmatrix} F^{1} \\ F^{2} \end{bmatrix} \qquad n=1,2$$

where D is

(4.2.28) $$D = \begin{vmatrix} \frac{\partial F^{2}}{\partial x^{2}} & \frac{\partial F^{1}}{\partial x^{2}} \\ \frac{\partial F^{2}}{\partial x^{1}} & \frac{\partial F^{1}}{\partial x^{1}} \end{vmatrix}$$

In order to calculate the Jacobian of the system in consideration we must decide first the interpolation formulae for picking up values of the function B^{3}/X^{4} at mid-points. Far from the horizon we can use the same formulae used for B/X in the previous case considered. Approaching the horizon both B and X go to zero and B^{3}/X^{4} tends to infinity, therefore no polynomial interpolation there could give the right behaviour of the function. This is the most difficult task of the test problem in consideration. It is important to solve it definitely since as long as an horizon is present in the configuration we look for equilibrium we will face with this divergence. Again to make experiments for this interpolation we used Dirichlet boundary conditions and as boundary conditions at r=50 the analytic value of X, ω and B were used. The best interpolation of this function which we have found so far is based on the following argument. In the Schwarzschild case the function B^{3}/X^{4} has the following dependence on r

$$\frac{B^9}{X^4} = \frac{(r+1)^7}{r^6(r-1)} \tag{4.2.29}$$

For a given value of ϑ, B^9/X^4 is only a function of r, then we can construct an interpolation formulae from the assumption that B^9/X^4 on r grid lines behaves like

$$\frac{B^9}{X^4} = \mathbb{R}\, a + b \tag{4.2.30}$$

where a and b are two arbitrary constants and

$$\mathbb{R} = \frac{(r+1)^7}{r^6(r-1)} \tag{4.2.31}$$

The constants a and b can be determined supposing that (4.2.30) holds for two different points giving two equations. After some trivial algebra we get, for i=2

$$\left[\frac{B^9}{X^4}\right]^h_{3/2,j} = \frac{(\mathbb{R}_{3/2}-\mathbb{R}_3)\left[\frac{B^9}{X^4}\right]^h_{2,j} + (\mathbb{R}_2-\mathbb{R}_{3/2})\left[\frac{B^9}{X^4}\right]^h_{3,j}}{\mathbb{R}_2 - \mathbb{R}_3} \tag{4.2.32}$$

$$\left[\frac{B^9}{X^4}\right]^h_{5/2,j} = \frac{(\mathbb{R}_{5/2}-\mathbb{R}_3)\left[\frac{B^9}{X^4}\right]^h_{2,j} + (\mathbb{R}_2-\mathbb{R}_{5/2})\left[\frac{B^9}{X^4}\right]^h_{3,j}}{\mathbb{R}_2 - \mathbb{R}_3} \tag{4.2.33}$$

and for i>2

$$\left[\frac{B^9}{X^4}\right]^h_{i-1/2,j} = \frac{(\mathbb{R}_{i-1/2}-\mathbb{R}_i)\left[\frac{B^9}{X^4}\right]^h_{i-1,j} + (\mathbb{R}_{i-1}-\mathbb{R}_{i-1/2})\left[\frac{B^9}{X^4}\right]^h_{i+1,j}}{\mathbb{R}_{i-1} - \mathbb{R}_i} \tag{4.2.34}$$

$$\left[\frac{B^9}{X^4}\right]^h_{i+1/2,j} = \frac{(\mathbb{R}_{i+1/2}-\mathbb{R}_{i+1})\left[\frac{B^9}{X^4}\right]^h_{i,j} + (\mathbb{R}_i-\mathbb{R}_{i+1/2})\left[\frac{B^9}{X^4}\right]^h_{i+1,j}}{\mathbb{R}_i - \mathbb{R}_{i+1}} \tag{4.2.35}$$

For interpolating the values of the function of the mid-points which lie on r=const grid lines we used formulae similar to (4.1.47) and (4.1.48). Using then the equations (4.1.43)-(4.1.48),

(4.2.32)-(4.2.35) we can calculate the changes to the metric functions X and ω due to a Newton step by the following formulae

$$(4.2.36)\qquad \delta X^h_{i,j} = \left[\mathbb{D}^h_{i,j}(r^1)^h_{i,j} - \mathbb{B}^h_{i,j}(r^2)^h_{i,j}\right] / \left(\mathbb{A}^h_{i,j}\mathbb{D}^h_{i,j} - \mathbb{C}^h_{i,j}\mathbb{B}^h_{i,j}\right)$$

$$(4.2.37)\qquad \delta\omega^h_{i,j} = \left[-\mathbb{C}^h_{i,j}(r^1)^h_{i,j} + \mathbb{A}^h_{i,j}(r^2)^h_{i,j}\right] / \left(\mathbb{A}^h_{i,j}\mathbb{D}^h_{i,j} - \mathbb{C}^h_{i,j}\mathbb{B}^h_{i,j}\right)$$

where $(r^1)^h_{i,j}$ and $(r^2)^h_{i,j}$ are the residuals relative to the equation relative to X and to ω respectively. The grid functions $\mathbb{A}^h_{i,j}$, $\mathbb{B}^h_{i,j}$, $\mathbb{C}^h_{i,j}$ and $\mathbb{D}^h_{i,j}$ are defined in Appendix C.

The transfer operators are constructed using the diffusion coefficients of the differential equations. The residuals relative to the equation for X are transferred in the same way we have done in treating the Schwarzschild case. For the equation in ω again, including the ratio B^9/X^4 would require an unacceptable computational time for calculating the residuals so we use as weights only the function $r^9\sin^9\vartheta$ and the weights can be written from (4.1.27)-(4.1.28) replacing r^2 with r^9 and $\sin^2\vartheta$ with $\sin^9\vartheta$. The experiments were done using FMG with fixed FAS algorithm. The relaxation of the system and the residuals transfer were tested solving the problem with the analytic values of the metric functions at the boundaries. The results of these runs are shown in Figs. 29-31. In these pictures an average of the residuals of the three equations are shown in function of the number of relaxation sweeps for different levels and three different values of the specific angular momentum α (α=0.001, 0.5, 0.9). The algebraic convergence factor is still as good as would be expected, but it deteriorates increasing α. This is perhaps due to the increase of the non-linearity. In highly relativistic cases those terms which we have neglected in the relaxation may become important in some coarse grid and there we need to update the right hand side of the coarse grid equations with those terms. Table VI-VIII show the solution error for the metric functions X and ω defined in a similar way as in (4.1.40). The tables do not contain the same quantity calculated for the B metric function, since, being the relevant equation solved separately by the same algorithm used in the Schwarzschild case, the results are exactly

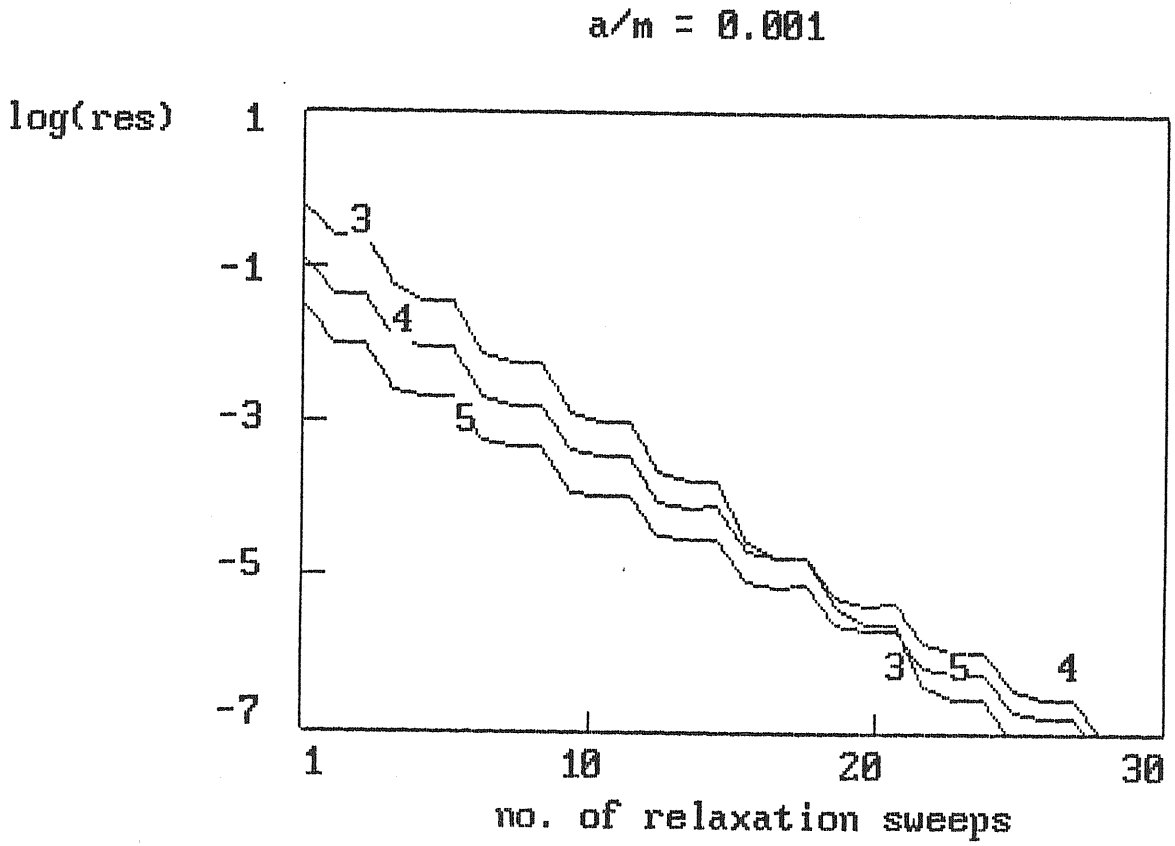

Fig. 29 - Residuals versus number of relaxations for the Kerr case with Dirichlet boundary conditions. Multigrid with 5 levels is used.

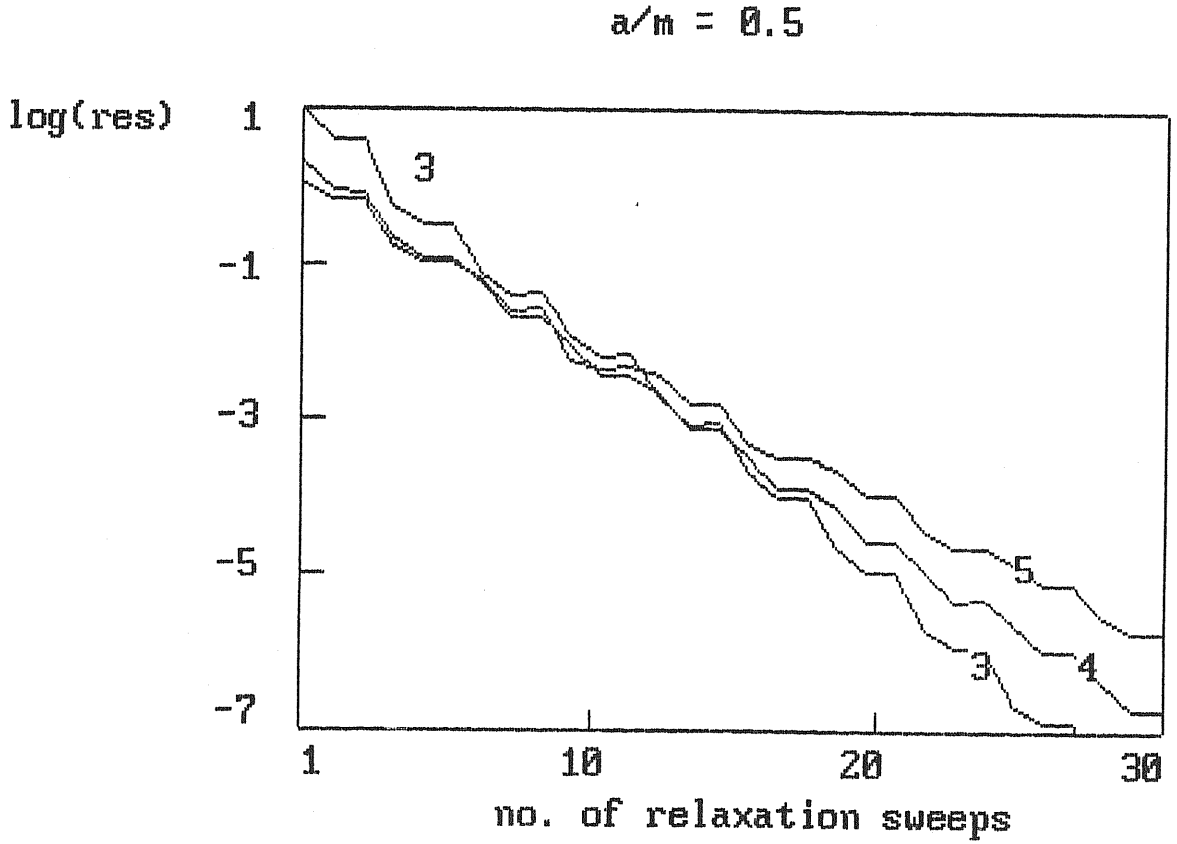

Fig. 30 - Residuals versus number of relaxations for the Kerr case with Dirichlet boundary conditions. Multigrid with 5 levels is used.

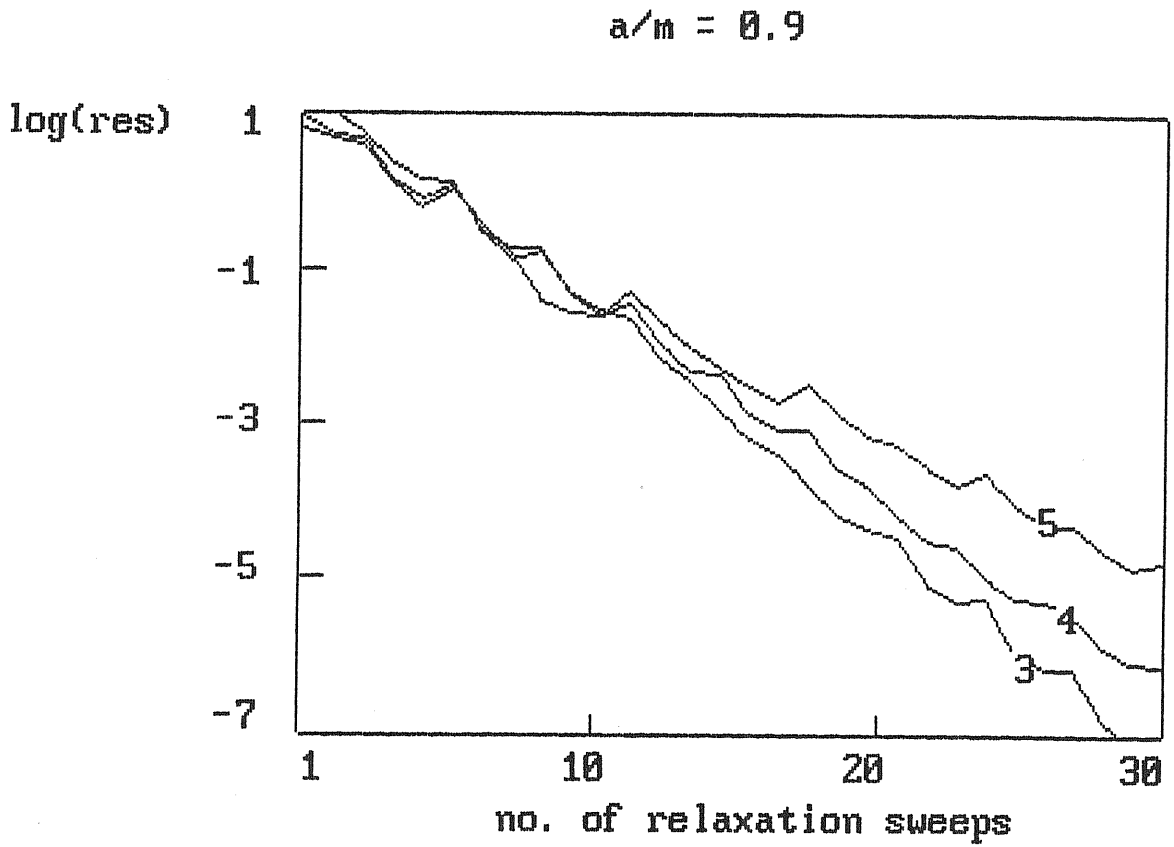

Fig. 31 - Residuals versus number of relaxations for the Kerr case with Dirichlet boundary conditions. Multigrid with 5 levels is used.

the same. Going from coarse grid to progressively finer grids the ratio of these errors should be asymptotically equal to four. From the tables we see that this tendency is clear for the slow rotating case (α=0.001). In the other cases is not as clear as it was for the Schwarzschild case. This is perhaps due to the way how the ratio B^9/X^4 is interpolated at half grid points near the horizon. Further numerical experiments using different interpolation formulae need to be done to improve the solution errors.

Fig. 32 show the history of the averaged residuals versus the number of relaxation sweeps in the case in which the Neumann boundary conditions were implemented. This is a clear example which shows how a bad treatment of non-Dirichlet boundary conditions completely destroy the efficiency of the Multigrid method. In this case the coupling of the boundary conditions residuals with the nearby interior residuals make some of the mode unstable (the residuals in the coarser grids are not smooth). These modes are very slow to converge in relaxation. Perhaps an averaging of the solution, done in the coarse grid where the cost is negligible, could annihilate these unstable mode. Further investigations and more numerical experiments need to be done to take care of this.

TABLE VI

$\alpha = 0.001$

level	grid	$\|x\|$	$\|\omega\|$
2	8x4	$2.8\text{x}10^{-2}$	$2.4\text{x}10^{-2}$
3	16x8	$1.9\text{x}10^{-2}$	$1.8\text{x}10^{-2}$
4	32x16	$3.4\text{x}10^{-3}$	$8.8\text{x}10^{-3}$
5	64x32	$5.9\text{x}10^{-4}$	$3.2\text{x}10^{-3}$

TABLE VII

$\alpha = 0.5$

level	grid	$\|x\|$	$\|\omega\|$
2	8x4	$3.4\text{x}10^{-2}$	$2.2\text{x}10^{-2}$
3	16x8	$1.7\text{x}10^{-2}$	$1.5\text{x}10^{-2}$
4	32x16	$6.4\text{x}10^{-3}$	$6.7\text{x}10^{-3}$
5	64x32	$2.2\text{x}10^{-4}$	$2.3\text{x}10^{-3}$

TABLE VIII

$\alpha = 0.9$

level	grid	$\|x\|$	$\|\omega\|$
2	8x4	$6.2\text{x}10^{-2}$	$2.2\text{x}10^{-2}$
3	16x8	$3.5\text{x}10^{-2}$	$7.7\text{x}10^{-3}$
4	32x16	$1.6\text{x}10^{-3}$	$2.1\text{x}10^{-3}$
5	64x32	$6.8\text{x}10^{-3}$	$6.5\text{x}10^{-4}$

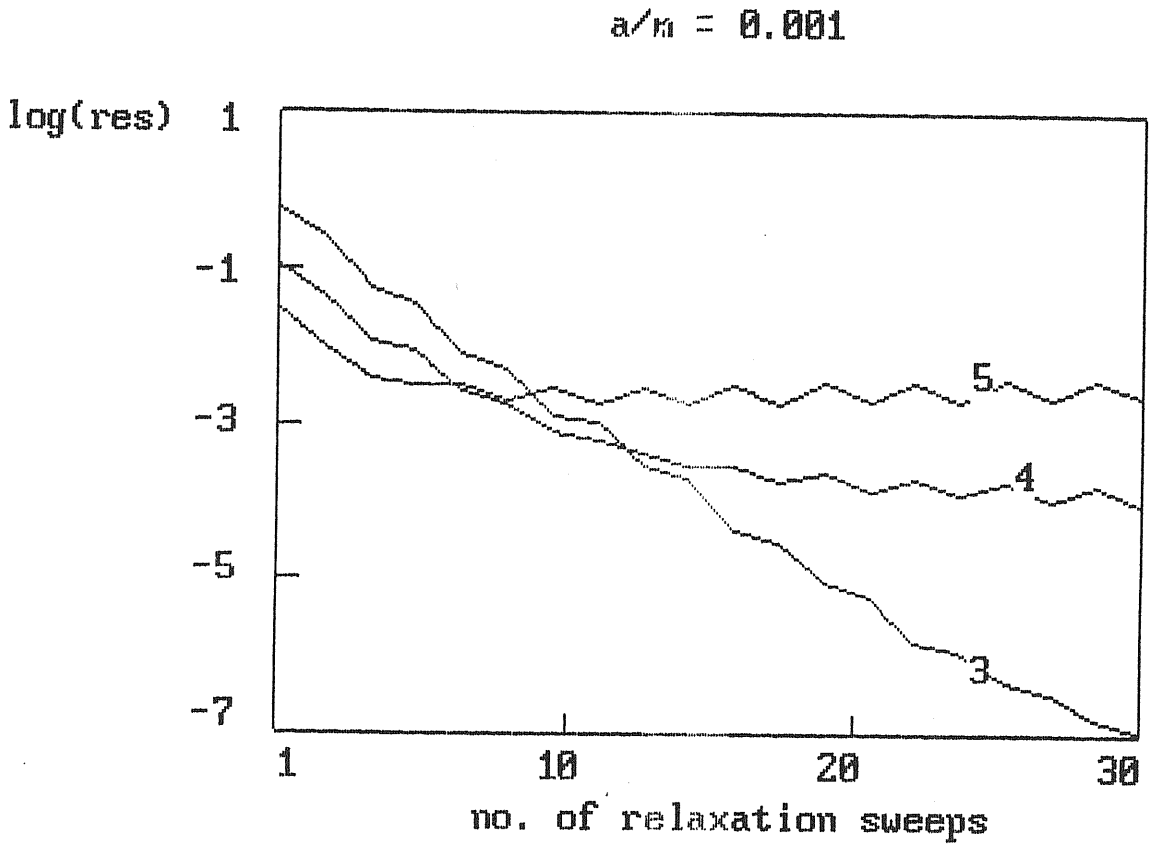

Fig. 32 - Residuals versus number of relaxations for the Kerr case with Neumann boundary conditions. Multigrid with 5 levels is used.

CHAPTER V

MULTIGRID IN GENERAL RELATIVITY: INFINITESIMALLY THIN DISKS

The next step on the way to developing a numerical code for finding the equilibrium configuration of a self-gravitating torus around a rapidly rotating black hole, is that of considering a zero pressure self-gravitating infinitesimally thin disk around a black hole. This configuration represent the simplest sort of rapidly rotating object which can be considered. The configuration without any black hole at the center has been extensively studied by Bardeen and Wagoner (1969, 1971) and we take this work as background for writing down the equations which we will solve numerically using the Multigrid. The solution of such a problem represent a new numerical solution of Einstein's equations which can give us a physical insight of the more complicated one, that is when the disk is supposed to have finite thickness. The simplicity of the problem stay on the fact that matter source terms enter into Einstein's equations only throughout the boundary conditions on the equatorial plane where the disk is supposed to lie representing a discontinuity and outside of it the space-time can be considered vacuum. Therefore, from the mathematical point of view the structure of the problem is the same as of the vacuum stationary and axisymmetric space-time described in the previous chapter, but with different boundary conditions.

Before writing down the relativistic equations for this configuration we consider the corresponding Newtonian case using a pseudo-Newtonian potential to describe the field generated by the black hole. This problem can be solved analytically and it is interesting to consider such a case because this will serve to test, again with an analytical solution, the performance of the numerical code in the case of no rotation and Newtonian limit. Since even in Newtonian theory this is a new solution we shall dedicate the next section on it.

5.1 Newtonian infinitesimally thin disks around a black hole.

Since Newtonian theory is linear the total potential of a configuration made of an infinitesimally thin disk and a black hole can be considered to be the sum of the pseudo-Newtoian potential plus the potential due to the disk, which is given by solving the Poisson equation for a given distribution of density representing the disk. The solution for an infinitesimal thin disk without central body was found by Hunter in 1963 for modeling spiral galaxy. We will use such a solution for constructing a sequence of new ones representing a disk around a black hole in the following way. We write down the potential ϕ_{in} of a disk whose radius is r_{in}, then we compute the potential ϕ_{out} of a disk with radius $r_{out}>r_{in}$. The difference $\phi_{out}-\phi_{in}$ between the two potentials then will be the potential of a disk whose inner edge is at r_{in} and outer edge at r_{out}, finally to this we add the pseudo-Newtonian potential.

To solve the Poisson equation for an infinitesimally thin disk we use oblate spheroidal coordinates since such a disk can be made a level surface of one of the spheroidal coordinates. In this coordinates Laplace's equation is separable and elementary solutions that represent matter distributed on the disk can be found. By superposition of such solutions, expressions for the density on the disk, the gravitational potential in its plane, and hence its rotational velocity can be derived in the form of series of functions. By means of these series, it is possible to derive the density distribution from a given rotational law or vice versa. For axisymmetric distribution of matter, these quantities are given in the form of a series of Legendre polynomials and functions have to be expressed in this form rather than as Fourier-Bessel integrals as required for not finite disk (Toomre, 1963).

An infinitesimally thin disk with radius r_{in} is a level surface $\zeta=0$ of one of the spheroidal coordinates defined by the relations

$$(5.1.3) \qquad r = r_o\left[(\zeta^2+1)(1-\mu^2)\right]^{1/2} \qquad z = r_o\zeta\mu$$

The surfaces ζ^2=const and μ^2=const are respectively confocal ellipsoids and hyperboloids of revolution around the z-axis (see Fig.). The coordinates ζ and μ in our case vary in the ranges $0 \leq \zeta \leq \infty$ and $-1 \leq \mu \leq 1$. In these coordinates Laplace's equation is separable and the solutions are of type (see e.g. Morse and Feshbach, 1956)

$$(5.1.2) \qquad P_n^m(\zeta) P_n^m(\mu) e^{im\vartheta} \quad \text{and} \quad q_n^m(\zeta) P_n^m(\mu) e^{im\vartheta}$$

where

$$(5.1.3) \qquad P_n^m(x) = i^{m-n} P_n^m(ix)$$

$$= \frac{(2n)!\,(1+x^2)^{m/2}}{2^n\, n!\, (n-m)!} \left\{ x^{n-m} + \frac{(n-m)(n-m-1)x^{n-m-2}}{2(2n-1)} + \cdots \right\}$$

and

$$(5.1.4) \qquad q_n^m(x) = (-1)^{m} \frac{(n+m)!}{(n-m)!} P_n^m(x) \int_x^{\infty} \frac{dy}{(1+y^2)\left[P_n^m(y)\right]^2}$$

where $P_n^m(x)$ are associated Legendre functions. Since as $x \longrightarrow \infty$, P_n^m becomes large, whereas q_n^m goes to zero we can consider, according to Hunter, the gravitational potential to be

$$(5.1.5) \qquad \psi = \frac{q_n^m(\zeta) P_n^m(\mu) e^{im\vartheta}}{q_n^m(0)}$$

This potential satisfies Laplace's equation at all points not on the disk, and decays at large distances from the disk as $(x^2+y^2+z^2)^{-(n+1)/2}$. It is continuous across the disk only if $(n-m)$ is an even integer and therefore $P_n^m(\mu)$ is an even function of μ. The normal component of $\nabla\psi$ however is discontinuous across the disk, therefore we must have a surface density of matter σ on the disk. Integrating Poisson's equation, imposing that the integral of a second normal derivative is equal to two times the normal derivative on the disk and that integrals of finite quantities on the disk are zero we get

$$(5.1.6) \qquad -4\pi G\, \sigma = 2\left[\frac{1}{h_\zeta} \frac{\partial \psi}{\partial \zeta}\right]_{\zeta=0}$$

where h_ζ is the scale factor relative to the spheroidal coordinate ζ, which is given by

$$(5.1.7) \qquad h_\zeta = r_o \left[\frac{\zeta^2+\mu^2}{\zeta^2+1}\right]$$

On the plane of the disk ($\zeta=0$), we have $h_\zeta=\pm\mu r_o$ on both sides of the disk. Defining $\xi=|\mu|$ we make use of the reflection symmetry around the equatorial plane and on the disk we can then write

$$(5.1.8) \qquad \xi = (1 - r^2/r_o^2)^{1/2} = h_\zeta/r_o \qquad 0\le\xi\le 1.$$

Using (5.1.5) and (5.1.6) we get then a relation for the surface density

$$(5.1.9) \qquad \sigma = \frac{P_n^m(\xi)e^{im\phi}}{2\pi^2\gamma_n^m G r_o \xi}$$

where

$$(5.1.10) \qquad \gamma_n^m = \frac{-q_n^m(0)}{\pi q_n^{m'}(0)} = \frac{(n+m)!\,(n-m)!}{2^{2n+1}\left[\left(\frac{n+m}{2}\right)!\right]^2\left[\left(\frac{n-m}{2}\right)!\right]^2}$$

For a derivation of this last formulae see Hunter (1963).

For an axisymmetric distribution of matter (m=0) on the disk, suppose that the surface density can be represented by the general series

$$(5.1.11) \qquad \sigma = \sum_{n=0}^{\infty} c_{2n} P_{2n}(\xi)/\xi$$

where P_{2n} are Legendre polynomials, then the gravitational potential can be written as

$$(5.1.12) \qquad \psi_D = 2\pi^2 G r_o \sum_{n=0}^{\infty} c_{2n}\gamma_{2n}^o P_{2n}(\xi)$$

where $\gamma_{2n}^o = 1/(2^{2n+1}n!)$. The coefficient c_{2n} can be determined as follows. Recall the orthonormality property of the Legendre polynomials

$$(5.1.13) \qquad \int_0^1 P_{2n}(\xi)P_{2m}(\xi)d\xi = \begin{cases} 0 & n-m \text{ even } n\neq 0 \\ 1/(4n+1) & n=m \end{cases}$$

Multiplying then (5.1.11) by $P_{2m}(\xi)$ and integrating over ξ we get

$$(5.1.14) \quad c_{2n} = (4n+1)\int_0^1 \xi\sigma(\xi)P_{2n}(\xi)d\xi.$$

Using such an expression we can write the potential on the disk as

$$(5.1.15) \quad \psi = 2\pi^2 G r_0 \sum_{n=0}^{\infty} (4n+1)\gamma_{2n}^0 P_{2n}(\xi)\int_0^1 \xi\sigma(\xi)P_{2n}(\xi)d\xi.$$

The mass of the disk can be calculated integrating the surface density function over the disk

$$(5.1.16) \quad m = \int_0^{r_0} 2\pi\,\sigma\, r dr$$

Using (5.1.8) we change variable of integration from r to ξ and then putting the expression (5.1.11) for the surface density we get the result

$$(5.1.17) \quad m = 2\pi\, r_0^2 c_0.$$

Therefore the surface density can also be written as

$$(5.1.18) \quad \sigma = \frac{m}{2\pi r_0^2 \xi} + \sum_{n=0}^{\infty} c_{2n} P_{2n}(\xi)/\xi.$$

We specialize now the surface density to be given only by the first term of the series (5.1.18)

$$(5.1.19) \quad \sigma = \frac{m}{2\pi r_0^2 \xi}$$

For this σ the potential on the disk is easily calculated from equation (5.1.15) giving as result

$$(5.1.20) \quad \psi = \frac{\pi}{2}\frac{Gm}{r_0}$$

We construct now a new solution of an annulus made by the difference of two disks with radii r_{out} and r_{in} ($r_{out} > r_{in}$). The surface densities of the two disks are chosen to be the following functions

$$(5.1.21)\qquad \sigma^{out} = \frac{m^{out}}{2\pi r_{out}^2 \xi} \qquad\qquad \sigma^{in} = \frac{m^{in}}{2\pi r_{in}^2 \bar{\xi}}$$

where $\xi=(1-r^2/r_{out}^2)^{1/2}$ and $\bar{\xi}=(1-r^2/r_{in}^2)^{1/2}$. Although the spheroidal coordinates ξ are different for the two disks the radial coordinate r must be the same. This condition allows to get a relationship between ξ and $\bar{\xi}$ through equation (5.1.1)

$$(5.1.22)\qquad \bar{\xi}^2 = 1 - \frac{r_{out}^2}{r_{in}^2}(1-\xi^2) \qquad \bar{\xi}d\bar{\xi} = \frac{r_{out}^2}{r_{in}^2}\xi d\xi .$$

For each of these disks the potential on their planes are formally given by an expression as (5.1.20). The potential on the plane of the annulus with mass $m=m^{out}-m^{in}$ is then

$$(5.1.23)\qquad \psi = \frac{\pi}{2} G \left[\frac{m^{out}}{r_{out}} - \frac{m^{in}}{r_{in}} \right] = \left[\frac{m^{out}}{r_{out}} - \frac{m^{out}}{r_{in}} + \frac{m}{r_{in}} \right]$$

A relation between m^{out} and m can be found imposing that in the region $r<r_{in}$ the surface density should be zero. Then

$$(5.1.24)\qquad \frac{m^{out}}{r_{out}^2 \xi} - \frac{m^{in}}{r_{in}^2 \bar{\xi}} = 0.$$

After some algebra using the definition of $m=m^{out}-m^{in}$ we get

$$(5.1.25)\qquad m^{out} = \frac{m\,\xi}{(\xi-\beta^2\bar{\xi})}$$

where $\beta=r_{in}/r_{out}$ is the ratio between the inner and outer radius of the disk. Putting (5.1.25) into equation (5.1.23) and using (5.1.22) after some algebra we obtain

$$(5.1.26)\qquad \psi = \frac{\pi}{2}\frac{Gm}{r_{out}} \frac{\xi - \left[\beta^2-(1-\xi^2)\right]^{1/2}}{\xi-\beta\left[\beta^2-(1-\xi^2)\right]^{1/2}}$$

By superposition of solutions like (5.1.5), the external potential can be written in the general form

$$(5.1.27)\qquad \psi^{ext} = \sum_{n=0}^{\infty} A_{2n} q_{2n}(\zeta) P_{2n}(\xi)$$

The constants A_{2n} are determined imposing continuity of the external potential on the surface of the disk

$$(5.1.28)\qquad \psi^{ext}\Big|_{\zeta=0} = \psi$$

By using (5.1.26) and (5.1.27) we have

$$(5.1.29)\qquad \sum_{n=0}^{\infty} A_{2n} q_{2n}(0) P_{2n}(\xi) = \frac{\pi}{2}\frac{Gm}{r_{out}}\,\frac{\xi - \left[\beta^2-(1-\xi^2)\right]^{1/2}}{\xi-\beta\left[\beta^2-(1-\xi^2)\right]^{1/2}}$$

Multiplying by $P_{2l}(\xi)$ and integrating over ξ we get

$$(5.1.30)\qquad A_{2l} q_{2l}(0) = \frac{\pi}{2}\frac{Gm}{r_{out}}(4l+1)\int_0^1 \frac{\xi - \left[\beta^2-(1-\xi^2)\right]^{1/2}}{\xi-\beta\left[\beta^2-(1-\xi^2)\right]^{1/2}} P_{2l}(\xi)\,d\xi$$

therefore the external potential of the disk is

$$(5.1.31)\qquad \psi^{ext} = \frac{\pi}{2}\frac{Gm}{r_{out}}\sum_{n=0}^{\infty}\frac{q_{2n}(\zeta)}{q_{2n}(0)}(4l+1)\,P_{2n}(\xi)$$
$$\int_0^1 \frac{\xi - \left[\beta^2-(1-\xi^2)\right]^{1/2}}{\xi-\beta\left[\beta^2-(1-\xi^2)\right]^{1/2}} P_{2l}(\xi)\,d\xi.$$

For obtaining the total potential of the configuration made by our disk and a black hole described by the pseudo-Newtonian potential we should add the expression

$$(5.1.32)\qquad \psi_{BH} = -\frac{GM}{R - R_G}$$

where $R=(r^2+z^2)^{1/2}$ and $R_G=2GM/c^2$ is the Schwarzschild radius (c is the velocity of light). The potential on the plane of the disk is then

$$(5.1.33)\qquad \psi = -\frac{GM}{r - R_G} + \frac{\pi}{2}\frac{Gm}{r_{out}}\,\frac{\xi - \left[\beta^2-(1-\xi^2)\right]^{1/2}}{\xi-\beta\left[\beta^2-(1-\xi^2)\right]^{1/2}}$$

while the total external potential is

$$(5.1.34)\qquad \psi^{ext} = -\frac{GM}{R - R_G} + \frac{\pi}{2}\frac{Gm}{r_{out}}\sum_{n=0}^{\infty}\frac{q_{2n}(\zeta)}{q_{2n}(0)}(4l+1)\,P_{2n}(\xi)$$
$$\int_0^1 \frac{\xi - \left[\beta^2-(1-\xi^2)\right]^{1/2}}{\xi-\beta\left[\beta^2-(1-\xi^2)\right]^{1/2}} P_{2l}(\xi)\,d\xi.$$

From the expression of the potential it is possible to study the theory of orbits around the black hole. In particular, calculating the specific Keplerian angular momentum and the binding energy we can locate the radius of the marginally stable and marginally bound orbits. Constructing then a disk whose radius is at the marginally stable orbit value we can study the runaway instability, varying the mass of the black hole and see how the location of the marginally orbits changes. This is one the aims to compute such a Newtonian solution. Another one is for purpose of testing the numerical code that we will develop to integrate the Einstein's equations for the analogous relativistic configurations. In the limit of small gravity and slow rotation the two solutions should be very similar.

5.2 Relativistic infinitesimally thin disks a black hole.

In this paragraph we specialize the Einstein's equation to the situation when a infinitesimally thin disk is present around the black hole. In relativity, in contrast with the Newtonian theory, the field equations are non-linear therefore it is not possible to approach the problem as described in the previous section. Here we need to solve numerically the Einstein equation. We assume that the disk is axially symmetric, time-independent, and embedded in an asymptotically flat space-time. The energy-momentum is taken to be that of a perfect fluid in the limit that the pressure p is infinitesimally small in comparison with the energy density e. In the limit of infinitesimal thickness $e \longrightarrow \infty$. The pressure gradient force per unit inertial mass in the equation of hydrostatic equilibrium is proportional to $\nabla p(e+p)^{-1}$. This force is significant in the direction perpendicular to the plane of the disk, where the infinitesimal thickness allows to ∇p to become large enough to compensate for the infinite energy. However along the plane of the disk ∇p is finite and the pressure force is negligible compared with the gravitational and centrifugal forces.

In the disk limit of the gravitational field equations the matter source terms can be treated as surface densities which

cause discontinuities in the normal derivatives of the gravitational potentials across the plane of the disk. The detailed distribution of matter perpendicular to the plane becomes unimportant. The metric functions themselves are continuous across the disk. Obtaining the solution of the field equations reduces to solving the vacuum field equations with boundary conditions on the disk, at infinity, on the horizon and on the axis.

In cylindrical coordinates (ρ,z) the disk is located at $z=0$ and $a_1 \leq \rho \leq a_2$. In spherical coordinates it will be at $\vartheta=\pi/2$ and $r_{in} \leq r \leq r_{out}$. We define a surface density σ by

$$(5.2.1) \qquad \sigma = \int e^{\frac{-2\gamma}{X^2}} r \, d\vartheta$$

The boundary conditions on the disk ($\vartheta=\pi/2$) are obtained by integrating the full equations trough the disk. In integrating we should take into account that the metric functions and their first derivatives are finite, but their second derivatives normal to the disk are infinite. The integral of a normal second derivative through the disk equals the discontinuity in the normal first derivative, equal to twice the first derivatives itself at the surface. Moreover the integral of a finite quantity through the disk vanishes. The normal derivative at $\vartheta=\pi/2$ is

$$(5.2.2) \qquad \frac{\partial}{\partial z} = -\frac{1}{r}\frac{\partial}{\partial \vartheta}$$

Consider the equation for X at $\vartheta=\pi/2$ for p=0, integrating over the disk we get

$$(5.2.3) \qquad \int r^2 \frac{B}{X} X_{,\vartheta\vartheta} d\vartheta = 4\pi \int r^3 \frac{Be^{2\gamma}}{X^2} e \, \frac{1+v^2}{1-v^2} d\vartheta$$

The equation for B gives

$$(5.2.4) \qquad \int r^3 B_{,\vartheta\vartheta} \, d\vartheta = 0 \qquad \text{then} \qquad B_{,\vartheta} = 0.$$

Therefore B is independent of ϑ. Moreover v is independent of ϑ then

$$(5.2.5) \qquad \frac{X_{,\vartheta}}{X} = 4\pi\sigma \, \frac{1+v^2}{1-v^2}$$

is the boundary condition to impose for the metric function X on the plane of the disk. It easy to verify that the equation for ω gives

$$(5.2.6) \qquad \omega_{,\theta} = -\,8\pi\,\sigma\,\frac{\Omega-\omega}{1-v^2}$$

The conditions to impose on the other boundaries are those already discussed in Chap. II and so we will not discuss them here.

In this approximation the material of the disk is pressure free and the stress energy tensor is

$$(5.2.7) \qquad T^{\alpha}{}_{\beta} = \sigma\, u^{\alpha} u_{\beta}$$

The hydrostatic equilibrium equation then gives

$$(5.2.8) \qquad (\Omega-\omega)^2 (r^2\sin^2\theta\frac{B^2}{X^2})_{,r} - 2(\Omega-\omega)\,\omega_{,r}(r^2\sin^2\theta\frac{B^2}{X^2}) - (X^2)_{,r} = 0$$

The angular velocity then can be determined in terms of the metric functions which in turn can be calculated once a surface density is specified. Therefore, choosing a surface density function we can determine the angular velocity. This point of view is different than that of Bardeen and Wagoner in which they specialize the angular velocity to be constant and so simplified the problem.

The configuration is completely specified when in addition to the surface density a value for the angular velocity of the black hole is given if the radial coordinate is rescaled by the horizon size in a way which is described in the next chapter.

An improved version (to take care of the present suboptimal performance) of the Multigrid method used to test the Kerr solution, will be used to solve such a problem. The modifications which are needed are in the treatment of the boundary conditions on the plane of the disk. In this case an higher order discretization of the boundary conditions may be needed. Moreover, local refinement only in the direction parallel to the plane of the disk and nearby it may be needed as well. The organization of the grids can be done in a way which is described in section 4 of the next chapter.

CHAPTER VI

MULTIGRID FOR SELF-GRAVITATING TORI AROUND BLACK HOLES: SOME PRELIMINARIES

So far we have discussed the necessary numerical experiments which needed to be done before solving the full problem of finding the equilibrium configurations of self-gravitating tori around rapidly rotating black holes. The full problem presents many difficulties which we will describe below, giving a prescription on how to deal with them using the Multigrid. Work is in progress towards obtaining a full numerical solution of this problem.

6.1 Initial configuration.

When the matter is put around a rotating black hole and the mass of it is not negligible compared with that of the black hole, the metric describing the exterior space-time will not anymore be the Kerr metric because of the contribution of the matter to the field. In particular we expect that the location and the shape of the horizon will change according to the quantity of matter we put around the black hole. This will complicate the mathematical nature of the problem since now the radius of the horizon is an eigenvalue. For avoiding this we decide to rescale the radial coordinate with the quantity $h/2$. With this rescaling the field equations will preserve the same form if we define the following new variables

$$(6.1.1) \qquad \hat{\omega} = h\omega/2 \qquad e^{\zeta} = he^{\gamma}/2$$

In the following, we will still use ω and γ as variables although they are the rescaled ones. The boundary conditions keep the same form as well, since we can repeat the derivation of them as in Chap. II writing the metric as

$$(6.1.2) \qquad ds^2 = -X^2dt^2 + r^2\sin^2\vartheta\,\frac{B^2}{X^2}(d\phi^* - \omega dt)^2 + \frac{e^{2\zeta}}{X^2}(dr^2 + r^2d\vartheta^2)$$

where $\phi^* = h\phi/2$. Using such a metric we can re-formulate all the

boundary conditions and write integral expressions for the rescaled total mass $M^{*}=2M/h$ and total angular momentum $J^{*}=4J/h$. The integral expressions for these quantities are formally equivalent to those for M and J.

Using such a rescaling a first solution will then be constructed as follows. We start off with the Kerr metric specifying a value for the specific angular momentum α. Given a value for α we can calculate, via equations (4.2.15)-(4.2.18), the metric functions X, B, ω and y. Knowing these quantities we can compute the quantities M_H and J_H. Then we choose a constant value of specific angular momentum ℓ_o in between the values $\ell_{ms}\leq\ell\leq\ell_{mb}$ (which correspond to values of the angular momentum for Keplerian orbits at the marginally stable and marginally bound values of the radial coordinate) and using the theory of equipotential surfaces of a fluid around a black hole we can determine the location of the cusp and of the center of the torus solving the non-linear equation $\ell_o=\ell_k(r)$. The value of the radius of the inner edge of the tori then is chosen in such a way that $r_{in}\geq r_{cusp}$ in order that matter cannot flow through the inner edge. Since the surface of the torus is an equipotential one (see section 2.4) the outer edge will be determined solving the equation $u^t_{out}(r,\pi/2)=u^t_{in}(r,\pi/2)$.

The surface of the torus is determined by the condition $p(r,\vartheta)=0$. This equation can easily be converted in the form $\vartheta=\vartheta(r)$ using the hydrostatic equilibrium equation (see Appendix E) giving as result the following differential equation

$$(6.1.3)\qquad \frac{d\vartheta}{dr}=\frac{(\ln u^t)_{,r}(1-\Omega\ell)-\ell\Omega_{,r}}{(\ln u^t)_{,\vartheta}(1-\Omega\ell)-\ell\Omega_{,\vartheta}}$$

The angular velocity Ω in terms of the metric functions and ℓ is given in (2.3.5). The four-velocity u^t is given by the formulae

$$(6.1.4)\qquad u^t=\frac{r\sin\vartheta\, B\, X}{\left[r^2\sin^2\vartheta B^2(\omega\ell-1)^2-\ell^2X^4\right]^{1/2}}$$

Knowing the inner and outer edges of the configuration, we can distribute the matter in between using the hydrostatic equilibrium, which written in terms of the metric functions is

$$(6.1.5)\qquad p = \left[\frac{\gamma - 1}{\gamma k^{1/\gamma}} \frac{u^t_{in}\ell X(1-v^2)^{1/2} - r\sin\vartheta B v}{r\sin\vartheta\, B\, v} \right]^{\gamma/(\gamma-1)}$$

where u^t_{in} is the value of the four-velocity calculated at the inner radius and v is the three-velocity which in terms of the metric functions can be expressed as

$$(6.1.5)\qquad v = \frac{\ell X^2}{(1-\omega\ell) r\sin^2\vartheta B}$$

Then the total energy density is calculated according to the equation of state

$$(6.1.5)\qquad e = \left(\frac{p}{k}\right)^{1/\gamma} + \frac{p}{\gamma - 1}$$

The model is then completed if we choose values for γ and k. These values will be fixed requiring that the torus is radiation dominated. In this case the equation of state can be specialized as

$$(6.1.6)\qquad p = \left[3\left(\frac{k_B}{m_p \beta}\right)^4 \frac{(1-\beta)}{a} \right]^{1/3} \rho^{4/3}$$

where $\beta = p_r/p_g$ is the ratio of radiation to gas pressure, k_B is the Boltzmann's constant, m_p is the proton mass and a is the radiation density constant. So, what we should really fix is a value for the pressure ratio β.

The choice of a value of the constant specific angular momentum is important because it determines the thickness of the tori. The closest is ℓ_o to ℓ_{mb} the thicker is the torus. For constructing the first model we will choose a value of ℓ_o close to ℓ_{ms} so that the torus is fairly small and we will make sure that the rest mass M_o of the torus, defined as,

$$(6.1.7)\qquad M_o = 2\pi \int_{r_{in}}^{r_{out}} \int_0^{\pi} \rho\, u^t B e^{2\gamma - 2\nu} r^2 \sin\vartheta\, dr\, d\vartheta$$

will be small so that the starting approximation for the metric functions (the Kerr metric) will not be so bad since the

contribution of the self-gravity of the torus to the field will be small as well. This is important from the numerical point of view because being Einstein's equations highly non-linear it is better to start off with a very good initial guess. If the requirement of having a small mass ratio is not satisfied then one can go back and try a different value of ℓ_o and/or a different value of β. Once the first model is constructed we use this as initial approximation to find the solution for another torus with slightly greater value of ℓ_o or β, keeping constant all the other parameters. in a such a way that this torus will have more mass. When the next solution is found, this is used to construct a further one with more mass in the torus and so on. Doing this we can find a set of solutions with increasing amounts of differential rotation. Different sequences can then be constructed using different values of Ω_H or r_{in}.

6.2 Multigrid for the full set of equations.

An efficient way of treating system of non-linear differential equations with the Multigrid is described in Brandt (1984). Since relaxation is a local process, only the local important terms contribute to smooth out the high-frequency components of the error, therefore it is enough to relax the principal part of the full system, that is the system of differential equations constituted only by the higher order derivatives terms (see Chap. IV). Since in the process of finding solutions for our problem we will consider the self-gravity of torus as a small perturbation to the previous constructed solution as described in the previous section, the principal part of the system can be considered to be the corresponding full system in the vacuum. So for the purpose of relaxation it is the vacuum system of equation that will be considered. This is not a bad approximation since in high relativistic situation the shear contributes more than the matter as source of the gravitational field. The right hand side of the Einstein's equations do not need to be update during the relaxation process, but they will be transferred to the coarser grids as well as all the algebraic

relations which describe the matter configuration like the hydrostatic equilibrium equation the definition of the total mass, angular momentum and so on. Only in coarser grids we will update the right hand sides of Einstein's equations and the fluid variables with the updated metric functions. This can be done if we use the FMG with FAS and write the coarse grid equations like (3.4.10).

6.3 Treatment of the interface of the torus

The surface of the torus represents an interface between two region of the space-time in which the physical conditions are different. Inside the torus we have a pressure different than zero, whereas outside the pressure is zero. Since we are using a polytropic equation of state the surface of the matter configuration does not introduce any discontinuity in the metric functions being the pressure a smooth decreasing function as one goes towards the surface. However the field equations nearby the surface need to be discretized with care. In general the surface of the torus will not be a coordinate line and the discretization will be very complicated. The most effective discretization is made in terms of coordinates in which the boundary is a coordinate line. In such coordinates it is much easier to formulate high-order approximations near and on the boundary. With the Multigrid this can be combined with local refinement. One can introduce a coordinate transformation only near the boundary such that the boundary is a grid line and create a subset of grids in such coordinates and apply the Multigrid cycle on them. The result of this local refinement then can be transformed back to the original coordinates. This process is not very much time consuming because it will be limited only to a small region of the entire domain therefore the number of grid points involved in such an operation will be small as well (however see next section). Since the transformation has to be done only locally, it can be obtained by a simple and standard transformation. In our case the boundary is given by the differential equation (6.1.3) which introducing the arclength υ can be split in the following two differential

equations

$$(6.2.1) \qquad \frac{d\hat{\vartheta}}{d\upsilon} = F_1(r,\hat{\vartheta}) \Big/ \sqrt{F_1^2 + F_2^2}$$

$$(6.2.2) \qquad \frac{dr}{d\upsilon} = F_2(r,\hat{\vartheta}) \Big/ \sqrt{F_1^2 + F_2^2}$$

where $F_1(r,\hat{\vartheta})$ and $F_2(r,\hat{\vartheta})$ are the numerator and denominator of equation (6.1.3) respectively, and

$$(6.2.3) \qquad \left(\frac{dr}{d\upsilon}\right)^2 + \left(\frac{d\hat{\vartheta}}{d\upsilon}\right)^2 = 1$$

After solving the equations (6.2.1) and (6.2.2) we get a parametric form of the equations describing the boundary $r=r(\upsilon)$ and $\hat{\vartheta}(\upsilon)$. To get a coordinate system $(\hat{\theta},\upsilon)$ in which the surface of the torus coincides with the grid line $\hat{\theta}=0$, we can use the standard transformation

$$(6.2.4) \qquad r(\hat{\theta},\upsilon) = r(\upsilon) - \hat{\theta}\,\frac{d\hat{\vartheta}}{d\upsilon}, \quad \hat{\vartheta}(\hat{\theta},\upsilon) = \hat{\vartheta}(\upsilon) + \hat{\theta}\,\frac{dr}{d\upsilon}$$

The differential formulae which allows to go from the $(r,\hat{\vartheta})$ to the $(\hat{\theta},\hat{\vartheta})$ coordinates are the following

$$(6.2.5) \qquad \frac{\partial}{\partial r} = -\frac{d\hat{\vartheta}}{d\upsilon}\frac{\partial}{\partial\hat{\theta}} + \frac{dr}{d\upsilon}\frac{1}{1+\hat{\theta}q}\frac{\partial}{\partial\upsilon} \qquad \frac{\partial}{\partial\hat{\vartheta}} = \frac{dr}{d\upsilon}\frac{\partial}{\partial\hat{\theta}} + \frac{d\hat{\vartheta}}{d\upsilon}\frac{1}{1+\hat{\theta}q}\frac{\partial}{\partial\upsilon}$$

where

$$(6.2.6) \qquad q(\upsilon) = \frac{d^2r}{d\upsilon^2}\Big/\frac{d\hat{\vartheta}}{d\upsilon} = -\frac{d^2\hat{\vartheta}}{d\upsilon^2}\Big/\frac{dr}{d\upsilon}$$

Therefore the discretization of the field equations should be done according to the transformation (6.2.5). In this approach (Brandt, 1984) the curved grids are regarded as finer levels which correct the finest grid near the surface boundary.

This process should be done together with the a more general local refinement needed near the horizon.

6.4 Organization of non-uniform grids.

In our problem there are three lengthscales which characterize the solution: the horizon size, the scale

corresponding to the structure of the torus and infinity. In order to have a good resolution of these scales the organization of the grids must be done carefully. Near the horizon and inside the torus a sequence of local finer grids will be used while the position of the artificial edge where the boundary condition at infinity is to be imposed can be decided during the solution process by extending the coarsest grid as required by the solution as described in section 3.4f. This avoids the necessity of computing the multipole moments appearing in the asymptotic expansions of the metric functions which are usually needed when *infinity* is put near to the configuration being studied. As we already said in section 3.4f, this can be done in an accommodative way or in a fixed way if an estimation of the truncation error can be obtained. In our case we do not have an apriori estimation of the truncation error but we know approximately where we need more resolution, therefore we will use a fixed scheme to do local refinement based on the so-called λ-FMG algorithm (Bai and Brandt, 1985). This is designed for reducing the computational work that a regular FMG would invest when local levels of refinement are used. In this case in fact, when finer levels cover much smaller subdomains the number of points on coarser grids is not necessarily small in comparison with the finest grid, therefore the computational work of FMG will not be anymore proportional to the number of grid points of the finest grid since now the coarser grids have not fewer points. In λ-FMG algorithm the problem is solved for a given sequence of different values of the exchange rate of accuracy for work λ introduced in section 3.4f such that $\lambda_0>\lambda_1>\ldots>\lambda_n$. For large value of λ we get an optimized grid with less work and poorer accuracy, for smaller value of λ, we invest more work and get more accuracy. For each value of λ a sequence of grids is constructed and a Multigrid cycle is applied to it. The first value of λ, λ_0 is chosen large enough so that a crude solution is obtained by investing a small amount of work. For each λ_i ($i\geq 1$) the first approximation is obtained by interpolating the λ_{i-1} solution to the relative grids. Assuming λ_{i-1} close enough to λ_i then only a small number of cycles on the grids relative to λ_i would be enough to obtain the solution to the level of the

TABLE IX

	h	h/2	h/4	h/8	h/16
λ_0	100	100	20	10	0
λ_1	100	100	40	20	10
λ_2	100	100	80	40	20
λ_3	100	100	100	80	40
λ_4				100	80
λ_5					100

truncation error. An example of organization of the grids is shown in Table IX. For each value of λ the table shows the values of the radial coordinate used as outer edge of the grid for five levels with different mesh-sizes. The values in the table are only indicative because the value of the radial coordinate at the outer edge depends on the configuration which we are dealing with. In particular it depends on how far from the hole, the torus does extends. For each λ those are the grids to which the Multigrid will be applied.

6.4 Treatment of the boundary conditions at infinity.

To impose the boundary conditions at infinity we need to evaluate the total mass and total angular momentum. The source for these quantities is not only the matter, but even the geometry and in order to evaluate them we should know the metric functions. Therefore the evaluation of them should be done consistently inside the solution process. With the help of Multigrid this can be done without spending too much computational time.

Being global relations since they involve integral expressions these quantities do not need to be treated at all on fine grid. There is no error smoothing related to such relations. What one has to do is to transfer the residual of the relation to serve as right hand side for a similar relation on the coarser grid. In the coarsest grid the condition must be imposed in order to solve the problem.

The boundary conditions are then treated in a similar fashion

like the Neumann boundary conditions, with the difference that they are not relaxed but only transferred to coarser grids.

Several numerical experiments have been done for developing a numerical code which is able to deal with quite complicated general relativistic equilibrium configurations. The main interest is that of solving Einstein's equations for self-gravitating fluid tori around a rapidly rotating black hole, but the flexibility of the code is such that only small changes need to be done to consider spheroidal type of configurations.

The difficulty of the problem is a good challenge for using the Multigrid method. Although today's computers are very fast and have a large capacity, one should always try to solve any problem in the best efficient way and the Multigrid provides this high efficiency. Moreover the impact of new techniques is always source of new ideas.

The construction of numerical code able to make large scale calculations is, in general, a long process. Testing and debugging are very important tools that any computational physicists should always consider as the only way to approach the final goal, although they take most of their time. This is particularly true when the equations to solve are complicated partial differential equations, for which no general packages exits (and perhaps will never exists) which are able to solve a large spectra of physical problems.

With this in mind, we considered first those significant test problems which contains separately several features that are present together in the full problem. The results of the tests considered so far show that the method is so efficient that numerical relativists should consider to use it even in different applications. The complicated structure of the method very often discourages people on using it, objecting that it is not worth spending several months of human time more to get as result a decrease on computational time. However, this is true when one is dealing with a small scale numerical calculations, but it is questionable for problems which are already complicated in structure and their solution requires in any case a lot of human

time to spend on it. Moreover, after one understands the structure of the Multigrid method and has already constructed the inter-grids communication routines, the human time spent for solving the problem is at most comparable with that one would spent using any other method.

More work needs to be done for solving the full problem. However, this thesis contains the solution of many crucial related problems (treatment of the horizon, relaxation schemes, etc.) which were necessary to test using simplified models.

The physical components of the Riemann tensor in the locally non-rotating frame take on a relatively simple form when expressed in terms of the metric functions defined by equation (2.1.15). Direct calculation gives

$$R_{(0)(1)(0)(1)} = \left(\nu_{,2}\psi_{,2}e^{-\mu_2} + \nu_{,3}\psi_{,3}e^{-\mu_3}\right) + \frac{1}{4}\left(\omega_{,2}\omega_{,2}e^{-\mu_2} + \omega_{,3}\omega_{,3}e^{-\mu_3}\right)e^{2\psi-2\nu}$$

$$R_{(0)(2)(0)(2)} = e^{-\mu_2-\nu}\left[e^{-\mu_2}\left(e^{\nu}\right)_{,2}\right]_{,2} + e^{-2\mu_3}\nu_{,3}\mu_{2,3} - \frac{3}{4}e^{-2\mu_2}\omega_{,2}\omega_{,2}e^{2\psi-2\nu}$$

$$R_{(0)(3)(0)(3)} = e^{-\mu_3-\nu}\left[e^{-\mu_3}\left(e^{\nu}\right)_{,3}\right]_{,3} + e^{-2\mu_2}\nu_{,2}\mu_{3,2} - \frac{3}{4}e^{-2\mu_3}\omega_{,3}\omega_{,3}e^{2\psi-2\nu}$$

$$R_{(1)(2)(1)(2)} = -e^{-\mu_2-\psi}\left[e^{-\mu_2}\left(e^{\psi}\right)_{,2}\right]_{,2} + e^{-2\mu_3}\psi_{,3}\mu_{2,3} - \frac{1}{4}e^{-2\mu_2}\omega_{,2}\omega_{,2}e^{2\psi-2\nu}$$

$$R_{(1)(3)(1)(3)} = -e^{-\mu_3-\psi}\left[e^{-\mu_3}\left(e^{\psi}\right)_{,3}\right]_{,3} + e^{-2\mu_2}\psi_{,2}\mu_{3,2} - \frac{1}{4}e^{-2\mu_3}\omega_{,3}\omega_{,3}e^{2\psi-2\nu}$$

$$R_{(2)(3)(2)(3)} = -e^{-\mu_2-\mu_3}\left\{\left[e^{-\mu_2}\left(e^{\mu_3}\right)_{,2}\right]_{,2} + \left[e^{-\mu_3}\left(e^{\mu_2}\right)_{,3}\right]_{,3}\right\}$$

$$R_{(0)(2)(0)(3)} = e^{-\mu_2-\mu_3}\left[e^{-\nu}(e^{\nu})_{,23} - \nu_{,2}\mu_{2'3} - \nu_{,3}\mu_{3'2} - \frac{3}{4}\omega_{,2}\omega_{,3}e^{2\psi-2\nu}\right]$$

$$R_{(1)(2)(1)(3)} = -e^{-\mu_2-\mu_3}\left[e^{-\psi}(e^{\psi})_{,23} - \psi_{,2}\mu_{2'3} - \psi_{,3}\mu_{3'2} + \frac{1}{4}\omega_{,2}\omega_{,3}e^{2\mu-2\nu}\right]$$

$$R_{(0)(2)(1)(2)} = \frac{1}{2}e^{-2\psi-\mu_2}\left[e^{3\psi-\nu-\mu_2}\omega_{,2}\right] + \frac{1}{2}e^{-2\mu_3}\omega_{,3}\mu_{2'3}e^{\psi-\nu}$$

$$R_{(0)(3)(1)(3)} = \frac{1}{2}e^{-2\psi-\mu_3}\left[e^{3\psi-\nu-\mu_3}\omega_{,3}\right] + \frac{1}{2}e^{-2\mu_2}\omega_{,2}\mu_{3'2}e^{\psi-\nu}$$

$$R_{(0)(2)(1)(3)} = \frac{1}{2}e^{\psi-\nu-\mu_2-\mu_2}\left[\omega_{,23} + 2\omega_{,2}\psi_{,3} + \omega_{,3}\psi_{,2} - \omega_{,2}\nu_{,3} - \omega_{,2}\mu_{2'3} - \omega_{,3}\mu_{3'2}\right]$$

$$R_{(0)(1)(2)(3)} = \frac{1}{2}e^{\psi-\nu-\mu_2-\mu_2}\left[\omega_{,2}(\psi-\nu)_{,3} - \omega_{,3}(\psi-\nu)_{,2}\right].$$

The remaining non-zero components are equivalent to these though the symmetries of the Riemann tensor. The Ricci tensor can then be computed using

$$R_{(\alpha)(\beta)} = R^{(\gamma)}{}_{(\alpha)(\gamma)(\beta)}.$$

APPENDIX B

The energy momentum tensor for a perfect fluid is

$$(B.1) \quad T^{\alpha\beta} = (e + p)\, u^{\alpha} u^{\beta} + p\, g^{\alpha\beta}$$

applying the normal projector tensor to the divergence of it we get

$$(B.2) \quad (g_{\alpha\beta} + u_{\alpha} u_{\beta})\, \nabla_{\gamma} T^{\gamma\beta} = 0$$

since the four velocity is a time-like unit vector

$$(B.3) \quad u^{\alpha} u_{\alpha} = -1 \qquad \longrightarrow \qquad u^{\alpha} \nabla_{\beta} u_{\alpha} = 0.$$

Applying equations (B.3), then after some trivial algebra equation (B.2) becomes

$$(B.4) \quad a_{\alpha} = \frac{\nabla_{\alpha} p}{e+p}$$

where a_{α} is the four-acceleration.

On the other hand the four velocity can be expressed as a linear combination of the Killing vectors

$$(B.5) \quad u^{\alpha} = A(\eta^{\alpha} + \Omega \xi^{\alpha})$$

The four-acceleration is then

$$(B.6) \quad a^{\alpha} = u^{\beta} \nabla_{\beta} u^{\alpha} = A^2 (\eta^{\beta} + \Omega \xi^{\beta})\, \nabla_{\beta} (\eta^{\alpha} + \Omega \xi^{\alpha}).$$

Since

$$(B.7) \quad \eta^{\beta} \nabla_{\beta} \eta^{\alpha} = \frac{1}{2} \nabla^{\alpha} (\underline{\eta}, \underline{\eta})$$

we have

$$(B.8) \quad a^{\alpha} = \frac{1}{2} A^2 \left[\nabla^{\alpha} (\underline{\eta}, \underline{\eta}) + 2\Omega \nabla^{\alpha} (\underline{\eta}, \underline{\xi}) + \nabla^{\alpha} (\underline{\xi}, \underline{\xi}) \right]$$

From the condition $u^{\alpha} u_{\alpha} = -1$ we get

(B.9) $$A^2(\eta^\alpha + \Omega\xi^\alpha)(\eta_\alpha + \Omega\xi_\alpha) = -1$$

(B.10) $$A^{-2} = -\left[(\underline{\eta},\underline{\eta}) + 2\Omega(\underline{\eta},\underline{\xi}) + \Omega^2(\underline{\xi},\underline{\xi})\right].$$

Taking the derivative of equation (B.10) we obtain

(B.11) $$\nabla^\alpha(\underline{\eta},\underline{\eta}) + 2\Omega\nabla^\alpha(\underline{\eta},\underline{\xi}) + \nabla^\alpha(\underline{\xi},\underline{\xi}) = \nabla^\alpha\left(A^{-2}\right) - 2(\underline{\eta},\underline{\xi})\nabla^\alpha\Omega - 2\Omega(\underline{\xi},\underline{\xi})\nabla^\alpha\Omega$$

therefore equation (B.8) can be written as

(B.12) $$a^\alpha = \nabla^\alpha(\ln\alpha) + \frac{\left[(\underline{\eta},\underline{\xi}) + \Omega(\underline{\xi},\underline{\xi})\right]}{\left[(\underline{\eta},\underline{\eta}) + 2\Omega(\underline{\eta},\underline{\xi}) + \Omega^2(\underline{\xi},\underline{\xi})\right]}\nabla^\alpha\Omega.$$

Recalling the definition of the specific angular momentum per inertial mass we can write

(B.13) $$\ell = -\frac{(\underline{u},\underline{\xi})}{(\underline{u},\underline{\eta})} = -\frac{\left[(\underline{\eta},\underline{\xi}) + \Omega(\underline{\xi},\underline{\xi})\right]}{\left[(\underline{\eta},\underline{\eta}) + \Omega(\underline{\eta},\underline{\xi})\right]}$$

therefore equation (B.12) can be written

(B.14) $$a^\alpha = \nabla^\alpha(\ln A) - \frac{\ell\nabla^\alpha\Omega}{1-\Omega\ell}.$$

Using the relations (2.3.3) which link Ω and ℓ, equation (B.14) can also be written as

(B.15) $$a^\alpha = -\nabla^\alpha(\ln u^t) + \frac{\Omega\nabla^\alpha\ell}{1-\Omega\ell}.$$

Consider a disk with constant specific angular momentum ℓ, equation (B.15) now can be integrated

(B.16) $$\int_0^p \frac{dp}{e+p} = -\ln\frac{u^t}{u^t_{in}}$$

where u^t_{in} is the four-velocity at the inner edge of the disk. If the matter compounding the torus is modelled by a polytropic equation of state

(B.17) $$p = k\rho^{\gamma}$$

and

(B.18) $$p = (\gamma - 1)\rho\,\varepsilon \qquad e = \rho + \frac{p}{\gamma - 1}$$

then the hydrostatic equilibrium equation is trivially integrated to the expression

(B.19) $$p = \left[\frac{\gamma - 1}{\gamma k^{1/\gamma}}\left[\frac{u_{in}^{t}}{u^{t}} - 1\right]\right]^{\gamma/(\gamma-1)}$$

or

(B.20) $$\rho = \left[\frac{\gamma - 1}{\gamma k}\left[\frac{u_{in}^{t}}{u^{t}} - 1\right]\right]^{1/(\gamma-1)} .$$

APPENDIX C

We derive here the Schwarzschild solution in our coordinates. For convenience we report again the equations to solve with the relative boundary conditions

(C.1) $\nabla\cdot(B\nabla\nu) = 0$

(C.2) $\nabla\cdot(r\sin\vartheta\nabla B) = 0$

(C.3) $\nu \longrightarrow 0, \qquad B = 1 \qquad\qquad r \longrightarrow \infty$

(C.4) $e^{\nu} = 0 \qquad B = 0 \qquad Be^{-\nu}$ regular ar $r = 1$.

Here the radial coordinate has already been rescaled by h/2. In the Schwarzschild case the space-time is spherical symmetric therefore the metric functions are only function of the radial coordinate r. Equation (C.2) then becomes

(C.5) $$\frac{d}{dr}\left(r^2\frac{dB}{dr}\right) = 0$$

whose general solution is

(C.6) $$B = c_1 + \frac{c_2}{r^2}$$

the boundary conditions determine the constants c_1 and c_2 to be uniquely equal to $c_1=1$ and $c_2=-1$, hence the solution is

(C.7) $$B = 1 - \frac{1}{r^2}$$

Equation (C.1), when the value of B given by (C.7) is substituted, becomes

(C.8) $$\frac{d}{dr}\left[(r^2-1)\frac{d\nu}{dr}\right] = 0$$

whose general solution is

(C.9) $$\nu = c_3\ln\left(\frac{r-1}{r+1}\right) + c_4$$

the constant c_4 is determined by the boundary condition at

infinity and its value is $c_4=0$. The constant c_3 is not uniquely determined by the requirement that $X=e^{\nu}=0$ at the horizon, but we need to impose the regularity of the ratio B/X

$$(C.10) \qquad \frac{B}{X} = \frac{r^2-1}{r^2}\left[\frac{r+1}{r-1}\right]^{c_3} = \frac{(r+1)^{c_3+1}}{r^2(r-1)^{c_3-1}}$$

this ratio is regular at $r=1$ when $c_3=1$, therefore the solution is

$$(C.11) \qquad \nu = \ln\left[\frac{r-1}{r+1}\right]$$

or in terms of $X=e^{\nu}$

$$(C.12) \qquad X = \frac{r-1}{r+1} .$$

The grid functions used in equation (4.2.36) and (4.2.37) $\mathbb{A}^h_{i,j}$, $\mathbb{B}^h_{i,j}$, $\mathbb{C}^h_{i,j}$ and $\mathbb{D}^h_{i,j}$ are defined as follows

(D.1) $$\mathbb{A}^h_{i,j} = q^h_{i,j} - 4\frac{B^9}{X^5}\Big[m^h_{i,j}(\tilde{\omega}^h_{i+1,j}-\tilde{\omega}^h_{i,j})(\tilde{\omega}^h_{i,j}-\tilde{\omega}^h_{i-1,j}) + p^h_{i,j}(\tilde{\omega}^h_{i,j+1}-\tilde{\omega}^h_{i,j})(\tilde{\omega}^h_{i,j}-\tilde{\omega}^h_{i,j-1})\Big] - e^h_{i,j}(\tilde{X}^h_{i+1,j}-\tilde{X}^h_{i,j})\frac{\partial}{\partial X}_{i,j}\left[\frac{B}{X}\right]^h_{i+1/2,j}$$

$$w^h_{i,j}(\tilde{X}^h_{i-1,j}-\tilde{X}^h_{i,j})\frac{\partial}{\partial X}_{i,j}\left[\frac{B}{X}\right]^h_{i-1/2,j} - n^h_{i,j}(\tilde{X}^h_{i,j+1}-\tilde{X}^h_{i,j})\frac{\partial}{\partial X}_{i,j}\left[\frac{B}{X}\right]^h_{i,j+1/2}$$

$$s^h_{i,j}(\tilde{X}^h_{i,j-1}-\tilde{X}^h_{i,j})\frac{\partial}{\partial X}_{i,j}\left[\frac{B}{X}\right]^h_{i,j-1/2}$$

(D.2) $$\mathbb{B}^h_{i,j} = \left[\frac{B^9}{X^4}\right]^h_{i,j}\Big[p^h_{i,j}(\tilde{\omega}^h_{i+1,j}-2\tilde{\omega}^h_{i,j}+\tilde{\omega}^h_{i-1,j}) + m^h_{i,j}(\tilde{\omega}^h_{i,j+1}-2\tilde{\omega}^h_{i,j}+\tilde{\omega}^h_{i,j-1})\Big]$$

(D.3) $$\mathbb{C}^h_{i,j} = -e^h_{i,j}(\tilde{\omega}^h_{i+1,j}-\tilde{\omega}^h_{i,j})\frac{\partial}{\partial X}_{i,j}\left[\frac{B^9}{X^4}\right]^h_{i+1/2,j}$$

$$w^h_{i,j}(\tilde{\omega}^h_{i-1,j}-\tilde{\omega}^h_{i,j})\frac{\partial}{\partial X}_{i,j}\left[\frac{B^9}{X^4}\right]^h_{i-1/2,j} - n^h_{i,j}(\tilde{\omega}^h_{i,j+1}-\tilde{\omega}^h_{i,j})\frac{\partial}{\partial X}_{i,j}\left[\frac{B^9}{X^4}\right]^h_{i,j+1/2}$$

$$s^h_{i,j}(\tilde{\omega}^h_{i,j-1}-\tilde{\omega}^h_{i,j})\frac{\partial}{\partial X}_{i,j}\left[\frac{B^9}{X^4}\right]^h_{i,j-1/2}$$

(D.4) $$\mathbb{D}^h_{i,j} = e^h_{i,j}\left[\frac{B^9}{X^4}\right]^h_{i+1/2,j} + w^h_{i,j}\left[\frac{B^9}{X^4}\right]^h_{i-1/2,j} + n^h_{i,j}\left[\frac{B^9}{X^4}\right]^h_{i,j+1/2} + s^h_{i,j}\left[\frac{B^9}{X^4}\right]^h_{i,j-1/2}$$

The grid functions $e^h_{i,j}$, $w^h_{i,j}$, $n^h_{i,j}$ and $s^h_{i,j}$ are defined in

(4.1.52), while $e^h_{i,j}$, $w^h_{i,j}$, $n^h_{i,j}$, $s^h_{i,j}$, $m^h_{i,j}$ and $p^h_{i,j}$ are defined as follows

$$
\begin{aligned}
e^h_{i,j} &= \frac{h_\vartheta}{h_s} r^9_{i+1/2} \sin^9 \vartheta_j \\
w^h_{i,j} &= \frac{h_\vartheta}{h_s} r^9_{i-1/2} \sin^9 \vartheta_j \\
n^h_{i,j} &= \frac{h_s}{h_\vartheta} r^9_i \sin^9 \vartheta_{j+1/2} \\
s^h_{i,j} &= \frac{h_s}{h_\vartheta} r^9_i \sin^9 \vartheta_{j-1/2} \\
m^h_{i,j} &= \frac{1}{2} \frac{h_\vartheta}{h_s} r^9_i \sin^9 \vartheta_j \\
p^h_{i,j} &= \frac{1}{2} \frac{h_s}{h_\vartheta} r^9_i \sin^9 \vartheta_j
\end{aligned}
\tag{D.5}
$$

The derivatives are easily calculated and the result is, for i=2

$$\frac{\partial}{\partial X_{i,j}} \left(\frac{B}{X}\right)^h_{i-1/2,j} = -\frac{15}{8} \frac{B_{i,j}}{X^2_{i,j}} \tag{D.6}$$

$$\frac{\partial}{\partial X_{i,j}} \left(\frac{B}{X}\right)^h_{i+1/2,j} = -\frac{9}{8} \frac{B_{i,j}}{X^2_{i,j}} \tag{D.7}$$

$$\frac{\partial}{\partial X_{i,j}} \left(\frac{B}{X}\right)^h_{i,j-1/2} = -\frac{1}{2} \frac{B_{i,j}}{X^2_{i,j}} \tag{D.8}$$

$$\frac{\partial}{\partial X_{i,j}} \left(\frac{B}{X}\right)^h_{i,j+1/2} = -\frac{1}{2} \frac{B_{i,j}}{X^2_{i,j}} \tag{D.9}$$

$$\frac{\partial}{\partial X_{i,j}} \left(\frac{B^9}{X^4}\right)^h_{i-1/2,j} = -4 \frac{\mathbb{R}_{i-1/2} - \mathbb{R}_{i+1}}{\mathbb{R}_{i-1} - \mathbb{R}_i} \frac{B^9_{i,j}}{X^5_{i,j}} \tag{D.10}$$

$$\frac{\partial}{\partial X_{i,j}} \left(\frac{B^9}{X^4}\right)^h_{i+1/2,j} = -4 \frac{\mathbb{R}_{i+1/2} - \mathbb{R}_{i+1}}{\mathbb{R}_i - \mathbb{R}_{i+1}} \frac{B^9_{i,j}}{X^5_{i,j}} \tag{D.11}$$

$$(D.12)\qquad \frac{\partial}{\partial X_{i,j}}\left[\frac{B^{9}}{X^{4}}\right]^{h}_{i,\,j-1/2} = -2\,\frac{B^{9}_{i,j}}{X^{5}_{i,j}}$$

$$(D.13)\qquad \frac{\partial}{\partial X_{i,j}}\left[\frac{B^{9}}{X^{4}}\right]^{h}_{i,\,j+1/2} = -2\,\frac{B^{9}_{i,j}}{X^{5}_{i,j}}$$

for $i=9$, the derivatives that have different expressions are

$$(D.14)\qquad \frac{\partial}{\partial X_{i,j}}\left[\frac{B}{X}\right]^{h}_{i-1/2,j} = -\frac{9}{4}\,\frac{B_{i,j}}{X^{2}_{i,j}}$$

$$(D.15)\qquad \frac{\partial}{\partial X_{i,j}}\left[\frac{B}{X}\right]^{h}_{i+1/2,j} = -\frac{9}{4}\,\frac{B_{i,j}}{X^{2}_{i,j}}$$

$$(D.16)\qquad \frac{\partial}{\partial X_{i,j}}\left[\frac{B^{9}}{X^{4}}\right]^{h}_{i-1/2,j} = -4\,\frac{\mathbb{R}_{i-1}-\mathbb{R}_{i-1/2}}{\mathbb{R}_{i-1}-\mathbb{R}_{i}}\,\frac{B^{9}_{i,j}}{X^{5}_{i,j}}$$

the others are exactly the same expressions as for $i=2$.

APPENDIX E

Since the pressure is, in general, a function of the coordinates r and ϑ, the surface of the matter configuration can be expressed as an equation

$$p(r,\vartheta) = 0 \tag{E.1}$$

being an equipotential surface. Taking the differential of equation (E.1) we have

$$\frac{\partial p}{\partial r}\,dr + \frac{\partial p}{\partial \vartheta}\,d\vartheta = 0 \tag{E.2}$$

therefore

$$\frac{d\vartheta}{dr} = -\frac{P_{,r}}{P_{,\vartheta}} \tag{E.3}$$

then using the expression of the hydrostatic equilibrium equation (2.3.1) we get

$$\frac{d\vartheta}{dr} = \frac{(1-\ell\Omega)(\ln u^{t})_{,r} - \ell\Omega_{,r}}{(1-\ell\Omega)(\ln u^{t})_{,\vartheta} - \ell\Omega_{,\vartheta}}\,. \tag{E.4}$$

REFERENCES

Abramowicz, M.A., Astrophys.Lett., 7, 23, 1970.

Abramowicz, M.A., Acta Astron., 21, 81, 1971a.

Abramowicz, M.A., Acta Astron., 21, 221, 1971b.

Abramowicz, M.A., Acta Astron., 21, 449, 1971c.

Abramowicz, M.A., Acta Astron., 24, 45, 1974.

Abramowicz, M.A., Ap.J., 254, 748, 1982.

Abramowicz, M.A. and Wagoner R.V., Ap.J., 204, 896, 1976.

Abramowicz, M.A., Calvani, M., Nobili, L., Nature, 302, 597, 1980.

Abramowicz, M.A., Jaroszyński M. and Sikora M., Astron.Astrophys. 63, 221, 1978.

Alcouffe, R.E., Brandt, A., Dendy, J.E. and Painter J.W., SIAM Sci.Stat.Comput., 2, 430, 1981.

Backer, D.C. et al., Nature, 300, 615, 1982.

Bai, D. and Brandt, A., *Local Mesh Refinement Multilevel Techniques*, Weizmann Inst., Rehovot, Israel, 1985.

Bardeen, J., Ap.J., 162, 171, 1970.

Bardeen, J., Ap.J., 167, 425, 1971.

Bardeen, J., *Rapidly Rotating Stars, Disks, and Black Holes*, in *Black Holes*, eds. De Witt B. and De Witt C., Gordon and Breach, New York, 1973.

Bardeen, J. and Wagoner R.V., Ap.J., 158, L65, 1969.

Bardeen, J. and Wagoner R.V., Ap.J., 167, 359, 1971.

Bardeen, J., Carter B., Hawking S.W., Comm.Math.Phys., 31, 161, 1973.

Bardeen, J., Friedman J., Schutz, B. and Sorkin, R., Ap.J., 217, L49, 1977.

Baumgart, D. and Friedman, J., Proc.R.Soc.Lond.A, 405, 65, 1986.

Birchoff, G. and Lynch, R.E., *Numerical Solution of Elliptic Problems*, SIAM studies in Applied Mathematics, 1984.

Bodenheimer, P. and Ostriker, J., Ap.J., 180, 159, 1973.

Bonazzola, S. and Schneider, J., Ap.J., 191, 173, 1974.

Bowen, J.M. and York, J.W., Phys.Rev.D, 21, 2047, 1980.

Boyer, R.H., Proc.Camb.Phil.Soc., 61, 527, 1965.

Boyer, R.H., Proc.Camb.Phil.Soc., 62, 495, 1966.

Boyer, R.H. and Lindquist, R.W., Journ.Math.Phys., 8, 265, 1967.

Brandt, A., *Multi-Level Adaptive Technique (MLAT) For Fast Numerical Solutions To Boundary Value Problems*, Proc. 3rd Internat.Conf. on Numerical Methods in Fluid Mechanics (Paris, 1972), *Lecture Notes in Physics* 18, Springer-Verlag, Berlin, 1973.

Brandt, A., Math of Comp., 31, 333, 1977.

Brandt, A., *Multi-Level Adaptive Techniques (MLAT) For Partial Differential Equations: Ideas and Software*, in *Mathematical Software* III, ed Rice, J.R., Academic Press, New York, 1977.

Brandt, A., *Numerical Stability and Fast Solutions To Boundary Value Problems*, in *Boundary and Interior Layers-Computational and Asymptotic Methods*, ed. Miller J.J.H., Boole Press, Dublin 1980.

Brandt, A., *Multigrid Solvers For Non-Elliptic And Singular Perturbation Steady State Problems*, Weizmann Inst., Rehovot, Israel, 1981.

Brandt, A., *Multigrid Techniques: 1984 Guide with Applications to Fluids Dynamics*. GMD-Studien n. 85, St. Augustin, Germany, 1894.

Brandt, A. and Dinar, N., *Multigrid Solutions to Elliptic Flow Problems*, in *Numerical Methods for PDEs*, ed. Parter S., Academic Press, New York, 1979.

Brandt, A. and Ta'asan, *Multigrid Method for Nearly Singular and Slightly Indefinite Problems*, Weizmann Inst., Rehovot, Israel, 1985.

Butterworth, E.M., Ap.J., 204, 561, 1976.

Butterworth, E.M., Ap.J., 231, 219, 1979.

Butterworth, E.M. and Ipser, J.R., Ap.J., 200, L103, 1975.

Butterworth, E.M. and Ipser, J.R., Ap.J., 204, 200, 1976.

Carter, B., *General Theory of Stationary Black Hole State*, in *Black Holes*, eds. De Witt B. and De Witt C., Gordon and Breach, New York, 1973.

Carter, B., *The General Theory of the Mechanical, Electromagnetic and Thermodynamic Properties of Black Holes*, in *General Relativity: An Einstein Centenary Survey*, eds. Hawking

S.W. and Israel W., Cambridge University Press, Cambridge, 1979.

Chandrashekar, S., Ap.J., 142, 1513, 1965.

Chandrashekar, S., Ap.J., 147, 334, 1967.

Chandrashekar, S., Phys.Rev.Lett., 24, 611, 1970.

Chandrashekar, S., Ap.J., 167, 447, 1971a.

Chandrashekar, S., Ap.J., 167, 455, 1971b.

Chandrashekar, S., *The Mathematical Theory of Black Holes*, Oxford University Press, Oxford, 1983.

Chandrashekar, S. and Miller J.C., Mon.Not.R.astr.Soc., 167, 63, 1974.

Choptuik, M., Unruh W., G., Gen.Rel.Grav., 18, 813, 1986.

Comins, N., Mon.Not.R.astr.Soc., 189, 233, 1979a.

Comins, N., Mon.Not.R.astr.Soc., 189, 255, 1979b.

de Felice, F., Miller, J.C., Yunqiang Yu, Ap.J., 298, 480, 1985.

Dendy, J.E., Journ.Comp.Phys., 48, 366, 1982.

Dendy, J.E., *Apriori Local Grid Refinement in the Multigrid Method*, in *Elliptic Problem Solvers II*, eds. Birkhoff G. and Schoenstadt A., Academic Press, 1984.

Detweiler, L. and Lindblom, L., Ap.J., 213, 163, 1977.

Durisen, R.H. and Inamura, J.N., Ap.J., 243, 612, 1981.

Dyson, F.W., Phil.Trans.Roy.Soc.London A, 184, 43, 1893.

Eriguchi, Y., Talk given at the Numerical Relativity Workshop at the GR11 Conference, Stockholm, Sweden, 1986.

Eriguchi, Y. and Hachisu, I., Prog.Theor.Phys., 69, 1131, 1983.

Eriguchi, Y. and Hachisu, I., Astron.Astrophys., 148, 289, 1985.

Eriguchi, Y. and Sugimoto D, Prog.Theor.Phys., 65, 1870, 1981.

Fishbone, L.G., Ap.J, 215, 323, 1977.

Fishbone, L.G. and Moncrief, V., Ap.J., 207, 962, 1976.

Friedman, J., Comm.Math.Phys., 62, 247, 1978.

Friedman, J., Phys.Rev.Lett., 51, 11, 1983.

Friedman, J. and Ipser, J.R., *On the Maximum Mass of a Uniformly Rotating Neutron Star*, preprint, 1986.

Friedman, J. and Schutz, B.F., Ap.J., 199, L157, 1975.

Friedman, J. and Schutz, B.F., Ap.J., 221, 937, 1978a.

Friedman, J. and Schutz, B.F., Ap.J., 222, 281, 1978b.

Friedman, J., Ipser, J.R. and Parker, L., Nature, 312, 255, 1984.

Friedman, J., Ipser, J.R. and Parker, L., Ap.J., 304, 115, 1986.
Hachisu, I, Ap.J.Suppl., 61, 479, 1986.
Hachisu, I and Eriguchi, Y., Mon.Not.R.astr.Soc., 204, 583, 1983.
Hachisu, I and Eriguchi, Y., Publ.Astron.Soc.Japan, 36, 497, 1984.
Hackbusch, W., Math.Comp., 34., 425, 1980.
Hackbusch, W., *Multigrid Convergence Theory*, in *Multigrid Methods*, eds. Hackbusch, W. and Trottenberg U., Lecture Notes in Mathematics, 960, Springer-Verlag, Berlin, 1981.
Hackbusch, W., *Multi-Grid Methods and Applications*, Springer-Verlag, Berlin, 1985.
Harrison, B.K., Thorne, K.S., Wakano, M.S. and Wheeler, J.A., *Gravitation Theory and Gravitational Collapse*, 1965.
Hartle, J.B., Ap.J., 150, 1005, 1967.
Hartle, J.B. and Sharp D.W., Phys.Rev.Lett., 27, 529, 1965.
Hartle, J.B. and Sharp D.W., Ap.J., 47, 317, 1967.
Hartle, J.B. and Thorne, K.S., Ap.J., 153, 807, 1968.
Hunter, C., Mon.Not.R.astr.Soc., 126, 23, 1963.
Hunter, C., Ap.J., 213, 497, 1977.
Ipser, J.R. and Managan, R.A., Ap.J., 250, 362, 1981.
Inamura, J.N., Friedman, J. and Durisen, R.H., Ap.J., 294, 474, 1985.
James, R.A., Ap.J., 140, 552, 1964.
Jaroszyński, M., Abramowicz, M. and Paczyński, B, Acta Atron., 30, 1, 1980.
Komar, A., Phys.Rev., 113, 934, 1959.
Komatsu, H., Eriguchi, Y. and Hachisu, I., *Rapidly Rotating General Relativistic Polytropes*, in Proc. of the XIV Yamada Conference on Gravitational Collapse and Relativity, Kyoto, to appear, 1986.
Kozłowski, M., Jaroszyński, M. and Abramowicz, M., Astron.Astrophys., 63, 209, 1978.
Kuwahara, F., Ishizuka, T., and Yokosawa, M, Prog.Theor.Phys., 75, 828, 1986.
Laplace, P.S., *Memorie sur la théorie de l'anneau de Saturne*, Mem.Acad.Sci., 1789, summarized in Randers, 1940.
Lindblom, L., Ap.J., 267, 402, 1983.
Lindblom, L. and Detweiler, L., Ap.J., 211, 565, 1977.

Lindblom, L. and Hiscock, W.A., Ap.J., 267, 384, 1983.

Managan, R.A., Ap.J., 294, 463, 1985.

Mann, P.J., D.Phil. Thesis, University of Oxford, 1982.

Mann, P.J., Comp.Phys.Comm., 30, 127, 1983.

Mann, P.J., Journ.Comp.Phys., 58, 377, 1985.

Marcus, P.S., Press, W.H. and Teukolsky, S.A., Ap.J., 214, 584, 1977.

Maxwell, J.C., *On the stability of the motions in Saturn's rings*, 1859, Adams Price Essay, reprinted in Scientific papers of James Clerk Maxwell, Cambridge University Press, 1, 286.

Miller, J.C. and de Felice, F., Ap.J., 298, 47, 1985.

Morse, P.M. and Feshbach, H., *Methods of Theoretical Physics*, MacGraw-Hill, New York, 1953.

Nakamura, T., Progr.Theor.Phys.,65, 1876, 1981.

Ostriker, J., Ap.J., 140, 1056, 1964a.

Ostriker, J., Ap.J., 140, 1067, 1964b.

Ostriker, J. and Bodenheimer, P, Ap.J., 180, 159, 1973.

Ostriker, J. and Mark, J.W., Ap.J., 151, 1075, 1968.

Ostriker, J. and Tassoul, J.L., Ap.J., 155, 987, 1969.

Paczyński, B and Wiita, P.J., Astron.Astrophys., 88, 23, 1980.

Papaloizou, J and Pringle, J.E., Mon.Not.R.astr.Soc., 184, 501, 1978.

Piran, T. and Stark, R., F., *Gravitational Radiation, Gravitational Collapse and Numerical Relativity*, talk given at the XII Texas Symposium, December 1984, Jerusalem, Israel.

Poincaré, H., 1891, summarized in Tisserand F., *Mécanique Céleste*, Gauthier-Villars, Paris.

Press, W.H. and Teukolsky, S.A., Ap.J., 181, 513, 1973.

Press, W.H., Flannary, B.P., Teukolsky, S.A. and Vetterling, W.T., *Numerical Recipes: The Art of Scientific Computing*, Cambridge University Press, 1986.

Randers, G., Ap.J., 95, 88, 1942.

Roberts, P.H., Ap.J., 136, 1108, 1962.

Sciama, D.W., Waylen, P.C. and Gilman, R.C., Phys.Rev., 187, 1762, 1969.

Shapiro, S.L. and Teukolsky, S.A., *Black Holes, White Dwarfs, and Neutron Stars. The Physics of Compact Objects*, John Wiley & Sons, New York, 1983.

Smarr, L., Phys.Rev.Lett., 30, 71, 1973.

Steguin, F.H., Ap.J., 197, 745, 1975.

Stoeckly, R., Ap.J., 142, 208, 1965.

Tassoul, J,L., *Theory of Rotating Stars*, Princeton University Press, Princeton, 1978.

Tassoul, J.L. and Ostriker, J., Ap.J., 154, 613, 1968.

Tassoul, J.L. and Ostriker, J., Astron.Astrophys., 4, 423, 1970.

Thorne, K.S., *Relativistic Stars, Black Holes and Gravitational Waves (including a in-depth review of the theory of relativistic, rotating stars)*, in *Gravitation and Cosmology*, ed. Sachs, R.K., Academic Press, New York, 1971.

Toomre, A., Ap.J., 138, 385, 1963.

Tsuruta, S. and Cameron A.G.W., Canad.J.Phys., 44, 1895, 1966.

Vandervoort, P.O., Ap.J., 241, 316, 1980.

Vandervoort, P.O. and Welty, D.E., Ap.J., 248, 504, 1981.

Wagoner, R.V., Ap.J., 278, 345, 1984.

Wald, R.M., *General Relativity*, The University of Chicago Press, Chicago, 1984.

Wiita, P., Phys.Reports, 123, 118, 1985.

Will, C.W., Ap.J., 191, 521, 1974.

Will, C.W., Ap.J., 196, 41, 1975.

Wilson, D., B., Nature, 312, 620, 1984.

Wilson, J.R., Ap.J., 176, 195, 1972.

Wong, C.-Y., Ap.J., 190, 675, 1974.